VILNIUS UNIVERSITY

CENTER FOR PHYSICAL SCIENCES AND TECHNOLOGY

INGA MORKVĖNAITĖ-VILKONČIENĖ

SCANNING ELECTROCHEMICAL MICROSCOPY AS A TOOL FOR THE INVESTIGATION OF MODIFIED ELECTRODE SURFACES

Doctoral dissertation

Physical sciences, chemistry (03 P)

Vilnius, 2016

Dissertation was prepared 2012 – 2016 years at Vilnius University

Supervisor – prof. habil. dr. Arūnas Ramanavičius (Vilnius University, physical sciences, chemistry − 03P)

Scientific advisor – prof. dr. Henrikas Cesiulis (Vilnius University, physical sciences, chemistry − 03P).

VILNIAUS UNIVERSITETAS

FIZINIŲ IR TECHNOLOGIJOS MOKSLŲ CENTRAS

INGA MORKVĖNAITĖ-VILKONČIENĖ

SKENUOJANČIOS ELEKTROCHEMINĖS MIKROSKOPIJOS TAIKYMAS MODIFIKUOTŲ ELEKTRODŲ PAVIRŠIŲ TYRIMUOSE

Daktaro disertacija

Fiziniai mokslai, Chemija (03 P)

Vilnius, 2016

Disertacija rengta 2012 – 2016 metais Vilniaus universiteto Chemijos fakultete

Mokslinis vadovas – prof. habil. dr. Arūnas Ramanavičius (Vilniaus universitetas, fiziniai mokslai, chemija − 03P).

Mokslinis konsultantas – prof. dr. Henrikas Cesiulis (Vilniaus universitetas, fiziniai mokslai, chemija − 03P).

Acknowledgements

I would like to acknowledge prof. habil. dr. Arūnas Ramanavičius for his supervision. I would like to thank for support of all my ideas and showing the best way to realize them. I was excited to work in very new for me bioelectrochemistry, and to learn many things, which will be very useful in a future: experimental work, data analysis, and writing of publications. It was a rare gift to have been able to work in such enthusiastic scientific group of young scientists, leading by great supervisors - prof. habil. dr. Arūnas Ramanavičius and prof. habil. dr. Almira Ramanavičienė. I would like to thank her for patience explaining basics of writing articles, and to improving manuscripts.

I would like to acknowledge my scientific advisor prof. dr. Henrikas Cesiulis for showing my mistakes, and for possibility to participate in some projects' activities. For great time, spend in these activities, I would like to thank my new friends: dr. Urtė Samukaitė-Bubnienė, dr. Natalia Tintaru, and PhD student Edita Vernickaitė.

I would like to thank PhD student Povilas Genys for basic knowledge and common work in electrochemical impedance area, and help to combine two techniques in one. Also, I would like to thank PhD student Aura Kisieliūtė for discussions about processes, which occurred in living cells, and knowledge in biochemistry.

I would like to thank dr. Lina Mikoliūnaitė for administration support, and dr. Ieva Balevičiūtė for encouraging and explaining that all of difficulties will be overcome. These two girls was an example of diligence and intelligence at the highest level.

I would like to acknowledge dr. Antoni Kozič, Head of Electronics department at Vilnius University of Applied Sciences for giving me job. Without these finances it would be impossible to have pleasure to study PhD. Also, I would like to thank all my friends in this institution, Antoni, Eugenijus, Viktorija and Andžej for nice communication and funny lunch times.

I would like to acknowledge my excellent student Rita Šareikaitė for accurate and correct experiments.

Many thanks for great working atmosphere to PhD student Jurate Petroniene, dr. Jaroslav Voronovič, PhD student Anton Popov, Mindaugas Gicevičius, and PhD student Dominykas Juknelevičius.

I would like to thank habil. dr. Etienne Mathieu for acceptance in Laboratory of Physical Chemistry and Microbiology for the Environment, for help acquiring knowledge in SECM, for communication and collaboration.

And the most important supporters and encouragers are my family. Especially my loving husband Raimundas, for the orders ‘to rest’, ‘to eat’, ‘to get fun’ (it is really difficult to live with workaholic like me). Also, I would like to thank for courage to have children with me after such difficult experience; for staying with me in spite of everything; and for supporting me in all situations. I would like to thank my mother for the first encouragement to go ‘learn something’, and for practical examples from her life ‘how to start life anew’. It was easier, with such strong women example, to go to the new city and to study in a new area. Also, I would like to thank for Raimundas parents – my children were grown on their hands.

At last, thank God for great opportunity, favourable circumstances and hope.

Table of contents

List of abbreviations

AC-SECM – alternating current scanning electrochemical microscopy

ADIFDM - alternating-direction finite implicit difference method

AFM – atomic force microscopy

AFM-SECM – atomic force scanning electrochemical microscopy

Ag/AgCl/KClsat – Ag/AgCl electrode in saturated KCl

A-PBS – sodium acetate - sodium phosphate buffer, pH 6.0, with 0.1 M KCl

AzBTS – 2,2-azinobis-(3-ethylbenzothizoline-6-sulfonic acid)

BEM - the boundary element method

BFCs - biofuel cells

BOx - bilirubin oxidase

CDH – cellobiose dehydrogenase

CNTs – carbon nanotubes

DCPIP – 2,6-dichlorophenolindophenol sodium salt hidrate

DET - direct electron transfer

EDC–NHS - 1-ethyl-3-(3-dimethylaminopropyl) carbodiimide hydrochloride and N-hydroxysuccinimide

E-BFC – enzymatic biofuel cell

EIS – Electrochemical impedance spectroscopy

ET - electron transfer

FB – Feedback

FB-SECM – feedback (FB) mode Scanning electrochemical microscopy

FDM - the finite difference method

GC-SECM – generation-collection mode scanning electrochemical microscopy

GOx – Glucose oxidase

GOx/PD/GRE – GRE consequently modified by PD and GOx

GRE – graphite electrode

HRP - horseradish peroxidase

HRP/GRE – HRP-modified GRE

$i_{max(\text{for FeCN})}$ – maximal current value for ferricyanide

$i_{max(\text{for PQ})}$ – maximal current value for 9,10-phenantrenequinone

$K_{M(\text{app. for FeCN})}$ – apparent Michaelis constant for ferricyanide

$K_{M(\text{app. for PQ})}$ – apparent Michaelis constant for 9,10-phenantrenequinone

$K_{M(app.)}$ – apparent Michaelis constant

LAC - laccase

ME – microelectrode (diameter in micrometers range)

M_{ox} / M_{red} – oxidized/reduced form of electroactive species

NAD-GDH – NAD-dependent glucose dehydrogenase

NMMRL – nominal minimal mass retention limit

NPNWs – Nafion poly(vinyl pyrrolidone) compound nanowires

pBQ – p-benzoquinone

PBS – sodium phosphate buffer solution

PD – 1,10-phenantroline-5,6-dione

PD/GRE – PD-modified GRE electrodes

PEGDGE – poly(ethyleneglycol) (400)diglycidyl ether

PnDs – phenananthroline derivatives

PQ – 9,10 phenantrenequinone

PQQ-GDH – PQQ-dependent alcohol dehydrogenase

RC-SECM – redox competition mode scanning electrochemical microscopy

SECM – scanning electrochemical microscopy

SEIM – scanning impedance microscopy

SG/TC - substrate generation/tip collection

SICM - scanning ion conductance microscopy

SWNT – single-walled carbon nanotubes

TG/SC - tip generation/substrate collection

UME – ultramicroelectrode (diameter up to 25 μm)

Introduction

Scanning electrochemical microscopy (SECM) is an innovative method, which could be applied for the surface-activity analysis of enzymatic biosensors [1-3]. The SECM is based on electrochemical measurements performed by ultramicroelectrode (UME), which is scanning 3D space close to surface of the interest, which could contain catalytic, redox or other electrochemically active sites. In such experiments the UME is mostly connected as a working electrode in electrochemical setup, and the current, which is measured by the UME, depends on the local concentration of electroactive species. Thus, the concentrations of chemicals produced and/or consumed by immobilized enzyme at different position can be determined by SECM. For the first time electron transfer kinetics of non-conducting surfaces modified by enzymes were investigated by Bard's group using feedback (FB) mode of SECM [4]. Since then, the investigation of heterogeneous reactions catalysed by immobilized enzymes using the SECM has been applied in many biosensorics-related researches: for high-resolution imaging of the chemical reactivity [5, 6], electrocatalytic activity [7-10], and topography of enzyme-based interfaces formed in enzyme immunoassays [11], biosensors and biochips [12].

The most important part of the SECM is an UME with a radius ranging from few nm to 25 μm [13]. The UME usually is moved by positioners in three directions – x, y, z in the solution close to the surface of interest. Mostly the UME is switched as a working electrode in the electrochemical system consisting of two, three or four electrodes [13]. One of the most informative SECM modes is based on vertical movement of UME *vs* sample because it allows to register the current changes *vs* distance over the sample. From these curves measured in FB mode the distance of UME from sample surface can be determined, the evaluation

of electrochemically active surfaces can be performed, and reaction kinetics can be calculated [4, 14-17]. Current flow in FB mode is caused by oxidation/reduction reaction, occurred at the UME.

The main aim of this study was to evaluate surfaces of electrochemical biosensors and biofuel cells based on bio-recognition elements such as enzymes and living cells by mean of SECM. For this purpose, enzyme *Glucose oxidase* and yeasts cells *Saccharomyces cerevisiae* were immobilized on selected substrates and different modes of SECM were applied using ultra micro electrodes of different geometry.

The main tasks set to achieve the aim were following:

1. To evaluate how RC-SECM and GC-SECM modes could be used in separated and combined way for the determination of UME distance from bio sensing surface and for the evaluation of GOx catalysed reaction.

2. To determine how Michaelis constant ($K_{M(app.)}$) depends on the distance of UME-based probe from the GOx-modified biosensor's surface and how this $K_{M(app.)}$ value depends on the conductivity (gold-based – conducting or plastic-based non-conducting) of substrate, which is used for the immobilization of GOx.

3. To merge EIS with SECM methods into joint SEIM system and to apply developed SEIM system for the investigation of solution conductivity at different distance from the surface, in order to demonstrate the suitability of SEIM for the evaluation of the diffusion of reaction products from enzyme-modified surface in real time.

4. To create mathematical model of RC-SECM mode, in order to describe kinetics of reactions on the GOx-modified surface.

5. To evaluate the possibility to investigate electrochemical activity of biosensor's surfaces modified by yeast cells by GC-SECM mode of SECM based on two redox mediators based system.

6. To develop and evaluate enzymatic biofuel cell based on GOx/PD/GRE anode powered by glucose and HRP/GRE cathode powered hydrogen peroxide.

Statements for defence:

1. GC-SECM and RC-SECM modes are suitable for the investigation of biosensor's surface, when together the formation of product of enzymatic reaction (H_2O_2) and the kinetics' of the reactant (O_2) consumption can be determined and visualized.

2. Determination of Michaelis constant ($K_{M(app.)}$) can be simplified using RC-SECM mode, when 'approaching curves' are recorded and kinetics can be determined using specialized mathematical models.

3. Determination of diffusion of reaction products in real time can be performed by combined SECM/EIS system.

4. Using created mathematical model, it is possible to calculate oxygen consumption rate, to evaluate enzymatic reaction kinetics, and to determine diffusion coefficients for oxygen diffusion in the media of varying composition.

5. The surface of biosensors, which are based on application of living cells, devoted for the determination of toxicity can be investigated by GC-SECM using two redox mediators based system, one of those mediators is lipophilic toxic quinone, and a second one is hydrophilic ferricyanide.

6. New design of biofuel cell based on GOx/PD/GRE anode powered by glucose and HRP/GRE cathode powered hydrogen peroxide allows to utilize glucose as a fuel for the anode, and H_2O_2 formed during the catalytic action of GOx, which is immobilized on anode, could be utilized as a fuel at the cathode of the same biofuel cell.

1 Literature review

1.1 Scanning electrochemical microscopy

Scanning electrochemical microscopy (SECM) concept was determined by A. J. Bard in 1989 [18]. SECM was introduced as a technique, using which the local electrochemical activity of surfaces can be visualized. The advantage of SECM is that the technique can be applied for in-situ study without any damage to the system of interest. SECM could be applied for the surface-activity analysis of enzymatic biosensors [2, 3]. For the first time electron transfer kinetics of non-conducting surfaces modified by enzymes were investigated by Bard's group using feedback (FB) mode [4]. Since then, the investigation of heterogeneous reactions catalysed by immobilized enzymes using the SECM has been applied in many biosensorics-related researches [2, 19-23]. In addition the SECM was applied for high-resolution imaging of the chemical reactivity [5, 6], electrocatalytic activity [7-10], and topography of enzyme-based interfaces formed in enzyme immunoassays [11], biosensors and biochips [12]. Until now, SECM is widely used for the investigation of living cells viability [24], biocatalytic activity [25], and even for some chemicals toxicity to the cells [26]. Depending on the type of single live cells studied, cellular processes addressable by SECM range from the membrane transport of metabolites to the stimulated release of hormones and neurotransmitters and processes such as cell respiration or cell death and differentiation [27]. Living cells electrochemical activity can be imaged, and zones of different electrochemical activity can be distinguished. Different kind of cell treatment can be investigated in real-time, because reaction products concentration, diffused out of the cell, can be measured directly by SECM.

The SECM is based on electrochemical measurements performed by ultramicroelectrode (UME), which is scanning 3D space close to

surface of the interest, which could contain catalytic, redox or other electrochemically active sites. In such experiments the UME is mostly connected as a working electrode in electrochemical setup, and the current, which is measured by the UME, depends on the local concentration of electroactive species. Thus, the concentrations of chemicals produced and/or consumed by immobilized enzyme or living cell at different position can be determined by SECM. UME is the electrode with a radius ranging from few nm to 25 μm [13]. One of the most informative SECM modes is based on vertical movement of UME *vs* sample because it allows to register concentration profile. From these current *vs* distance dependencies, measured in feedback (FB) modes, the distance of UME from sample surface can be determined, the evaluation of electrochemically active surfaces can be performed, and reaction kinetics can be calculated [4, 14-17]. Current flow in FB modes is caused by oxidation/reduction reaction, occurred at the UME. Current *vs* distance dependencies could be measured at several SECM modes, such as feedback (FB-SECM), generation-collection (GC-SECM) or redox competition (RC-SECM). Feedback modes are described mathematically, and from such measurements it is possible not only determine kinetics of surface of interest, but also calculate electrode geometry and quality [28]. GC-SECM modes are used mostly for imaging of the surface of interest. RC-SECM mode is very useful for cells respiration measurement [29, 30], but also could be applied for oxygen consumption determination in other systems, like enzymatic biosensors.

SECM scheme of experiment is shown in Fig. 1.1. Here four electrodes electrochemical cell is shown with UME as a moving working electrode, reference and counter electrodes, and substrate is connected as second working electrode. All electrodes are connected to the bipotentiostat. Control of UME movement and current record at the same time are realized by computer program.

Widely applied experiments are amperometric, but some other electrochemical measurements can be applied, such as Electrochemical Impedance Spectroscopy (EIS), Alternating Current SECM (AC-SECM) [31], or measurements of conductivity or pH [32, 33]. SECM allows use all these techniques while scanning the surface, and the result is topographic image or current *vs* distance dependence.

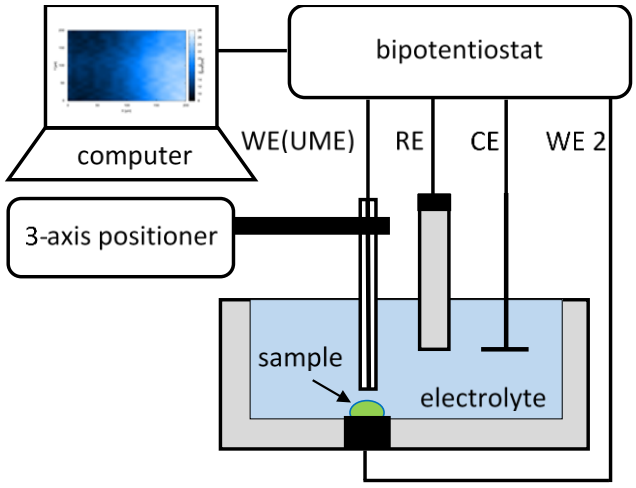

Fig. 1.1. Scheme of typical SECM experiments. WE(UME) – working ultramicroelectrode, RE – reference electrode, CE – counter electrode, WE 2 – second working electrode, connected to substrate.

1.1.1 SECM operating modes

All SECM experiments can be carried out in constant height and constant distance modes. In constant height mode the UME is moved only laterally in the x and y directions, while in constant distance mode UME can be moved in x-y-z directions [34]. The constant height mode is appropriate for the evaluation of smooth surface (roughness is smaller than the UME radius) samples [35]. In this mode the UME current depends on the distance between UME and surface of interest and on the reactivity of compounds immobilized on the surface. Resolution studies of SECM in constant height mode shows quantitative correlation of decrease in resolution and the increase in distance between UME and sample [36]. To determine the distance, which is the most suitable for appropriate resolution of SECM constant height mode measurement, the

current *vs* distance dependence could be measured in feedback mode by approaching the UME to the surface of interest; and distance between UME and sample could be calculated from the SECM theory, where $i_T/i_{T,\infty}$ (ratio of UME current and steady-state current far from electrochemically active surface) can be related to d/a (the ratio of distance between sample and UME and UME radius) [34]. However, this approach is not accurate and can lead to tip crash or biological sample damage. Attempts to overcome these restrictions include among others positioning of the tip to distances outside the feedback range [37], into cavities [24, 38-42], embedding of the cells or efforts to subtract topographic contributions after cell death [43]. Moreover, as living cells are irregular in dimension, the tip-to-cell distance varies with the tip position.

These limitations can be overcome by using a shear-force based constant-distance control [44]. The microelectrode vibrates at its resonance frequency with typical amplitudes of only a few nanometers with use of a piezo-pusher [45]. Simultaneously, a laser beam is focused onto the very end of the vibrating electrode and the resulting Fresnel diffraction pattern is projected onto a split photodiode. Amplitude and phase information about the vibrating tip is obtained by the amplification of the difference signal from the split photodiode with respect to the agitation signal using a lock-in amplifier. With decreasing tip-to-sample distance, increasing shear forces between tip and sample surface lead to a damping of the vibration amplitude and to a phase shift, which can be used to continuously keep a predefined damping value related to a constant distance of about 50 ± 100 nm by means of a software-controlled feedback loop [45].

Another method of the shear-force detection is accomplished by mechanically attaching a set of two piezoelectric plates to the scanning probe [46]. One of the plates is used to excite the SECM tip causing it to resonate, and the other acts as a piezoelectric detector of the amplitude

of the tip oscillation. Increasing shear forces in close proximity to the sample surface lead to a damping of the vibration amplitude and a phase shift, effects that are registered by connecting the detecting piezoelectric plate to a dual-phase analogue lock-in amplifier [46]. Also, a shear force-based method is able to work at various tip-to-sample separations. It can hence detect complete diffusion profiles in the surroundings of sources or sinks of redox-active species [47]. In particular, coupling SECM with scanning probe techniques, such as atomic force microscopy (AFM) [48] and scanning ion conductance microscopy (SICM) [49], shear force [44, 46, 50, 51] and impedance-based techniques, [52] as well as led to efficient strategies to control the tip-to-sample separation.

In combined technique of AFM-SECM, AFM tip is used as a working electrode and as the force sensor at the same time [53, 54]. This technique allows achieving the best resolution and measure different properties of surface. For living cells, it could be force curves measured at the same time with current-distance curves. To investigate some influence of toxic chemicals, or to distinguish cancer cells from healthy ones, both data are interesting: cells, depending on their healthy, become softer/harder and at the same time more/less active.

Feedback modes

SECM feedback modes can be distinguished in two parts: negative feedback and positive feedback [55]. Far from the surface, current depends only on concentration and diffusion of redox species (Fig. 1.2). Diffusion-limiting current can be calculated by *equation 1*. If current is decreasing when UME is approaching surface of interest, the resulting curve is of negative feedback behaviour (Fig. 1.2 A). It happens if surface is insulating. If current is increasing when UME is approaching the surface, the resulting curve is of positive feedback behaviour (Fig. 1.2 B) and can be achieved approaching conducting surface. When UME is

approaching living cells, negative feedback can only be achieved if no reaction in the cell occurs. Then the current depends only on distance.

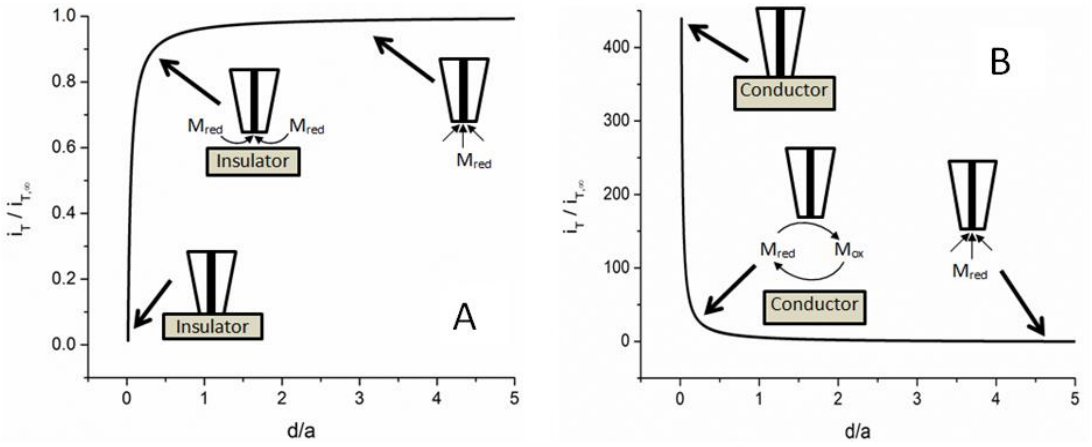

Fig. 1.2. Negative feedback (hindered diffusion) when UME is approaching insulating surface – A; Positive feedback when UME is approaching conducting surface - B. Negative feedback curve was calculated by Cornut and Lefrou equation [56] using RG=10; positive feedback curve was calculated by Cornut and Lefrou equation [57] using RG=10 and Λ=1.

In positive FB-SECM mode current can be increased when the UME is approaching conducting surface. Moreover, registered current at positive FB could increase even when conducting surface, which is evaluated by SECM, is not connected to the potentiostat [58]. In this case, the conducting surface is reacting with redox compounds, which are generated on the UME, and then the reversible oxidation-reduction reaction occurs on conducting surface [58]. Due to this reaction, the concentration of compounds, which are utilized by UME, increases close to the conducting surface. However, such reversible redox process can be observed only when the UME is close (at the distance equal to 1-2 radiuses of UME) to conducting surface. When the conducting surface is modified by enzyme, then particular redox mediator could be involved into two simultaneous processes: (i) electron uptake with immobilized enzyme and (ii) recycling to the corresponding oxidation state at the conducting surface, as it was well demonstrated by some redox mediators based on ferrocene derivatives [19]. Some attempts to separate both redox processes (the redox process related to enzymatic

reaction and the reverse redox reaction occurring on the conducting surface) by SECM-based imaging were also applied [59]. For this SECM based measurements were performed in (i) glucose containing solution and in (ii) glucose-free solution and such evaluation demonstrated that reversible reaction response from conducting surface dominates in overall response and only a very small fraction of overall response corresponds to the contribution of the enzymatic reaction [59]. Therefore, if the enzyme is immobilized on conducting surface, the determination of enzymatic kinetics by SECM is more complicated. But despite of this limitation, such investigations are important for the evaluation of enzyme-modified surfaces of biofuel cells or biosensors, where the enzymes are usually immobilized on conducting surfaces.

Generation-collection modes

In GC-SECM mode, the UME is only registering currents, which are caused by the reaction products [24, 60, 61]. Usually the UME passively detects the redox compounds, which are generated at the surface. The problem is that the reaction on the sample occurs continuously, independently on the operation of the UME. There are two SECM generation-collection modes: Substrate generation/Tip collection (SG/TC) (Fig. 1.3 A) and Tip generation/Substrate collection (TG/SC) (Fig. 1.3 B). In a SG/TC mode, solution initially contains redox species, which are not detectable. These redox species could be oxidized/reduced by sample and then they could be detected by UME. In a TG/SC mode, UME is generated electroactive species, which could be detected by substrate electrode. If redox species are detected on UME, and also consumed in the reaction of the surface, such mode is called Redox competition (RC-SECM) (Fig. 1.3 C).

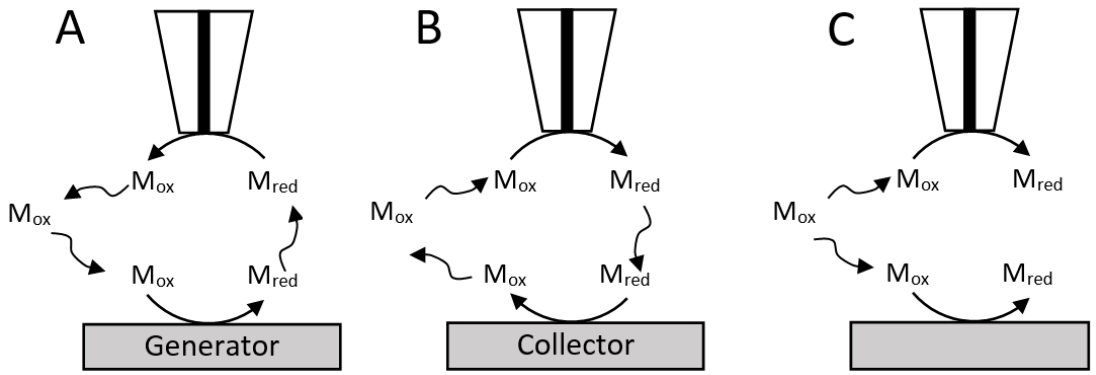

Fig. 1.3. Generation-collection mode SECM: **A** – species, generated by substrate electrode, are collected by UME; **B** – UME generated species are collected by substrate electrode. Redox competition mode SECM: **C** – species is detected on UME, and at the same time consumed on substrate electrode.

Redox competition mode

The RC-SECM mode, which was developed by Schuhmann's group [62], could be used for the evaluation of oxygen reduction reaction (Fig. 1.3 C). If 'bi-potentiostatic' mode is applied for the evaluation of conducting surfaces modified by enzymes, then dissolved oxygen is consumed in two competing reactions: one is running on the UME and another one – on the surface modified by enzyme (e.g. glucose oxidase (GOx)), which is utilizing O_2 as electron acceptor. In the case when electrically conducting substrate is modified with GOx, that conducting substrate could be switched into electrochemical setup as a second working electrode, and then the electrocatalytic activity of the surface could be visualized by horizontal scanning at selected distances over GOx-modified surface [63]. The same method has been applied for the characterization of the performance of biosensors, e.g. for the evaluation of local electrocatalytic activity of GOx [10] and bilirubin oxidase [64]: (i) the GOx was immobilized within a polymer hydrogel matrix on the surface of Prussian blue modified glassy carbon electrode, and then the potential, which was suitable for the re-oxidation of Prussian blue, was applied; in this research both the ME-based probe and GOx-modified glassy carbon electrode were competing for H_2O_2, which was formed in GOx-catalysed

reaction [10]; (ii) UME-based probe and electrode, which was based on glassy carbon electrode modified with Os-complex and bilirubin oxidase, were competing for dissolved oxygen [64]. The RC-SECM mode has been applied for the determination of laccase distribution within sol-gel processed silicate films deposited on glass plate, which was modified by redox mediator – 2,2'-azino-bis(3-ethylbenzothiazoline-6-sulfonate) [65]. In this research both the UME and laccase were competing for reduced form of the redox mediator [65]. SECM-based activity-mapping of carbon ceramic electrodes modified with laccase, which was encapsulated in sol-gel modified matrix, has been performed [1]. In this experiment both the UME-based probe and closely located laccase-modified electrode were competing for dissolved dioxygen [1].

In our work, the RC-SECM mode was used for the determination of UME distance from surface and for the evaluation of GOx catalysed reaction. The O_2 reduction current was registered and current decrease while approaching the GOx-modified surface was observed. This current decrease shows oxygen consumption by GOx. It should be noted that there are some principle differences between recent our work and previous reports [10, 62, 63] published by W. Schumann's group: (i) we have used redox competition mode for the evaluation of enzymatic reaction while the GOx was immobilized on insulating surface and no external potential was applied, (ii) in researches conducted by W. Schumann's group an redox mediator was used, while we have performed the SECM measurements without any redox mediator.

Mathematical models

Digital simulations are performed for different modes of SECM [55, 58, 66-71]. Such simulations are performed for different purposes: i) for the investigation of the influence of UME geometry to the SECM response [72], ii) for the determination of reaction kinetics, including

reaction rate constants and evaluation of enzymatic kinetics [4, 58, 66, 69]. The simulations could solve important problems, such as poor spatial resolution, negative effect of uncontrolled distance between UME and surface of interest during SECM investigations, and the effects of deviations from mathematically idealized SECM geometries [69, 73]. Such numerical simulations could be a basis for a quantitative interpretation of SECM results [74]. Mathematical simulations of SECM systems have been performed by: i) the finite difference method (FDM) [58, 72, 75]; ii) finite elements simulations, which were initially used [55, 76] and were recently revisited [55, 71, 76]; iii) the boundary element method (BEM) [77, 78]. The influence of electrode geometry for SECM simulations was shown by various authors [57, 72, 79]. However, according to our best knowledge, analytical equations for the determination of enzymatic kinetics in RC-SECM mode are still not well established.

1.2 Scanning electrochemical impedance microscopy

EIS is a powerful, non-destructive and informative technique, which has been successfully applied for the characterization of GOx-based biosensor surfaces [80-84]. Moreover the EIS could be applied for glucose concentration measurements in electrochemical systems based on GOx-modified electrodes. However, conventional EIS based techniques represent only averaged response of the entire electrochemical system. In order to get more advanced mapping of electrochemical system scanning electrochemical microscopy (SECM) merged with EIS (SEIM) eventually could be applied. In SEIM based technique localized impedance measurements could be performed in the range of frequencies when the surface of interest is scanned by ultramicroelectrode (UME). The result of SEIM could be visualized by mapping one of calculated parameters, e. g. charge transfer resistance or double layer capacitance as a function of 3D coordinates [85, 86].

The evaluation of enzymatic reaction intensity could be estimated by conventional SECM techniques [87, 88]. However in conventional SECM the most commonly used electrochemical method is based on faradaic response when fixed potential is applied to the UME in order to register the concentration of electrochemically active enzymatic reaction products [4, 89]. Moreover, it should be noted, that the potential applied to the electrode drives the electrochemical system far from the equilibrium, and then the response to this perturbation is observed as disturbing signal. In order to avoid this problem the applicability of technique based on SECM in which the UME is modulated by selected frequency alternating current (AC-SECM) can be applied. The AC-SECM based technique also allows to study local corrosion processes in the entire solution volume without any redox mediator [90]. Using AC-SECM method the approach curves were recorded at several different frequencies and they demonstrated negative feedback behaviour while the UME was approaching an insulating surface [91]. This phenomena is similar to that observed in faradaic SECM based methods, however, different approach curves were observed when different frequencies were applied [92]. In order to advance this technique, the entire electrochemical impedance spectra can be registered at every measurement point and then the electrochemical system can be evaluated using the most suitable and informative equivalent circuits. This technique is called scanning electrochemical impedance microscopy (SEIM). In the case of SEIM conventional approach curves, which represent ohmic resistance and/or other equivalent circuit parameters *vs* distance are plotted. The concept of SEIM was described recently in the evaluation of localized corrosion processes by Schuhmann's group [93, 94]. When SEIM was applied for localized evaluation of corrosion processes the sample was minimally influenced by UME, which was applied as a scanning probe, and it was demonstrated that domains, which have different electrochemical

properties, could be easily distinguished by SEIM even if they have similar topography and/or morphology [86]. In another research, impedance dependence on UME distance from insulating sample was revealed at feedback mode SEIM [95]. The spherical diffusion, which has most significant influence far from insulating surface, was evaluated by Cole-Cole impedance evaluation method, and the radial diffusion, which has most significant influence when the UME is approaching insulating surface, was evaluated by Cole-Davidson impedance evaluation method. It was determined that the low-frequency part of the EIS in a thin-layer between UME and surface of interest is controlled by both above mentioned types of diffusion. Moreover it was also demonstrated that the SEIM in feedback mode is suitable for constant-height based imaging. When SEIM was acting in feedback mode the local information on both topography and surface reactivity was obtained from the simultaneous analysis of the current and electrolyte-resistance variations [96]. Fundamental aspects of SEIM were investigated comparing UME responses while it was approaching to different surfaces e.g.: (i) insulator surface, (ii) conducting surface not-connected to electric circuit, and (iii) conducting surface, which was connected to electric circuit and was held at constant potential [97]. By this research it has been shown that the admittance of the UME located at relatively small distance from the surface of interest mostly depends on the distance between UME and the surface and on interfacial properties of the surface. Therefore the SEIM based imaging is informative even without any redox mediators. When AC-SECM and SECM methods are compared, it should be noted that the AC-SECM is performed at single frequency, while the SEIM is performed in broad range of frequencies what enables to select the most suitable equivalent circuit and to calculate number of EIS parameters. Therefore parameters, which are derived from SEIM evaluations, better describe an electrochemical system than the parameters that are derived from AC-SECM data. Thus, the SEIM could be suitable for the

investigation of biosensor and biofuel cell surfaces in order to evaluate localized activity of immobilized enzymes and/or to perform advanced evaluation of the diffusion of enzymatic reaction products.

1.3 Saccharomyces cerevisiae as a recognition element of cell-based biosensors

Saccharomyces cerevisiae (*S. cerevisiae*) is a simple eukaryotic cell, which is serving as a model system for eukaryotes, including humans, for the study of fundamental cellular processes such as cell cycle, DNA replication, recombination, cell division, and metabolism [98]. Yeast cells can be used as a recognition unit in biosensors [99-103]. Such biosensors can be used in environmental monitoring and control [104], and toxicity tests [99, 105-109]. Among many different types of recognition elements (e. g. enzymes, antibodies, receptors, micro-organisms, animal or plant cells and tissues), the micro-organisms have some advantages including sensitivity towards various chemical substances for a wide range of pH and temperature [110]. Yeast cells are attractive as a recognition element of cell-based biosensors, because they can remain viable in adverse conditions especially if they are immobilized on membranes and hydrogels [111]. Another application of yeast cells is in a model system for the investigation of toxic compounds [108, 109]. The yeast cell based model system is ideal for the evaluation and biosensing of toxic compounds because: (i) yeast cells are simple eukaryotic organisms with some homology to mammalian cells; (ii) the yeast genome is fully sequenced allowing facile manipulation of their genetics to control predictably their susceptibility/resistance to toxic compounds; (iii) yeast can survive under different conditions including anaerobic environment and varying pH, which allows the evaluation of toxicity at different growth conditions and/or cell environment; and (iv)

both handling and manipulation of yeast cells are simple and inexpensive [108].

Quinones interact with the plasma membrane oxido-reductase systems, which are accessible from the cell's periplasm [112]. Therefore, quinones can be applied to transduce internal cellular redox activity into electrode current. 2-Methyl-1,4-naphthoquinone (menadione, vitamin K3) and water soluble 2-methyl-1,4-naphthoquinone sodium bisulfite (menadione sodium bisulfite) were compared as artificial electron acceptors for their ability to transduce internal cellular redox activity into electrode current [113]. It was found that hydrophobic menadione was superior to its water-soluble bisulfite derivative for electrochemical evaluation of intact cells. The different behaviours of three lipophilic mediators including menadione, 2,6-dichlorophenolindophenol (DCPIP) and N,N,N',N'-tetramethyl-p-phenylenediamine (TMPD) in the evaluation of redox activity of the yeast *Saccharomyces cerevisiae* were studied by experiments based on the effect of several different factors [114]. It was found that under anaerobic condition, menadione interacts with the anaerobic respiration pathway, whereas DCPIP and TMPD interact with the fermentation pathway in the yeast [114]. However, in practice such lipophilic mediators usually cannot be used as the single mediators in such yeast cell based biosensing systems because their low aqueous solubility limits the mediator concentration in solution and therefore the magnitude of amperometric signal is very small [112]. Hence, in order to achieve better electrochemical signal, the application of additional hydrophilic mediators, such as ferricyanide, is very useful. Hydrophilic mediators are soluble in the aqueous environment of the cell, but they cannot cross the cell membrane to enter the cytoplasm [115]. Hydrophilic $[Fe(CN)_6]^{3-}$ was employed as an extracellular electron acceptor, and constituted a two-redox-mediator-based system together with lipophilic mediators [114]. In *S. cerevisiae*, the two redox mediators

based system response originates from the reduction of the lipophilic mediator by nicotinamide adenine dinucleotide phosphate (NAD(P)), which is produced in the pentose phosphate pathway. The single mediator signal arises from reduction of the hydrophilic mediator by an extracellular redox species produced in response to the presence of glucose [115].

The possibility to investigate a biosensors' surface by scanning electrochemical microscopy (SECM) and demonstration of the different properties of biosensors is provided by the use of various mediators to image mammalian and bacterial cell features using SECM [33, 116-118]. SECM has an advantage compared to other types of scanning microscopes, because the electrode is not in contact with the cell surface and the sample is not directly violated. SECM is also very convenient to investigate cells in their favoured medium. In our work, the GC-SECM mode was used, because this mode is characterized by a relatively high sensitivity compared to others modes of SECM. Therefore, it is suitable for the detection of small quantities of electroactive species, which are diffusing out from an immobilized cell. In addition, the UME in GC-SECM mode is used as a passive sensor, which causes minimal distortions to the surface during investigation.

1.4 Biofuel Cells

The fast technological progress in alternative energetics and biomedicine is leading to the development of new implantable micro- and nano-biodevices [119, 120]. Mostly such devices are still based on electronic circuits, therefore they need electric power sources. However chemical batteries and accumulators are lasting for limited time. Therefore, a new concept in the development of power sources is required in order to maintain the functions of various implantable miniaturized electronic devices during long periods [121-124]. Recently,

considerable attention has been paid to the development of biofuel cells (BFCs). The most suitable for in vivo application are biofuel cells based on enzyme catalysed reactions. There are some positive indications that some enzymatic biofuel cells (E-BFCs) are able to operate under physiological conditions and at low concentrations of natural biofuels [125], which are present in human body. In E-BFCs the redox enzymes are mostly applied because they are involved in oxidation and reduction of materials, which potentially could be served as fuels in BFCs [126-128], and enzymes, which could be involved in generation of electric current. Very suitable is that the most enzymatic reactions occur at physiological level (at mili- or micro-molar concentrations) of selected bio-fuel [129]. However just very few out of thousands recently available redox enzymes are capable to accept or to pass electrons correspondingly from/to electrode. Therefore one of the most important challenges in the development of biofuel cells is the establishment of electron transfer (ET) between immobilized enzymes and electrodes. The redox mediators could be applied for this purpose [130-133]. However, not all redox mediators are suitable for the development of biofuel cells due to their unsuitable redox potentials and/or some other physicochemical characteristics. Therefore the selection of optimal redox mediator needs satisfaction of many requirements, which are followed by experimental approval. Significant number of compounds, which are exhibiting proper redox mediating properties, are based on organic metal complexes, quinonic compounds or redox polymers [123, 129, 134-138]. In some researches it was shown that the metal ion complexes with phenanthroline derivatives (PnDs), which are classic bidentate ligands capable to chelate some metal ions (e.g., Os(III) or Ru(II)), could be applied as redox mediators [139, 140]. The PnDs are rigid planar, hydrophobic, electron-poor heteroatomic systems, in which nitrogen atoms are well placed to act cooperatively in the binding of metal ions [141]. Therefore the PnDs complexes with coordinated heavy metals are

mostly used for bioelectrochemical applications [139, 140]. However, the most of PnDs complexes with metal ions are not commercially available and the synthesis of these complexes is very complicated and time-consuming [142, 143]. Therefore the application of PnDs derivatives, which are not involved into metal complexes could be very attractive. However according to our best knowledge, there are only very few recently published studies related to bioelectrochemical application of PnDs, which are not involved as ligands of metal-based complexes [135, 136]. Recently it was reported that five different PnDs (1,10-phenanthroline monohydrate; 5-nitro-1,10-phenanthroline; 5-amino-1,10-phenanthroline; 5-amino,6-nitro-1,10- phenanthroline and 5,6-diamino-1,10-phenanthroline) with different functional groups have been investigated electrochemically in order to determine their ability to act as electron transfer mediators for glucose oxidase (GOx) [135]. PnDs containing amino groups, i.e., 5-amino-1,10-phenanthroline and 5,6-diamino-1,10-phenanthroline have been found to be suitable as redox mediators for GOx [144]. However up to now there are just very few published reports on the application of PnDs in enzymatic electrodes, which are suitable for the design of biofuel cells [145]. Therefore, the evaluation of other PnDs compounds, which are capable to serve as redox mediators for some other oxidases is highly interesting and important, especially if such redox mediator in combination with selected enzyme is suitable for the development of the enzymatic biofuel cells. Another important problem in the development of E-BFCs is the selection of proper design of E-BFC cathode. For this purpose some oxygen or hydrogen peroxide utilizing enzymes such as laccase (LAC) [144, 146-148], bilirubin oxidase (BOx) [149-153] and peroxidase [122, 129, 154-156] could be applied. It should be noted that due to unique direct electron transfer (DET) properties a number of peroxidases, i.e., microperoxidase-8 [122], microperoxidase-11 [157] and horseradish peroxidase (HRP) [158] have been used in the design of biofuel cell

cathodes. But among the other peroxidases the HRP is very attractive because it is relatively cheap and stable in comparison with other peroxidases [127]. The HRP-based cathode is fuelled by H_2O_2, which is a strong oxidizer, however electrochemical reduction of H_2O_2 at a carbon electrode occurs at a very high over-potential. The HRP reduces this over-potential [129] and it is capable for DET between enzyme and the carbon electrode [127, 159]. It should be noted that the H_2O_2 is one of products of GOx-catalysed reaction [122, 129], which could be exploited on the anode of E-BFC.

1.5 Influence of living cells preparation to AFM measurements

The most challenging cell preparation is cell fixation, which is required to protect cell from detachment and to eliminate their movements. Therefore measurement results strongly depend on cell fixation methods. Cell rigidity, comparing to unfixed cell, increases due to chemical fixation and for this reason image resolution becomes much higher. Fixation of round shape cells (yeasts, some bacteria) by capturing them in pores of membrane or filter causes the deformation of cells and therefore different diameter holes in membrane are needed for cells in various dimensions. However this method allows investigations of living cells without any additional procedures such as drying, coating or chemical treatment.

When cells are immobilised by electrostatic interactions (Fig. 1.4 A) and measurements are performed in phosphate buffer saline (PBS) or 3-(N-morpholino) propane sulfonic acid, they often are detached from the support. To solve this problem, Meyer et al. [160] proposed to use a layer of polyphenolic adhesive proteins formed on the surface for the attachment of cells (Fig. 1.4 B). Some other methods also could be applied for the immobilisation of cells, e.g.: (i) physical confinement by

capture in holes [161, 162] (Fig. 1.4 C), (ii) attractive electrostatic interactions [163] (Fig. 1.4 A), (iii) covalent binding to amine-functionalised surfaces after activation of carboxyl groups on the cell surface by 1-ethyl-3-(3-dimethylaminopropyl) carbodiimide hydrochloride and N-hydroxysuccinimide (EDC–NHS) [160] (Fig. 1.4 D), (iv) covalent binding to carboxyl-functionalised surfaces by EDC–NHS [160] (Fig. 1.4 E), (v) covalent binding to self-assembled monolayers [164] (Fig. 1.4 F) , (vi) covalent binding to amine-functionalised surfaces by glutaraldehyde [165] (Fig. 1.4 G).

Mechanical immobilization of cells. The cells can be fixed mechanically in porous membranes (Fig. 1.4 C) [166]. Wang et al. invented vacuum-based cell holding device [167]. Evenly spaced holes (diameter ~400 μm) are connected to a vacuum source. A sucking negative pressure of 7- 24 kPa (2-7 InHg) enables each through-hole to trap a single cell without damaging. To increase efficiency of immobilization during entrapment some processing conditions such as vacuum, pressure and cell concentration are controlled. However physical entrapment in membranes can cause severe structural and mechanical deformations of cell membrane [161]. In order to overcome the limitation and difficulties of imaging and manipulating living protein molecules by AFM, Fung et al. [168] propose to use a biocompatible and flexible polymer micromesh (parylene membrane) with 100 μm diameter openings that is specifically designed to immobilize mechanically living cell and protein structures. Human epithelial cells immobilized by this approach were successfully imaged using AFM tapping mode.

Electrostatic immobilisation of cells. For the immobilisation of cells using electrostatic interactions the surface have to be coated with positively charged substances, such as polyethyleneimine [163], poly-L-lysine, or gelatine. For example, bacteria *Staphylococcus sciuri* was suspended in distilled water or PBS were immobilised by electrostatic

interactions to the N-(2-aminoethyl)-3-aminopropyltrimethoxy-silane, 3-aminopropyltriethoxysilane, polyethyleneimine, poly-L-lysine, and gelatine coated slides [160].

Chemical fixation of cells. Fixation of cells is a process when cells are treated with different agents cross-linking proteins present at the cell surface, thereby ‘‘freezing’’ the morphology of the cell and fixing cells to the substrate and/or attaching cells to each other. Chemical fixation of cells simplifies measurement process and improves image resolution. Glutaraldehyde, formaldehyde, methanol, ethanol/acetic acid, paraformaldehyde, methanol/acetone are mostly applied for chemical fixation of cells. Chemical fixation dehydrates the cell and increases membrane stiffness, therefore small features, such as cytoskeletal fibbers are not revealed in topographical image [169].

It was demonstrated that chemically pre-treated yeast cells became much stiffer compared with intact ones. In addition, the morphology studies of the cell wall revealed that chemical treatment of cells enhanced roughness of the yeast cell surface [166].

Immobilization the cells on glass cover slip. In order to immobilize cells on transparent surface, cells can be grown on glass coverslip, plastic substrate, or mica. Glass coverslip can be coated with polyionic polymers like poly-L-lysine or poly-L-ornithine [170], which support attachment of cells to a surface. Flat pieces of fresh tissues can be ‘glued’ directly to the magnetic disks used for the fixation of AFM samples.

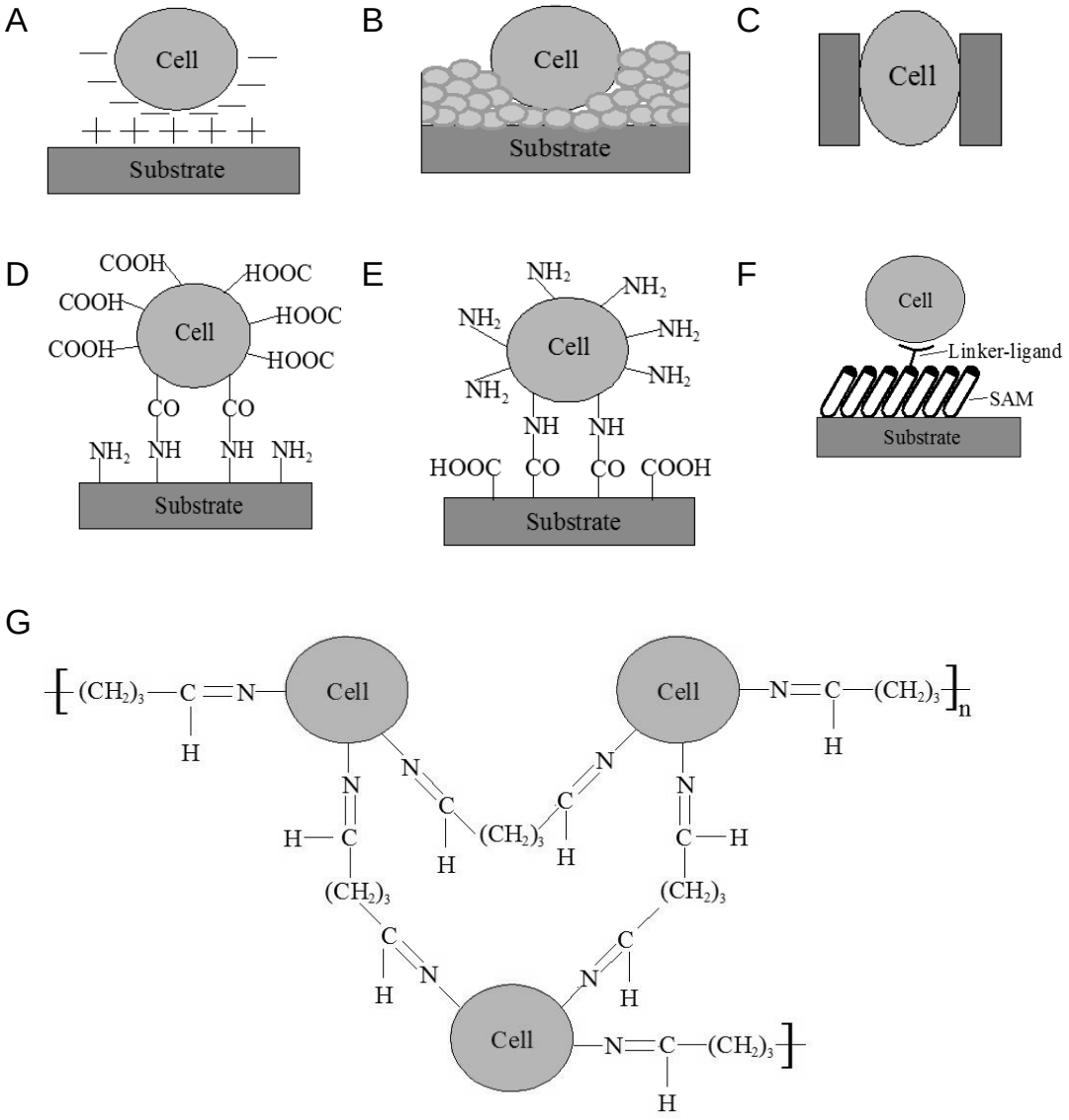

Fig. 1.4. A: Schematic representation of electrostatic interaction between cell and surface. **B**: Schematic representation of cell immobilization attaching them to polyphenolic adhesive protein. **C**: Schematic representation of mechanical immobilization of cell. **D**. Schematic representation of cell immobilization by covalent binding to amine-functionalised surfaces by EDC–NHS. **E**. Schematic representation of cell immobilization by covalent binding to carboxyl-functionalised surfaces by EDC–NHS. **F**. Schematic representation of cell immobilization on self-assembled monolayer. **G**. Schematic representation of covalent binding of cells to amino-functionalised surfaces by glutaraldehyde.

2 Materials and methods

2.1 Chemicals

Glucose oxidase (EC 1.1.3.4, type VII, from Aspergillus niger, 215.3 units mg^{-1}, molar mass 160 kDa, polymer length 583 amino acids [171]) and 25% glutaraldehyde solution were purchased from Fluka Chemie GmbH (Buchs, Switzerland). D-(+)-Glucose was obtained from Carl Roth GmbH&Co (Karlsruhe, Germany). Before investigations glucose solutions were allowed to mutarotate overnight. All solutions were prepared in deionized water purified with Millipore S.A. (Molsheim, France). Sodium acetate trihydrate, potassium chloride, sodium dihydrogen phosphate monohydrate, and disodium hydrogen phosphate dodecahydrate were obtained from Reanal (Budapest, Hungary) and Lachema (Neratovice, Czech Republic). Buffer solution (PBS) was prepared with 0.05 M CH_3COONa; 0.05 M NaH_2PO_4; 0.05 M Na_2HPO_4, and 0.1 M KCl in distilled water. Potassium chloride, monosodium and disodium phosphates, potassium ferricyanide $K_3[Fe(CN)_6]$, 9-10-phenanthrenequinone (PQ), p-benzoquinone, (pBQ), 1,10-phenanthroline-5,6-dione (PD), 2,6-dichlorophenolindophenol sodium salt hydrate (DCPIP) were obtained from Reanal (Budapest, Hungary) and Lachema (Neratovice, Czech Republic). Solutions of 0.5 M potassium ferricyanide and 1 M glucose were prepared in PBS. PQ, pBQ, PD, DCPIP were dissolved in 96 % ethanol. All solutions were stored in a light-proof container at 4°C.

Materials for biofuel cell

Glucose oxidase (β-D-glucose:oxygen 1-oxidoreductase, EC 1.1.3.4) (1572.8 U/mL enzymatic activity, 65.6 U/mg protein, contained 7.67×10^{-5} M of the enzyme) was recovered from cultural liquid after *P. funiculosum* 46.1 [172] fermentation with subsequent concentration and

purification of the enzyme using ultrafiltation complex. Ultrafiltration was performed using combined laboratory unit set designed by “Mifil” (Belarus), which was composed of hollow fiber membrane element and stirred ultrafiltration cell model 8400 from “Amicon” (USA). Hollow fiber membrane was based on aromatic polysulfonate with protected modified surface PS-10M nominal minimal mass retention limit (NMMRL) of 10 kDa. Membrane working surface was 0.2 m^2. Ultrafiltration cell was based on membranes with NMMRL 10 kDa UPM-10, from “Vladipore” (Russia) and 300 kDa PS-300, from “Mifil”, (Belarus).

25% glutaraldehyde and 30% hydrogen peroxide were purchased from AppliChem GmbH (Darmstadt, Germany). Horseradish peroxidase (HRP) (EC 1.11.1.7) of 1000 U/mg enzymatic activity, (for 2,2-azinobis(3-ethylbenzothizoline-6-sulfonic acid (AzBTS)). D-(+)-glucose was obtained from Carl Roth GmbH&Co (Karlsruhe, Germany). When needed, GOx of 4,7 U/mL (amount of enzyme was calculated for each enzyme individually) and HRP of 10 mg/mL solutions were freshly prepared from enzyme slurry in mixed 0.05 mol/L sodium acetate - sodium phosphate buffer, pH 6.0, with 0.1 M KCl (A-PBS).

2.2 Sample preparation

2.2.1 Immobilization of glucose oxidase

A cylindrical poly(methyl methacrylate) (plastic) cell (diameter 55 mm, height 13 mm) was kept in a closed vessel above a 25% glutaraldehyde solution for 10 min to adsorb/graft glutaraldehyde onto the plastic surface. Then surface was prepared depending on required GOx layer. For RC-SECM and GC-SECM mode measurements, 1.6 µL of 10 mg/mL GOx solution was dropped on the surface and it covered 1.13 mm^2 surface area. Then it was dried at room temperature, in order to get 14 µg/mm^2 GOx layer. For SEIM measurements, 6 µL of 40 mg/ml GOx solution were dropped on the surface and dried in room

temperature. For investigation of surfaces of different conductivity, in order to modify the non-conducting surface with aldehyde groups it was kept in a closed vessel over a 25% solution of glutaraldehyde for 10 min. Then 0.1 µL of 20 mg/mL solution of GOx was sprayed to get small drops on the surface and dried at room temperature. The gold surface was modified by GOx using the same sequence of chemical treatments and procedures.

After that, modified surface was kept in a closed vessel over a 25% solution of glutaraldehyde for 10 min at room temperature and then it was washed with buffer.

2.2.2 Preparation and immobilization of cells

Wild type strain of yeast *Saccharomyces cerevisiae* was obtained from Lithuania's Center of Physical Sciences and Technology. The yeast cells were maintained on agar slants containing (g/L): peptone 20, yeast extract 10, glucose 20, and agar 15 at 4 °C. Yeast cultures for the experiment were grown in 10 ml yeast extract peptone dextrose broth in test tubes rotated at 150 rpm for 20-24 h at 28 °C. Cells were then harvested by centrifugation at 3 g for 3 min and later washed 3 times with 0.1 M PBS, pH 6.5. The wet mass of the cell's pellet was weighed and suspended in PBS to a concentration of 0.33 g/mL.

A plastic petri dish, which was made of Poly(methyl methacrylate), was washed with 95 % ethanol solution. Then 0.5 ml of poly-L-lysine 0.01 % solution in water was dropped on the petri dish bottom and the solvent was allowed to dry out. After this the 0.5 µl of the yeast suspension was deposited on the surface modified by poly-L-lysine. The success of immobilization of yeast cells was evaluated by an optical microscope. Cells were immobilized in single 1.5 mm diameter toroid-shaped spot with increased density of the cell at the edges of the toroid.

For AFM measurements, 0.5 µl of the yeast suspension was deposited on the microscope slide. The sample was dried by shaking with MS1 Minishaker (IKA Works Inc, Wilmington, NC).

2.2.3 Preparation of electrodes for biofuel cell

Purification of enzymes

Extracellular GOx of *P. funiculosum* 46.1 was isolated according to the following scheme: Cultural filtrate of the fungus concentrated at hollow fiber membrane unit, the produced concentrate was passed through membrane PS-300 for the removal of high molecular impurities. Specific membrane flow rate was 287.98 $L \times h^{-1} \times m^{-2}$. Then GOx containing permeate was used for subsequent concentration. Separation of reducing substances and concentration of membrane-filtered protein (permeate) was carried out using membrane UPM-10. Specific membrane flow rate was 20.58 $L \times h^{-1} \times m^{-2}$. The pressure of process did not exceed 0.2 MPa, glucose oxidase in permeate was absent. For partial removal of trace proteins the preparations were frozen at –18°C. Total amount of impurity proteins in enzyme concentrate were determined by electrophoresis. Then we determined enzymatic activities of alleged impurity proteins by generally applicable enzymatic activity determination methods [173]. Impurity protein concentration in enzyme preparation was 34 – 38 % of the total protein content. The impurity proteins included some invertase (0.1 – 0.2 U/mL), phenoloxidases (0.004 – 0.006 U/mL), catalase (0.43 U/mL).

Electrode preparation and modification by PD and enzymes

In order to avoid contamination and to obtain a clean electrode surface, shortly before its modification, the surface of GRE was hand-polished with fine emery paper, rinsed with ethanol and distilled water and dried at room temperature. The basic method for rapid and simple preparation of enzyme-modified electrodes was applied [174]. In order to

get graphite electrode (GRE) consequently modified by PD and GOx (GOx/PD/GRE), 3 µL of 10 mM PD solution in ethanol was dropped and distributed on the electrode surface for three times. After each drop, the electrodes were dried at room temperature. The next drop was added just after completely drying the previously added one. Then PD-modified GRE electrodes (PD/GRE) were modified with 3 µL solution containing 4,7 U/mL of GOx and then electrodes were dried at room temperature.

The HRP-modified GRE (HRP/GRE) was prepared by a similar procedure just in the absence of PD. For this aim, after the cleaning procedure, the electrode surface was treated by 3 µL of 10 mg/mL HRP solution for three times. After each drop, the electrode was dried at room temperature. The next drop was added just after completely drying the previously added one.

All modified electrodes were stored for 20 hours over the 5% solution of glutaraldehyde at +4ºC in a closed vessel to cross-link enzymes adsorbed on the electrode. Prior to electrochemical measurements the modified electrodes were thoroughly rinsed with distilled water to remove non-cross-linked enzyme, then electrodes were dried and the lateral surface of the electrode was isolated with a silicone tube. Prepared electrodes were kept in a closed vessel over A-PBS buffer, pH 6.0, at +4°C until they were used in experiments.

2.3 Instrumentation

2.3.1 Scanning Electrochemical Microscopy

SECM and disk-shaped Pt UME with radius of 10 µm from Sensolytics (Bochum, Germany) and disk-shaped home-made Pt microelectrode (ME) based probe with radius of 100 µm were used for experiments. Before all measurements the UME was washed with 95 % ethanol solution and it was polished with polishing paper with grain size

of 0.3 µm and then the UME/ME was washed with buffer. The electrode quality was checked by cyclic voltammograms. Three electrode based electrochemical setup was applied, in this setup the UME/ME-based scanning probe was switched as a working electrode, Pt electrode – as a counter electrode and Ag/AgCl in 3M KCl – as a reference electrode.

Measurements in RC-SECM and GC-SECM modes

SECM measurements were performed in both RC-SECM and GC-SECM modes in buffer without mediator. First, the UME was moved with 1 µm s^{-1} speed in vertical direction until it touched the unmodified plastic surface to determine distance. Second, the UME was retracted out to required distance from the surface of interest, and the UME was approaching the GOx-modified or cells surface. All measurements were performed in phosphate-acetate buffer, pH 6.6. Each measurement was repeated for three times at different locations of enzyme modified surface, and the mean value of these measurements was used for further calculations and evaluations.

Impedance measurements

Scanning electrochemical microscope from Sensolytics (Bochum, Germany) was used for all experiments. The working electrode (WE) was situated as a SECM probe, which was approaching the substrate that was immersed in 0.1 M glucose solution in deionized water. Platinum wire was used as a counter/reference electrode (CE/RE). EIS measurements were performed in the range of frequencies from 100 kHz to 20 mHz with sinusoidal current of 5 mV of root mean square (RMS) amplitude in every step; the UME to the GOx-modified surface from 1.5 mm to 50 µm was approached stepwise, each step was of 250 µm. The speed of UME movement from one step to another was applied as 1 µm/s. The EIS measurements to acquire dependence of solution resistance on gluconic acid concentration were performed at constant

distance. Gluconic acid concentration was changed from 0.01 to 0.45 mmol/L and EIS measurements were performed in the same range of frequencies.

Measurements of living cells

Horizontal scans at GC-SECM mode at +400 mV *vs* $Ag/AgCl_{(3M\ KCl)}$ were performed. In order to determine an optimal concentration of PQ, 0.6 mM of potassium ferricyanide and 60 mM of glucose were added to the buffer solution. Then PQ concentration was changed from 0 until 0.25 mM, and horizontal scan was performed at each concentration. In order to determine an optimal potassium ferricyanide concentration, 0.04 mM of PQ and 60 mM of glucose were added to the buffer solution. Then potassium ferricyanide concentration was changed from 0.1 until 1 mM, and horizontal scan was performed at each of concentration. UME current dependence on time was registered by horizontal scanning (at scan rate of 20 μm/s) every 2 minutes after the addition of 60 mM of glucose to the buffer, pH 6.7, containing 0.6 mM of potassium ferricyanide and 0.04 mM of PQ. The UME current dependence on glucose concentration was registered by horizontal scanning after 18 min after the addition of glucose and initiation of metabolic reactions. Measurements were performed in buffer, pH 6.7, with 0.6 mM of potassium ferricyanide, 0 to 65.4 of glucose mM and 0.04 mM of PQ. SECM imaging was performed by scanning at the distance of 20 μm, in the presence of 0.6 mM of potassium ferricyanide, 0.04 mM of PQ, and 60 mM of glucose in buffer, pH 6.7.

Chronoamperometric measurements

Chronoamperometric measurements of not immobilized cells *Saccharomyces cerevisiae* were made by SECM UME-based probe using electrochemical cell mentioned above. Concentration of yeast cells dissolved in PBS, pH 6.5, was 6.7 mg/mL. Potassium ferricyanide was

used as a first redox mediator, PQ, pBQ, PD or DCPIP were used as second redox mediators.

2.3.2 AFM measurements

The AFM measurements were performed in air at contact mode using Veeco Bioscope II Atomic Force Microscope. The silicon nitride probes of NP series (Veeco MLTC) with the triangular cantilever of the spring constant below 0.1 N/m with the four-sided pyramidal tip from 20 to 60 nm radius were used for this experiment.

2.3.3 Electrochemical measurements

Electrochemical measurements were performed using an Autolab PGSTAT 30 Potentiostat/Galvanostat (Utrecht, Netherlands), and GPES software Eco Chemie (Utrecht, Netherlands). All experiments were carried out inside a Faraday-cage at ambient temperature (at 20^{o}C), while stirring in A-PBS, pH 6.0, under aerobic conditions. Graphite rod electrodes (GRE) (99.999 %, low density, 0.3 cm diameter with active surface area of 0.071 cm^{2}) were purchased from Sigma-Aldrich (Berlin, Germany) and used in design of GOx/PD/GRE and HRP/GRE electrodes.

Evaluation of GOx/PD/GRE and HRP/GRE electrode based biofuel cell was performed in two electrode mode, where GOx/PD/GRE and HRP/GRE electrodes were placed in different compartments, which were switched by electrolyte switch filled by A-PBS, pH 6.0, with 0.1 M KCl; 0 – 200 mM of glucose and 0.1 – 0.5 mM of H_2O_2 were added respectively into each compartment.

During some voltage measurements the external resistances (2 MΩ, 1 MΩ, 515 KΩ, 200 KΩ, 94 KΩ, 47 KΩ, 12 KΩ, 9.9 KΩ, 5 KΩ, 1 KΩ) were plugged in parallel to galvanostat to imitate the ‘work-load’ in electrical circuit for the assessment of power density of the complete

BFC. All potentiometric experiments were performed at room temperature while stirring in A-PBS, pH 6.0, under aerobic conditions.

Amperometric measurements

Amperometric measurements were performed in three electrode mode where Pt electrode with the electrochemically active area of 0.05 cm^2 was used as counter-electrode; Ag/AgCl electrode in saturated KCl ($Ag/AgCl/KCl_{sat}$) was used as a reference electrode. Dependence of GOx/PD/GRE generated anodic current on glucose concentration was studied at +150 mV *vs* $Ag/AgCl/KCl_{sat}$, while dependences of HRP/GRE generated cathodic current on hydrogen peroxide concentration were studied at –200 mV *vs* $Ag/AgCl/KCl_{sat}$ respectively.

Storage stability of potential and power of BFC at 1st, 2nd, 4th, 7th, 9th and 12th day were examined in two electrode mode by measuring of BFC potential at switched 'work-load' imitating resistance of 2 MΩ.

2.4 Calculations

2.4.1 Reaction kinetics

The steady-state diffusion-controlled current is related to the detectable material concentration when the UME-based probe is far from the surface [13]:

$$i_{T,\infty} = 4nFDCa \qquad (1)$$

where n is the number of electrons, which are involved in to the reaction, F is Faraday constant (9.65 10^4 C/mol), D diffusion coefficient, C is concentration of detectable material, and a is radius of the UME.

UME-based probe current was measured in GC-SECM mode when the UME was positioned over the center of enzyme-based spot, which was deposited on the surface of substrate, was calculated using assumptions presented by Saito [175]:

$$i_T = 4nFDC_s a \frac{2}{\pi} arctan \frac{r}{d} \quad (2)$$

where C_s is concentration of oxygen at the enzyme-modified spot, r is the radius of the enzyme-modified spot; d is the vertical working distance (measured in z direction).

The reactant/product consumption/generation rate (f) expressed in mol×cm^{-2}×s^{-1} was calculated using assumptions from [176]:

$$f = \frac{4DC_S}{\pi r} \quad (3)$$

The parameter f is the heterogeneous reaction rate for the formation of product per unit of time and at particular geometrical area; it characterizes the effectiveness of enzymatic reaction.

At steady-state conditions the heterogeneous reaction rate is expressed as [176]:

$$f = \frac{k_{cat}\Gamma_{enz}[S]}{K_{M(app.)}+[S]} \quad (4)$$

where f is the heterogeneous reaction rate for the formation of product (mol×cm^{-2}×s^{-1}); k_{cat} is enzyme turnover number; Γ_{enz} is the enzyme surface concentration (amount of enzyme per unit of geometric surface area); [S] is the concentration of substrate at the surface of the spot; $K_{M(app.)}$ is the apparent Michaelis constant.

From equations (2,3 and 4) the equation were derived:

$$K_{M(app.)} = \frac{8n\ F\ a\ D\ C_S\ [S]}{\pi\ i_T}\ arctan\left(\frac{r}{d}\right) - [S] \quad (5)$$

The equation (5) is suitable for the determination of apparent Michaelis constant ($K_{M(app.)}$). The $K_{M(app.)}$ was calculated by equation 5-2 using currents, which were registered during RC-SECM mode based measurements at 82.6 mM of glucose concentration and at 90 µm distance of UME from GOx-modified surface. Then we have fitted current

vs glucose concentration dependencies with theoretical results calculated using modified Michaelis-Menten equation:

$$i_T = \frac{i_{max}[S]}{K_{M(app.)} + [S]} \quad (6)$$

where i_{max} is maximal steady-state current, which is the function of maximal reaction rate, which is used as a parameter of standard Michaelis-Menten equation.

For initial evaluation and characterization of UME, theoretical curve of negative feedback, which was developed by Cornut and Lefrou [56] was applied:

$$\frac{i_T}{i_{T,\infty}} = \frac{A_1 L + A_2}{A_1 L + A_3 + \frac{LnR_g}{L} + \frac{2}{\pi R_g} + Ln\left(1 + \frac{\pi R_g}{2L}\right)} \quad (7)$$

Where L = d/a, A1, A2, A3 are fitting coefficients.

2.4.2 Electrochemical impedance

The mathematical impedance dependence, according to a simplified equivalent circuit, is expressed as:

$$Z = \frac{Z_{Cdl} \cdot (R_{ct} + W)}{Z_{Cdl} + (R_{ct} + W)} + R_s \quad (8)$$

where Z_{Cdl} is double-layer impedance (Eq. 9), R_{ct} – charge-transfer resistance, W – Warburg impedance (Eq. 10), and R_s is ohmic resistance of solution.

Double layer impedance is expressed as a constant-phase element:

$$Z_{Cdl} = \frac{1}{Q\,(j\omega)^{\alpha}} \quad (9)$$

where Q – the capacitance, j – imaginary unit, ω – angular frequency, α – empirical constant.

Infinite diffusion Warburg impedance was calculated as:

$$Z_W = \frac{1}{\sigma\sqrt{j\omega}} \qquad (10)$$

where σ – Warburg capacitance, j – imaginary unit, ω – angular frequency [177].

Solution resistance between the UME and counter electrodes was uncompensated. Over the course of time and within distance from the GOx-modified surface only concentrations of formed reaction products are varying in our system. Out of all in GOx-catalysed reaction formed products only gluconic acid tends to dissociate, therefore the concentration of gluconic acid mostly affects the conductivity of the solution and therefore changes of calculated R_S are mainly related to the variation of gluconic acid concentration.

2.4.3 Living cells

Current *vs* glucose concentration dependence was fitted to theoretical results calculated using general model, which is suitable for the description of chemical reactions between two compounds, which are forming an intermediate complex:

$$S + X \underset{k_{-1}}{\overset{k_1}{\rightleftarrows}} SX \overset{k_2}{\rightarrow} P \qquad (11)$$

where S is a substrate (glucose, PQ or potassium ferricyanide) the concentration of which was changed during particular experiment, X – the other compound, which interacted with the substrate of interest, SX – intermediate complex consisting of compounds S and X, P – product/products formed when the complex SX is dissociating.

The simplified model of two compound based reaction that was evaluated by ‘steady state approximation’ in a way, which is similar to that, which by Michaelis-Menten was adapted for enzymatic catalysis:

$$i_T = \frac{i_{max}[S]}{K_{SX} + [S]} \qquad (12)$$

where i_{max} is maximal steady-state current, which is a function of maximal reaction rate. [*S*] is the concentration of selected substrate (glucose, PQ or potassium ferricyanide) in solution; K_{SX} is the constant, which is showing the ratio of decay/increase of complex SX concentration (the meaning of this constant is similar to that of Michaelis constant, which is often used in enzymatic catalysis):

$$K_{SX} = \frac{k_{-1} + k_2}{k_1} \qquad (13)$$

where k_1, k_{-1} and k_2 are reaction rate constants of processes, which are presented in equation 11.

Hill equation, which was used for approximation of the current:

$$i = bkx^n/(1 + kx^n) = i_{max}\ x^n/(1/k + x^n) \qquad (14)$$

where: *b* – level of maximal 'saturation', or in our case it corresponds to the maximal current value (i_{max},) *k* – equilibrium constant of the reaction, n – Hill number, *x* – concentration of ligand, or in our case it corresponds to the concentration of chemicals, which is involved in cells metabolic reactions.

The change of registered current in time is affected by varying concentration of chemical compounds, which are affecting electrochemical signal. The dependence of current on the concentration of substrate (in this particular case it was glucose) could be rewritten taking into account the dependence of current on time. Therefore, for the evaluation of yeast cell viability, Hill's equation was modified is such a way:

$$i = i_{max} \cdot t^n/(k_M^n + t^n) \qquad (15)$$

where t – time, k_M – corresponds to the time at which half of maximal current is registered; according to a physical meaning the k_M is

similar to apparent Michaelis constant, which is often used in basic enzymatic catalysis described by Michaelis-Menten kinetics.

Ferrocyanide concentration is related to the UME current, and can be calculated using equation 1. The steady-state diffusion-controlled current is related to the initial ferrocyanide concentration when the UME-based probe is still relatively far from the surface.

2.4.4 Electric power of fuel cell

Calculation of electric power (*P*) of fuel cell was performed according this principle:

P = work done per unit of time = $U \times Q/t$; *and* Q/t=I

where U is electric potential or voltage in volts; *Q* is electric charge in coulombs; *t* is time in seconds; *I* is electric current in amperes;

Therefore:

$P = I \times U$; and I=U/R; (Ohm's law)

Therefore:

$P = U^2/R$;

U was determined from experimental results, while *R* was adjusted manually by switching fixed external resistances of 2 MΩ, 1 MΩ, 515 KΩ, 200 KΩ, 94 KΩ, 47 KΩ, 12 KΩ, 9.9 KΩ, 5 KΩ, 1 KΩ between the electrodes.

3 Results and discussion

3.1 Registration of approach curves in RC-SECM mode

The processes, which occur on the UME and GOx-modified surfaces, in RC-SECM mode when negative potential is applied to the UME, are revealed in Fig. 3.1. In the solution without any redox mediator the reduction of dissolved O_2 occurs on the UME, and additionally the O_2 is consumed by GOx catalysed reaction. Therefore the O_2 reduction based UME current decreases when the UME is approaching to the surface. However, in this case another factor such as blocked diffusion of O_2 to UME also has significant influence for the measurement of current *vs* distance.

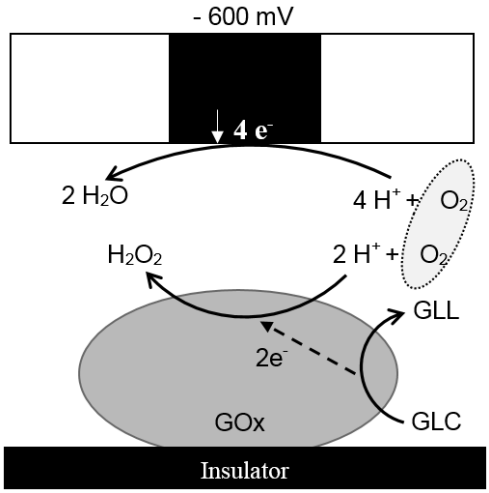

Fig. 3.1. Schematics of processes occurring during SECM measurements on both GOx-modified and UME surfaces in RC-SECM mode without any redox mediator. In this scheme gluconolactone is abbreviated as GLL, and glucose as GLC.

In order to determine the distance of UME from surface, the O_2 reduction current is usually measured while approaching electrode to the insulating surface [34]. The current *vs* distance dependence was registered in buffer, while applying -600 mV *vs* Ag/AgCl potential and approaching unmodified plastic surface (Fig. 3.2, buffer). Further

measurements by adding glucose to solution were performed in the same fixed x-y position, therefore results of SECM measurements were always mostly affected by two factors: (i) the hindered diffusion when the UME appears close to surface of interest and (ii) the consumption of O_2 by GOx catalysed reaction.

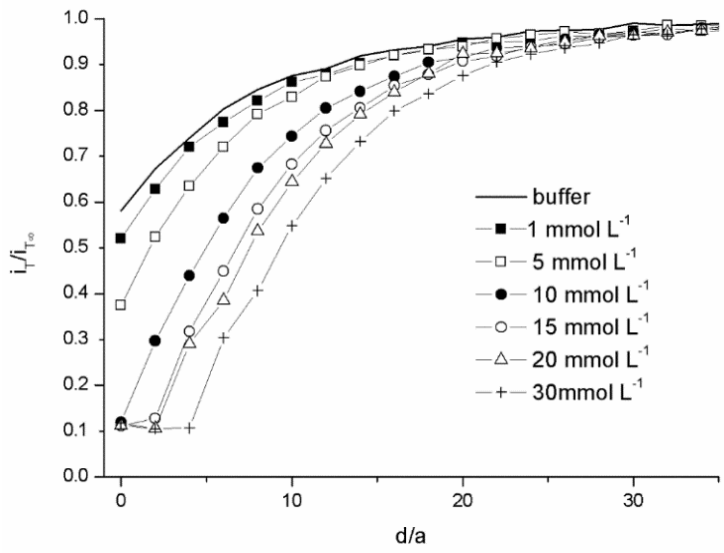

Fig. 3.2. Normalized current dependence on normalized distance at different glucose concentrations in buffer, at UME potential of –600 mV *vs* Ag/AgCl.

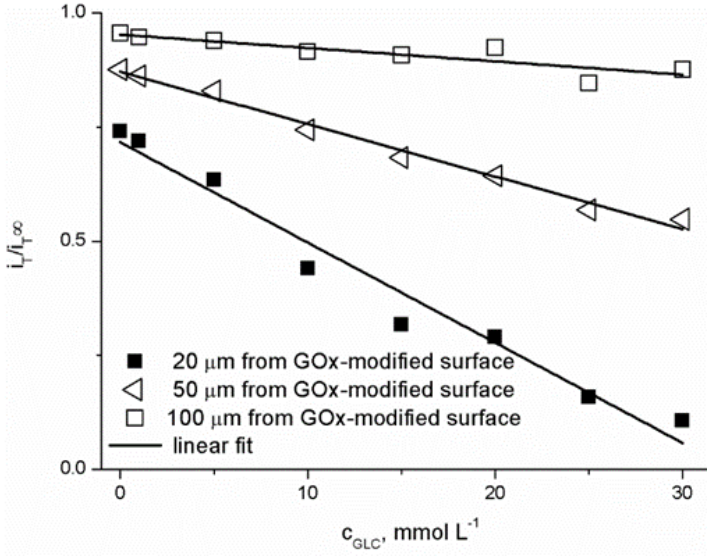

Fig. 3.3. Normalized current dependence on glucose concentration in buffer without any redox mediator, at UME potential of –600 mV *vs* Ag/AgCl.

Current *vs* distance dependences were registered in RC-SECM mode at different concentrations of glucose, in order to find which factor

has more significant influence on the current signal. Fig. 3.2 shows the O_2 reduction current dependence at initial glucose concentration. Approximately 250 μM of O_2 is initially present in the solution, which is exposed to air, and this dissolved O_2 is responsible for the generation of the UME background current in RC-SECM mode. In order to avoid current shielding effects, we compared currents, which are normalized by steady-state current. Since the O_2 is consumed in the enzymatic reaction, the addition of glucose to the solution facilitates the enzymatic reaction. The consumption of O_2 is registered when glucose is added to the solution: current decreases faster, comparing to measurements in the absence of glucose. If the decrease of current would be mostly related to the hindered diffusion, the character of current *vs* distance dependence should be the same. But results show that the layer of consumed O_2 is increasing by consecutive addition of glucose to solution. Hence, the most significant influence to the change of the current has O_2 concentration, but not blocked diffusion. Another evidence for this fact is that the current remains at the same level ($i_T/i_{T,\infty} = 0.1$) if glucose concentration is in the range from 10 mM to 30 mM and UME is at close distance (from 0 to 4 d/a) from surface of interest. In this case the layer, which contains lower concentration of O_2, is thicker due to much faster O_2 consumption. The dependence of O_2 consumption on glucose concentration at different distances from the GOx-modified surface is linear (Fig. 3.3). At closer distances the current decreases by 25–100% what is clear evidence of O_2 consumption.

3.2 GC-SECM mode based measurements

In the GC mode (Fig. 3.4), the H_2O_2 oxidation current on UME was registered. The highest concentration of H_2O_2, which is formed during GOx catalysed reaction, is close to the GOx-modified surface. Therefore the current of UME is significantly increasing when approaching to the

surface modified by GOx and this increase of UME current is related to the rate of enzymatic reaction.

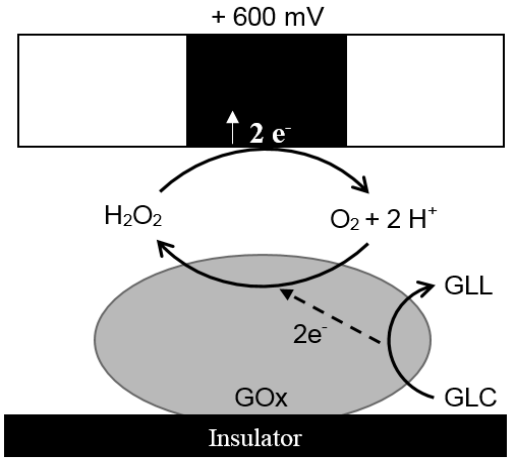

Fig. 3.4. Schematics of SECM processes occurring on GOx-modified and UME surfaces in GC mode without any redox mediator. In this scheme gluconolactone is abbreviated as GLL, and glucose as GLC.

The H_2O_2 concentration profile (Fig. 3.5) was determined by registration of current *vs* distance dependence. However, the estimation of registered current *vs* distance dependence at GC mode has some disadvantages: (i) the dependence of current *vs* distance is changing over the time, because the enzyme is continuously consuming both substrates (glucose and O_2) and the concentrations of products (H_2O_2 and gluconolactone) in solution are increasing within course of the reaction; (ii) the current increases by approaching the surface modified by GOx only at within certain distance range, at which the hindered diffusion effect still does not take place; (iii) from current *vs* distance dependence curves it is not possible to estimate exact distance of UME from the surface, therefore by approaching the surface of interest the UME could be crashed or sample could be damaged by UME. To avoid these negative effects, the measurement was performed immediately after the addition of glucose, and distance of measurement was chosen from negative feedback dependence of current *vs* distance, measured while approaching plastic surface at -600 mV (Fig. 3.2, in buffer). The measurement of GC current *vs* distance dependence was started at

1 mm distance between UME and surface. It was determined that the current in GC mode is decreasing more slowly, when the UME is approaching the surface of interest, comparing to that in RC-SECM mode. This phenomenon can be explained as follows: H_2O_2 diffusion from the GOx-modified surface is fast, therefore the increase in current comparing to the measurement without any glucose can be observed even at 1 mm distance. However, the concentration of H_2O_2 is highest at closest point, and this can be related to continuously proceeding enzymatic reaction, which is producing the H_2O_2. Here, the effect of hindered diffusion is not seen, because the measurement distance was calculated from negative feedback measurement carefully to avoid sample damage. Thus, both modes are important for the determination of the most suitable distance for the imaging. The distance of 40 μm was chosen from both approaching curves (Fig. 3.2, in buffer and Fig. 3.5), because: i) the current related to O_2 reduction at the UME is at 0.85 of normalized steady-state value (applied potential was -600 mV *vs* Ag/AgCl); ii) the current related to H_2O_2 concentration is at maximal value (applied potential was +600 mV *vs* Ag/AgCl).

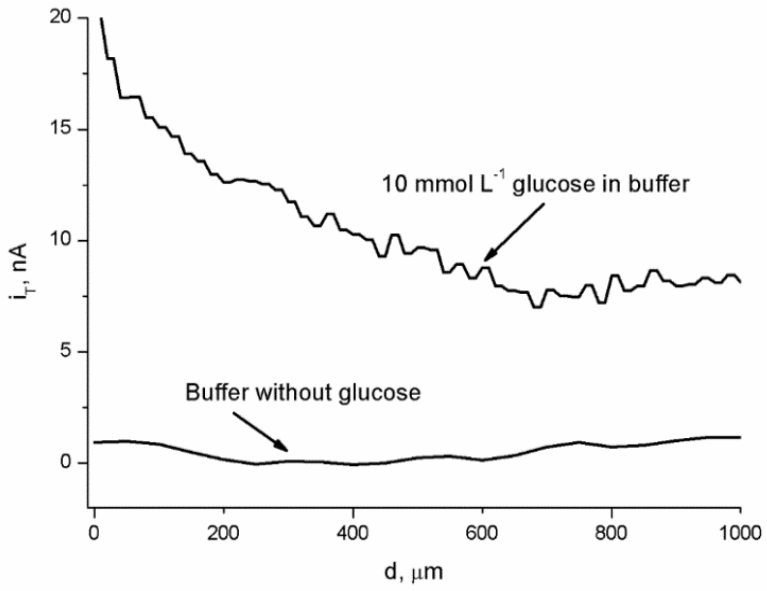

Fig. 3.5. Current *vs* distance curves registered while approaching the GOx-modified surface in the presence and absence of glucose. UME potential was +600 mV *vs* Ag/AgCl.

The similar results were obtained inside biosensor, based on GOx [178]. Authors of this research found that the distance is the same for maximal current while measuring H_2O_2 concentration by GC-SECM mode and for change of maximal current while measuring O_2 concentration by RC-SECM mode.

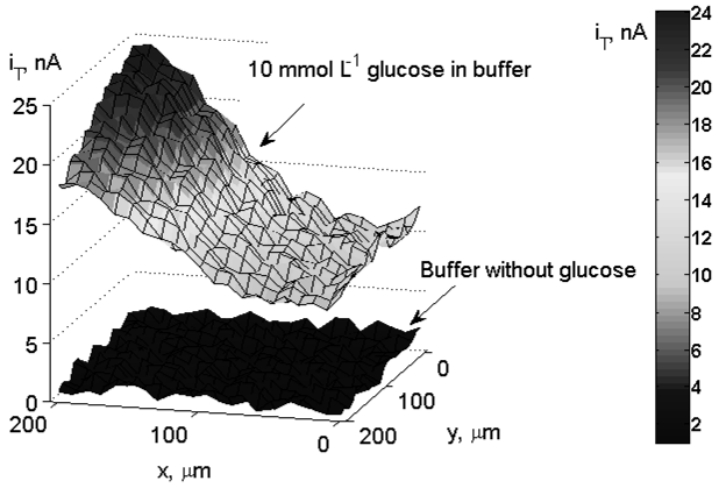

Fig. 3.6. UME current registered at the interphase between the GOx-modified and not modified surfaces in the presence and absence of glucose in buffer; the UME was operating in GC mode at +600 mV *vs* Ag/AgCl potential at 40 μm (d/a=8) distance.

These conditions allow to scan at the distance at which the hindered diffusion still does not take place – the current related to O_2 reduction at the UME (Fig. 3.2, in buffer) in this distance does not differs by more than 20 % from the steady-state value. On the other hand, the H_2O_2 concentration is at maximal level (Fig. 3.5) therefore it allows to perform the measurements at highest resolution.

The horizontal scanning, which was performed at constant 40 μm (d/a=8) from GOx-modified surface, is illustrating that the UME current in the absence of glucose is low (0-3 nA), and the UME current increases up to 24 nA in the presence of 10 mM of glucose (Fig. 3.6). The imaging was performed immediately after the addition of glucose, however the diffusion of H_2O_2 from GOx-modified surface is very fast and the current after addition of glucose increases not only in close proximity to the GOx-modified spot of surface (24 nA, x-coordinate from 100 to 200 μm), but

also in surrounding area (9 nA, x-coordinate from 0 to 100 μm). At the same time in current *vs* distance curve (Fig. 3.5) the current changes from 8 nA if UME is far (600-1000 μm) from GOx-modified surface to 20 nA close (20 μm) to GOx-modified surface. Tendencies in current changes of approaching curve (Fig. 2) and 3D images of UME current registered at the interphase between the GOx-modified and not modified surfaces (Fig. 3.5) are very similar, what is an evidence that appropriate distance was chosen for the imaging.

3.3 Evaluation of kinetics

3.3.1 Evaluation of distribution of immobilized glucose oxidase on surfaces of different conductivity

AFM images of non-modified and GOx-modified surfaces are presented in figure 3.7. The spots of GOx, which was of 1 mm diameter, were formed on both conducting and non-conducting surfaces. It was determined that the roughness of GOx layer on plastic was 4.5 times higher than that formed on gold surface. Measured Root Mean Square (RMS) value of plastic surface is 4 nm, while the RMS of the same plastic with immobilized GOx is 84 nm. The RMS of gold surface was 25 nm, while the RMS of the same gold surface with immobilized GOx was 386 nm. However GOx features formed on non-conducting plastic surface are denser and smaller than that for the GOx immobilized on the gold surface.

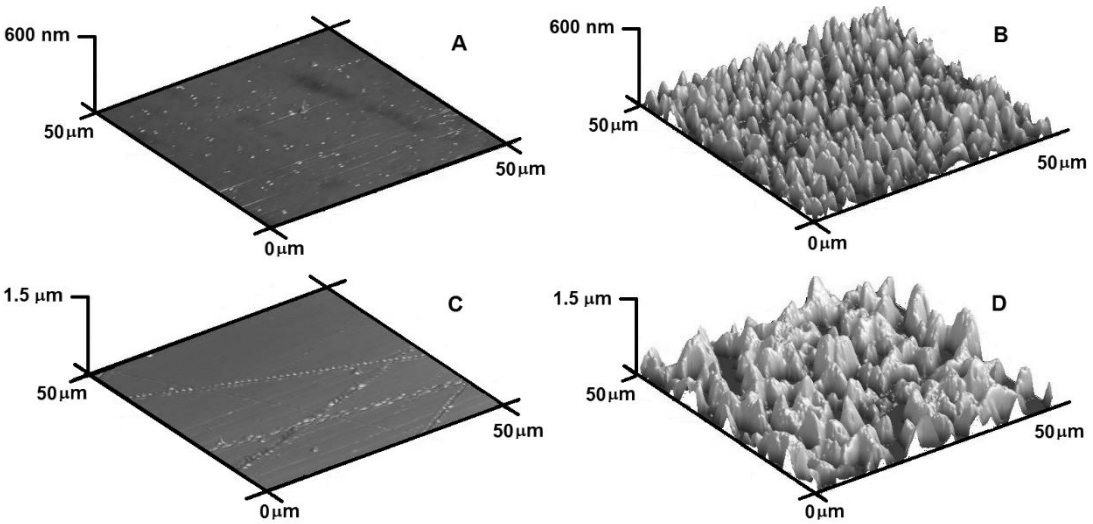

Fig. 3.7. AFM measurements of surfaces before and after enzyme immobilization: **A** – bare non-conducting plastic surface, **B** – non-conducting plastic surface modified by GOx, **C** – gold surface, **D** – gold surface modified by GOx. Evaluation of immobilized glucose oxidase kinetics at redox competition mode

3.3.2 Application of RC-SECM mode for determination of enzymatic kinetics

The RC-SECM mode can be applied for the determination of enzymatic kinetics. For such investigations, the rate of oxygen consumption on ME should be significantly lower than that on enzyme-modified surface in order to avoid the distortion of results [30]. In some particular cases at RC-SECM mode the oxygen consumption rates on the ME and on enzyme-modified surface are evaluated separately. Similar approach has been applied for the investigation of living cell respiration rate [30]. Oxygen consumption at the polarized ME was found by several orders of magnitude larger than the consumption of oxygen at individual living cells. There are three the most common ways to slow down the oxygen reduction rate on the ME: i) to decrease ME voltage *vs* reference electrode; ii) to apply ME of smaller radius; ii) to apply shorter potential pulses in order to avoid expansion of the diffusion zone and to reduce Faradaic currents of ME [30]. Schuhmann's group has reported that the local concentration of O_2 in the gap between ME, which was applied as SECM probe, and sample could be increased in comparison with that in the rest of the solution, when repetitive potential pulses with

the potential, which is sufficient to oxidize the hydroxyl ions (OH^-) into H_2O and O_2, are applied to the ME before the determination of O_2 reduction activity (Eq. 17) [179]. In this way, constant O_2 concentration could be generated in ME environment, when the ME-based probe is moving across the sample. In our research, the ME-based probe was moved in z-direction, and therefore O_2 concentration profile was determined by the distance between the ME-based probe and the sample. In such measurements O_2 concentration is varying along z-axis.

$$4OH^- \rightarrow 2H_2O + O_2 + 4e^- \quad (16)$$

Glucose oxidation in the presence of dissolved O_2 is catalysed by GOx, hydrogen peroxide and gluconolactone are produced according to equation (18). The ME-current value depends on the concentration of electrochemically active species close to the ME surface and on the potential applied to ME. In here evaluated RC-SECM measurement system (Fig. 3.8), the oxygen is consumed: (i) in the redox reaction occurring on ME surface (Equation 19), and (ii) in enzymatic reaction where oxygen serves as an electron acceptor, which is taking electrons from GOx (Equation 18).

$$GLC + O_2 + 2\,e^- + 2\,H^+ \xrightarrow{GOx} GLL + H_2O_2 \quad (17)$$

where GLC is glucose, GLL is gluconolactone.

$$O_2 + 4\,e^- + 4\,H^+ \rightarrow 2H_2O \quad (18)$$

The redox competition mode was used in order to measure O_2 reduction current, by applying negative potential of -750 mV to ME. The O_2 is reduced to water on the ME, according to the reaction, which is presented in equation (19). The GOx was immobilized on non-conducting (plastic) and conducting (gold) surfaces and current *vs* distance dependence measurements were performed in the buffer solution at glucose concentration ranging from 0 to 82.6 mM (Fig. 3.9).

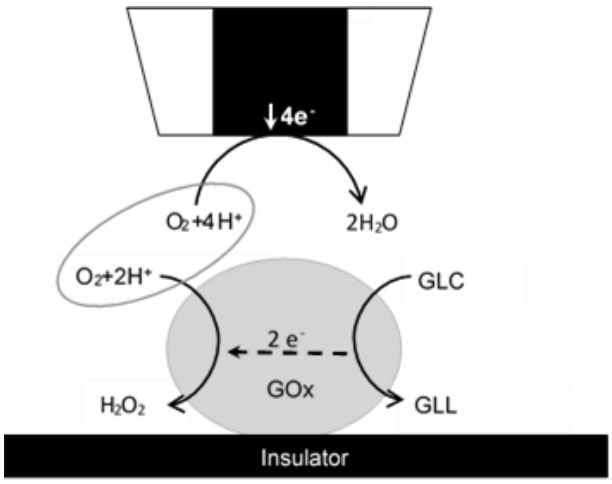

Fig. 3.8. Schematics of redox competition mode based SECM measurement. At -750 mV potential the oxygen on the ME surface is converted to H_2O. Oxygen is consumed in two ways: (i) in electrochemical reaction at ME surface and (ii) by GOx catalysed reaction. GLC – glucose, GLL – gluconolactone. The same process takes place when the GOx is immobilized on conducting surface.

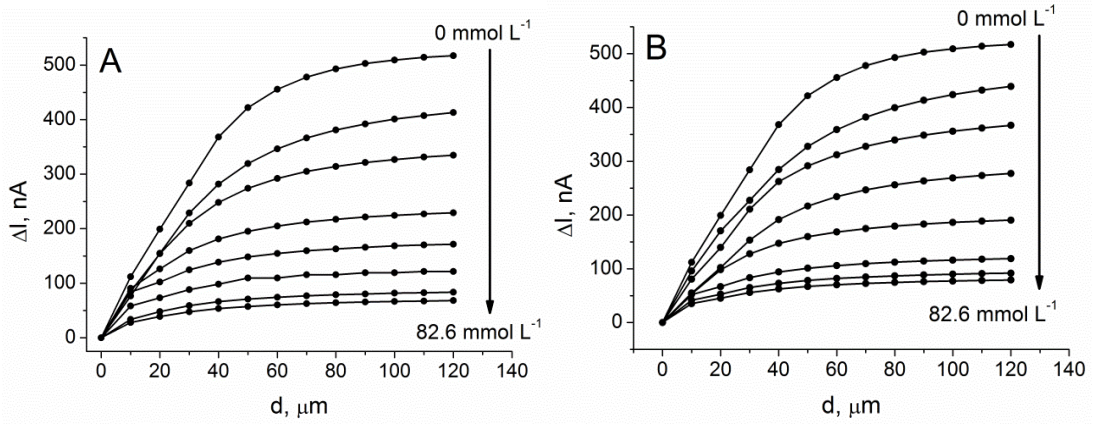

Fig. 3.9. Current *vs* distance dependencies registered when approaching the ME-based probe, to: **A** – non-conducting (plastic) surface modified with GOx; **B** – conducting (gold) surface modified with GOx. Measurements were performed in 0.1 M phosphate-acetate buffer containing 0-82.6 mM of glucose.

At 'zero distance' between ME-based probe and sample (when electrode was touching enzyme-modified surface) registered current (ΔI) was accounted as 'zero current'. Real current value registered at the 'zero distance' was subtracted from all other values presented in plot (Fig 3.9), which are representing dependence of ΔI *vs* distance between ME and enzyme-modified surface. The highest changes in current were observed at lower glucose concentrations. If the measurement was performed in buffer solution without glucose, current change was 500 nA, while for 82.6 mM of glucose the current change was only 40 nA at the

120 μm distance from the surface. The measurement in the absence of glucose shows only the effect of hindered diffusion because in this case O_2 concentration is the same in all solution. After the addition of glucose the ME current is decreasing due to O_2 consumption on the GOx-modified surface. The measurements of current *vs* distance dependencies showed similar results on both conducting and non-conducting surfaces (Fig. 3.9). This phenomena was also observed by other authors, when measurements close to conducting and non-conducting surfaces were performed in the presence and in the absence of redox mediator [19]. When concentration of oxygen was measured at negative ME potential, then no positive feedback was observed in the system, because in this case oxygen cannot be regenerated at gold surface. Therefore, we did not expected any increase of current when ME was approaching to the conducting surface. The decrease of current when ME was approaching the GOx-modified surface is mostly related to two phenomena: i) O_2 consumption by ME at negative potential and by GOx-modified surface; ii) hindered diffusion determined by insulating layer of ME, which is well described by negative FB-SECM theory [56]. However, this theory can be applied only if concentration of O_2 is similar in all bulk solutions, and then the decrease of current in close proximity to the surface of the sample is mainly related to ME geometry and thickness of insulator layer, which is surrounding conducting part of the ME-based probe. In addition to mentioned factors in our system, the O_2 concentration between ME-based probe and the GOx-modified surface depends: (i) on the distance between ME-based probe and sample and (ii) on glucose concentration, which affects GOx catalysed reaction rate. It should be noted that the diffusion limited current (at 100-60 μm distance) after the addition of glucose to the solution, also changes and it is different in comparison with the current observed in buffer without any glucose. Therefore, it is complicated to determine exact influence of hindered diffusion when the concentration of glucose is varying in large

concentration diapason. Because at the lowest concentration of glucose the hindered diffusion of O_2 towards ME-based probe is observed at 60-70 μm distance, while at high concentrations of glucose the hindered diffusion of O_2 is observed at 10 μm distance (Fig. 3.9). However, for the determination of distance, where hindered diffusion is observed, we can apply only the measurements at negative feedback at conditions when the measurement is performed in the buffer without any glucose. From this measurement it can be concluded that hindered diffusion at ME-based probe, which consist of 100 μm radius platinum wire wrapped within 380 μm radius insulating glass is observed at distances lower than 60 μm from surface. Therefore, at lower than 60 μm distances of ME-based probe from the surface the hindered diffusion should be taken into account.

Very interesting finding is that the current has decreased not only when ME-based probe was positioned close to modified surface, but also when ME-based probe was relatively far from modified surface where hindered diffusion does not take place. This phenomena is similar to that observed in GC-SECM mode [178], therefore, the calculations of enzymatic kinetics can be performed using the theory of GC-SECM. However, for these calculations the distance should be chosen taking into account results of measurement, which were performed without any glucose because by this experiment the distance, at which hindered diffusion do not have any effect, could be clearly identified. The distance for GC-SECM mode calculations should be chosen at diffusion-limited zone, where the ME current is the highest [176].

Another method for the determination of enzymatic kinetics by SECM is based on the determination of dependence of current *vs* concentration, which was fitted by Michaelis-Menten equation (Equation 6) [180-183]. From current *vs* distance dependencies, which were measured at different glucose concentrations (Fig. 3.9), we have

deducted current *vs* concentration dependencies (Fig. 3.10). The highest current change was registered at larger distances of ME-based probe from the sample; for example, at 100 μm distance the ME current change was 500 nA, and at 10 μm distance current change was 40 nA. This effect is related to hindered diffusion, because at closer distances this phenomenon has more influence to measured result. Also close to GOx-modified surface the concentration of O_2 is significantly lower due to consumption of O_2 by GOx.

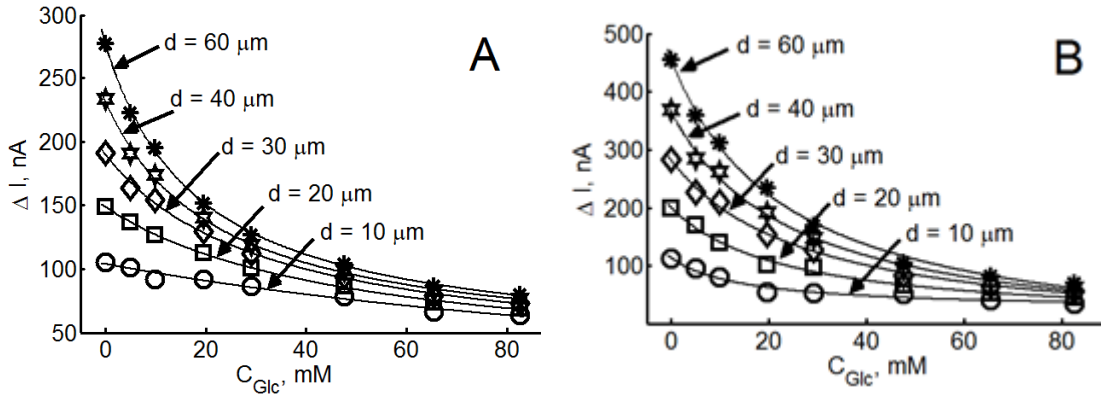

Fig. 3.10. The dependence of O_2 reduction current on glucose concentration: **A –** GOx immobilized on non-conducting (plastic) surface, and **B –** GOx immobilized on conducting (gold) surface. Lines are approximated according to Michaelis-Menten kinetics.

We have applied Michaelis-Menten kinetics (Eq. 6) for the fitting of current *vs* concentration dependencies in order to calculate $K_{M(app.)}$ (Fig. 3.11). Theoretically the $K_{M(app.)}$ value for GOx-based layer should be constant; using SECM, analytical equation suitable for the calculation of $K_{M(app.)}$ value using current *vs* distance data, which are measured at positive feedback mode using redox mediator, was reported earlier [184]. But differently from this report we have not used any redox mediators in order to avoid the effect of positive feedback on conducting (gold) surface, which can influence the ME response [19, 59]. Since we used RC-SECM mode without any redox mediator (except dissolved oxygen, which was serving as oxidator for reduced form of GOx), we have observed different $K_{M(app.)}$ values, which were dependent on the distance

of ME-based probe from the sample (Fig. 3.11). Such differences in $K_{M(app.)}$ values can be explained in the following way: in our measurement system the ME-based probe is always at some distance from enzyme-modified surface, and the solution, which is present between GOx-based sample and ME-based probe, is acting as diffusional layer trough which dissolved oxygen is diffusing. Therefore, if standard method which is suitable for the calculation of Michaelis constant is applied, the dependence of $K_{M(app.)}$ value on the distance of ME-based probe from enzyme-based layer could be determined.

Curves, which are characterizing the $K_{M(app.)}$ *vs* distance between ME and GOx-modified surface in both experimental cases (when GOx was immobilized on (i) non-conducting (plastic) or (ii) conducting (gold) surface) have similar dependencies (Fig. 3.11 A). The $K_{M(app.)}$ value remains the same within the distances in the range of 100-60 μm where hindered diffusion does not take place. At the distances ranging from 60 μm to 20 μm the $K_{M(app.)}$ value increases together with the distance when the GOx is immobilized on non-conducting (plastic) surface, and in the distance from 60 μm to 30 μm the $K_{M(app.)}$ value increases with the distance when GOx is immobilized on conducting (gold) surface. Only at very close distance (below 20-30 μm) the $K_{M(app.)}$ significantly decreases: in the case when the GOx is immobilized on non-conducting (plastic) surface, $K_{M(app.)}$ is 23 mM; in the case when the GOx is immobilized on conducting (gold) surface, $K_{M(app.)}$ is 18 mM. The same $K_{M(app.)}$ values was obtained for both curves at the distance of 36 μm and it was 26 mM.

The equation (*5)* was used to calculate the $K_{M(app.)}$ values from results registered using GC-SECM mode. In this case the $K_{M(app.)}$ values were calculated only when the ME-based probe was positioned at the distance where the highest current was observed. In order to prove $K_{M(app.)}$ values, which were calculated using traditional approach, we fitted current *vs* distance dependencies to calculate $K_{M(app.)}$ values at all

distances of ME-based probe from the GOx-modified surface. We have determined that $K_{M(app.)}$ values are equal to that, which were calculated at distance where diffusion-limited current was observed: for GOx immobilized on insulating surface such $K_{M(app.)}$ value was 18 mM, while for GOx immobilized on conductive surface it was 23 mM.

Calculated i_{max} values show that ME current similarly depend on the distance of ME-based probe from both conducting and non-conducting GOx-modified surfaces (Fig. 3.11 B). Therefore the $K_{M(app.)}$ and i_{max} values, which were calculated for GOx immobilized on both insulating and conductive surfaces modified by GOx, similarly depend on the distance of ME-based probe from surface of interest.

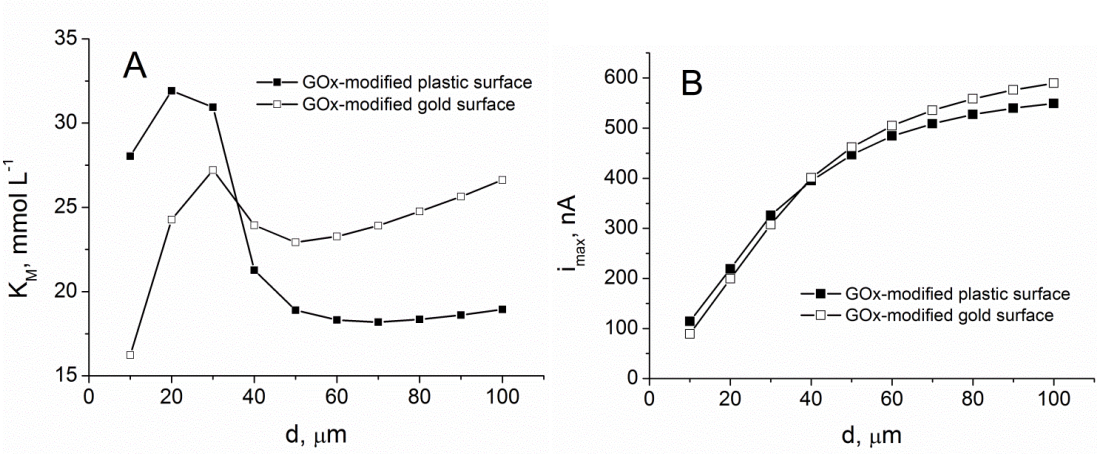

Fig. 3.11. Calculated dependence of **A** – apparent Michaelis constant and **B** – i_{max} on the distance of ME from GOx-modified conducting (gold) and non-conducting (plastic) surfaces.

3.3.3 Modelling of Scanning Electrochemical Microscopy at Redox Competition Mode Using Diffusion and Reaction Equations

Theoretical background

Glucose oxidation in the presence of dissolved oxygen (O_2^*) is catalysed by GOx. During this process the O_2^* is consumed the hydrogen peroxide and gluconolactone are produced according to equations (19-21). The value of UME-current depends on the concentration of dissolved oxygen and presence of all other electrochemically active species in

close proximity to the UME surface and on the potential applied to UME. In here evaluated RC-SECM measurement system (Fig. 3.12), the oxygen is consumed in two ways: (i) in the redox reaction occurring on UME surface (Equation 22), and (ii) in enzymatic reaction where oxygen serves as an electron acceptor, which is accepting electrons from GOx in the way presented below (Equation 19) and is passing them to the oxygen (Equation 20-21):

$$GOx^{ox} + GLC \underset{k_{-1}}{\overset{k_1}{\rightleftarrows}} GOx \cdot Glc \xrightarrow{k_2} GOx^{re} + Gll \qquad (19),$$

$$GOx^{re} + O_2^* \underset{k_{-3}}{\overset{k_3}{\rightleftarrows}} GOx \cdot O_2^* \qquad (20),$$

$$GOx + O_2^* + 2H^+ \underset{k_{-4}}{\overset{k_4}{\rightleftarrows}} GOx^{ox} + \cdot H_2O_2 \qquad (21),$$

where *Glc* is glucose, *Gll* is gluconolactone.

$$O_2 + 4e^- + 4H^+ \longrightarrow 2H_2O \qquad (22).$$

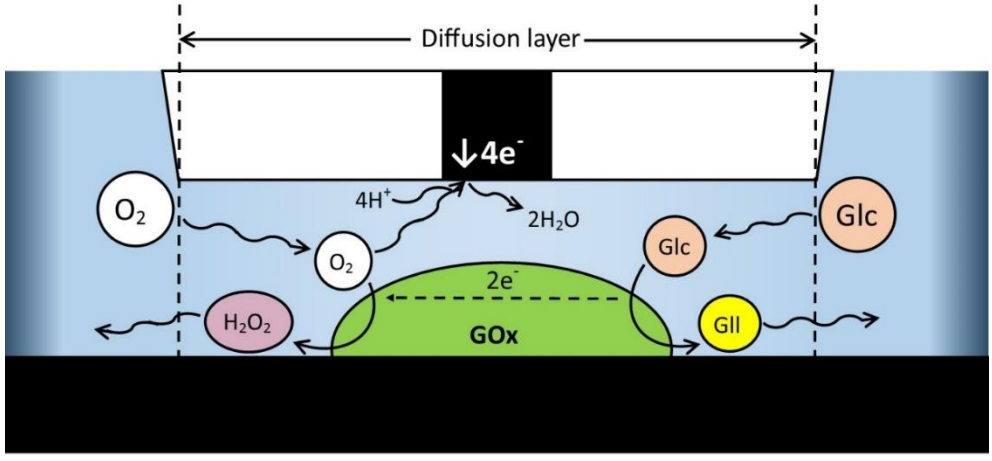

Fig. 3.12. Schematics of redox competition mode based SECM measurement. Oxygen is consumed in two ways: (i) by GOx catalyzed reaction and (ii) in electrochemical reaction on UME surface, at -500 mV *vs* $Ag/AgCl_{(3\ M\ KCl)}$ the oxygen in the presence of H^+ is converted to H_2O. Glc – glucose, Gll – gluconolactone.

The redox competition mode was used in order to register O^*_2 reduction current, at negative UME potential of -500 mV. Under such conditions the O^*_2 is reduced into water on the UME surface, according to the reaction, which is presented in equation (22). Mathematical model, which describes the SECM acting in redox-competition mode, was created taking into account conditions, revealed in Fig. 3.12. The diffusion layer was formed in confined space between the surface with immobilized GOx and UME. Both oxygen and glucose are diffusing from external solution to the diffusion layer, as it is shown in Fig. 3.12. During GOx catalytic action formed reaction products (H_2O_2 and gluconolactone) are diffusing from diffusion layer to external solution. At UME surface electrons are transferred to the oxygen, which is reduced in the presence of H^+. The oxygen is also consumed on the surface modified by GOx and due to this competition current, which is registered by UME, is decreasing proportionally to oxygen concentration consumed by GOx. Oxygen concentration in bulk of the electrochemical cell is 253 μM.

In order to achieve steady-state conditions in enzymatic reactions, electrochemical processes and diffusion the SECM experiments were performed 10 min after the initiation of enzymatic reaction.

Proper selection of reaction rate constants is an important issue during the further modelling of enzymatic reactions based processes. Mathematical models which are incorporating convection, diffusion and enzymatic reactions were developed to simulate the concentration of dissolved oxygen inside the microchannels [185]. The kinetic constants for reactions (19-21) were gathered from references [186-188] and adjusted to fit experimental results better (Table 1). Kinetic constants k_{-1}, k_{-3}, k_{-4} for equations (19-21) were determined from the model and were set to the following values: k_{-1}=10 s^{-1}, k_{-3}=2000 $M^{-1}s^{-1}$. The constant k_{-4} was set to zero, noting that the backward reaction (21) is much slower than other reactions and diffusion-related processes.

Table 1. Kinetic constants and thermodynamic parameters for the GOx catalysed reaction with β-D-glucose and dioxygen at pH 5.5.

Sugar substrate or thermodynamic parameter	k_1 (M^{-1} s^{-1})	k_2 (s^{-1})	k_3 (M^{-1} s^{-1})	k_4 (s^{-1})	Ref.
β-d-Glucose-1-^{1}H at 25 °C	≈200	≈6000	1.8×10^6	1440	[187]
β-d-Glucose-1-^{1}H at 25 °C	13.158		1.8×10^6	1440	[186]
β-d-Glucose-1-^{1}H at 27 °C	10,000		2.1×10^6	1.150	[188]
Used in the model	3000	6000	1.5×10^6	1500	

Mathematical model

Diffusion is one of the most important processes during the SECM evaluations, because during the SECM experiment small but the most important part of reaction vessel is confined by UME and the surface of interest and therefore if some dimensions of this confined space are reaching critical values the diffusion becomes limiting step and influences heavily chemical reactions and electrochemical processes occurring on the UME surface. Diffusion processes are expressed by second Fick's law [189]:

$$\frac{\partial[O_2]}{\partial t} = \mathrm{D}_{\mathrm{O}_2}\,\Delta[O_2], \qquad \frac{\partial[Glc]}{\partial t} = \mathrm{D}_{Glc}\,\Delta[Glc],$$
$$\frac{\partial[H_2O_2]}{\partial t} = \mathrm{D}_{H_2\mathrm{O}_2}\,\Delta[H_2O_2], \qquad \frac{\partial[Gll]}{\partial t} = \mathrm{D}_{Gll}\,\Delta[Gll] \tag{23}$$
$$for\ 0 < t \le T, 0 < z < d,\ 0 < r < r_{glass},$$

where d is the distance between the enzyme-modified surface and the electrode, which is varying from 1 μm to 120 μm. *[O_2], [Glc], [H_2O_2], [Gll]* are concentrations of corresponding reagents and expressed as functions of time t and spatial coordinates z and r. D_{O2}, ..., D_{Gll} are diffusion coefficients of O_2,...,*Gll* and Laplace operator Δ for O_2 in cylindrical coordinates is

$$\Delta[O_2] = \frac{\partial^2[O_2]}{\partial z^2} + \frac{\partial^2[O_2]}{\partial r^2} + \frac{1}{r}\frac{\partial[O_2]}{\partial r} \qquad (24)$$

Differential reaction equations for non-diffusing reagents on the surface z=0 are deduced from chemical equations (19-21):

$$\begin{aligned}
\frac{\partial[GOx^{ox}]}{\partial t} &= -k_1[GOx^{ox}][Glc] + k_{-1}[GOx\cdot Gll] + k_4[GOx\cdot O_2^*][H^+]^2 - \\
&\quad - k_{-4}[GOx^{ox}][H_2O_2], \\
\frac{\partial[GOx\cdot Gll]}{\partial t} &= k_1[GOx^{ox}][Glc] - (k_{-1}+k_2)[GOx\cdot Gll], \\
\frac{\partial[GOx^{red}]}{\partial t} &= k_2[GOx\cdot Gll] - k_3[GOx^{red}][O_2^*] + k_{-3}[GOx\cdot O_2^*], \\
\frac{\partial[GOx\cdot O_2^*]}{\partial t} &= k_3[GOx^{red}][O_2^*] - k_{-3}[GOx\cdot O_2^*] - k_4[GOx\cdot O_2^*][H^+]^2 + \\
&\quad + k_{-4}[GOx^{ox}][H_2O_2]
\end{aligned} \qquad (25)$$

$$for\ 0 < t \le T,\ 0 < r < r_{glass}$$

where $[GOx^{ox}]$, $[GOx\cdot Gll]$, $[GOx^{red}]$, $[GOx\cdot O_2^*]$ are concentrations depending on time *t* and radius *r*.

Reaction equations for diffusing substances on the base z=0 are also deduced from equations (19-21) and are used as the boundary conditions on z=0:

$$\begin{aligned}
D_{O_2}\frac{\partial[O_2^*]}{\partial z} &= k_3[GOx^{red}][O_2^*] - k_{-3}[GOx\cdot O_2^*], \\
D_{Glc}\frac{\partial[Glc]}{\partial z} &= k_1[GOx^{ox}][Glc] - k_{-1}[GOx\cdot Gll], \\
D_{H_2O_2}\frac{\partial[H_2O_2]}{\partial z} &= -k_4[GOx\cdot O_2^*][H^+]^2 + k_{-4}[GOx^{ox}][H_2O_2], \\
D_{Gll}\frac{\partial[Gll]}{\partial z} &= -k_2[GOx\cdot Gll] \qquad for\ 0 < t \le T,\ 0 < r < r_{glass}.
\end{aligned} \qquad (26)$$

During the development of mathematical model it was accounted that at the start of enzymatic reaction, oxygen concentration in the diffusion layer is 253 μmol/L and surface concentration of active GOx is

2.114 mol/m^2. Therefore, at the time t=0 initial concentrations of the materials and intermediate products are following:

$$\begin{aligned}
&[O_2^*] = 253\mu mol/L, \quad [Glc] = [H_2O_2] = [Gll] = 0\, mol/L \\
&for\ 0 < z < d,\ 0 < r < r_{glass} \\
&[GOx^{ox}] = 2.114 mol/m^2, \\
&[GOx \cdot Gll] = [GOx^{red}] = [GOx \cdot O_2^*] = 0\, mol/m^2 \\
&for\ z = 0,\ 0 < r < r_{glass}.
\end{aligned} \tag{27}$$

We consider [*H*+] = 1 to note that the process is not influenced by variation of [*H*+]. Furthermore, boundary conditions are expressed only for diffusing materials with condition on z=0 already given as equation set (25). Due to the symmetry, in the center r=0 there is no flow:

$$\frac{\partial[O_2^*]}{\partial r} = \frac{\partial[Glc]}{\partial r} = \frac{\partial[H_2O_2]}{\partial r} = \frac{\partial[Gll]}{\partial r} = 0 \qquad for\ 0 < t \le T, 0 < z < d\,. \tag{28}$$

For the border r=r_{glass}, i.e. on the edge of the insulating surface, boundary conditions are

$$[O_2^*] = 253\mu mol/L, \quad [Glc] \in (0-0.6) mmol/L \quad \text{for } t > 0,\ 0 < z < d\,.$$

All $[H_2O_2]$ and $[Gll]$ are considered to be diffusing away on the border $r = r_{glass}$, so

$$[H_2O_2] = [Gll] = 0 \quad \text{for } 0 < z < d,\ t > 0 \text{ and } r = r_{glass}. \tag{29}$$

Finally, for the border z=d on the insulator r>r_{el} there is no flow:

$$\frac{\partial[O_2^*]}{\partial z} = \frac{\partial[Glc]}{\partial z} = \frac{\partial[H_2O_2]}{\partial z} = \frac{\partial[Gll]}{\partial z} = 0 \quad \text{for } z = d \text{ and } r_0 < r < r_{glass}. \tag{30}$$

On the electrode ($r < r_{el}$) all O_2^* is consumed due to the speed of the reaction 22:

$$[O_2^*] = 0 \quad \text{for } z = d \text{ and } 0 < r < r_{el}. \tag{31}$$

The other 3 materials are blocked by electrode and insulator

$$\frac{\partial[Glc]}{\partial z} = \frac{\partial[H_2O_2]}{\partial z} = \frac{\partial[Gll]}{\partial z} = 0 \quad \text{for } z = d \text{ and } 0 < r < r_{glass}. \tag{32}$$

Numerical experiment

The resulting system of differential equations with corresponding initial and boundary conditions is solved using the alternating-direction finite implicit difference method (ADIFDM) by the house-made program. The effectiveness of ADIFDM was shown by various research groups [68, 190, 191]. Particular care has to be taken of the joining point between the insulator and electrode (z = d, r = r_{el}) and the chosen mesh is much thicker around thus point.

The model allows to calculate the concentration of diffusing materials O_2^*, Glc, H_2O_2, Gll and reagents GOx^{ox}, $GOx \cdot Gll$, GOx^{red}, $GOx \cdot O_2^*$ at any time t and position z, r. The current through the tip is calculated as a function of time

$$i(t) = 2\pi n F D_{O_2} \int_0^{r_{el}} \left. \frac{\partial [O_2^*]}{\partial z} \right|_{z=d} r\,dr, \qquad (33)$$

where n = 4 is number of electrons exchanged and *F* is the Faraday's constant.

For comparison with experimental data, steady state current $I = \lim i(t), t \to \infty$ has been calculated. Because of computational reasons, it was enough to take modelling parameter T large enough to ensure that relative error for i is smaller than 0.001% between two following time steps. Modelling results show that depending on the model parameters (distance *d* and Glc concentration) it takes T=~6-8s to achieve here determined accuracy.

Comparison to experimental results

Simulations were compared with real RC-SECM experiments (Fig. 3.13). Diffusion-limiting current values have changed together with varying glucose concentrations.

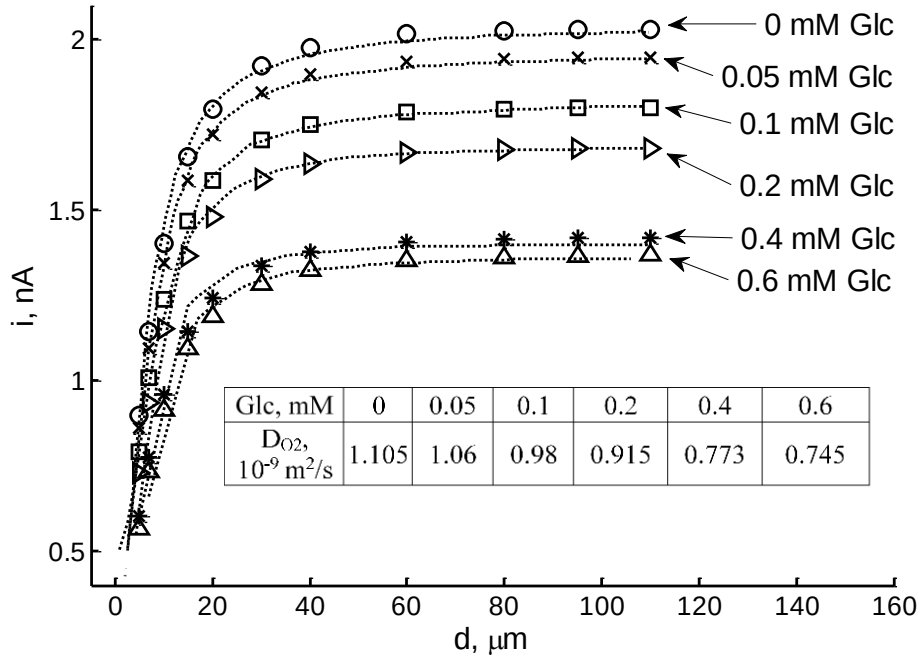

Glc, mM	0	0.05	0.1	0.2	0.4	0.6
D_{O2}, 10^{-9} m^2/s	1.105	1.06	0.98	0.915	0.773	0.745

Fig. 3.13. Current *vs* distance dependencies, when different concentrations of glucose were added to the buffer solution. Glc – glucose, D_{O_2} – oxygen diffusion coefficient. Rg = 33. Symbols – model data, line – experimental data.

The concentration of oxygen (and UME current) in zone, which was not affected by diffusion was considered to be the same at all in this research applied glucose concentrations. However, current value is proportional not only to oxygen concentration, but also it significantly depends on the diffusion rate of oxygen through the solution. Oxygen diffusion coefficients depends on the presence and concentration of some compounds, which are present in the solution: salts (e.g. NaCl, KH_2PO_4, K_2HPO_4), which are present in buffer solution, glucose, etc. [192]. Additionally, the diffusion coefficient significantly depend on the glucose concentration in solution, and it is decreasing by increasing glucose concentration [192]. Therefore during the comparison of real experimental data with that generated using here proposed mathematical model diffusion coefficient was adapted for each here evaluated glucose concentration. We have tested the influence of diffusion to the current of UME by SECM experiment, which was performed on the bare surface without any immobilized enzyme at different glucose concentrations in the buffer solutions. This experiment showed noticeable decrease of

diffusion coefficients observed when compared to that observed in buffer solution (Fig. 3.14). Therefore, to fit well absolute current values, which were registered during the experiment, the diffusion coefficient was one of the most significant parameters, which is affecting the UME current.

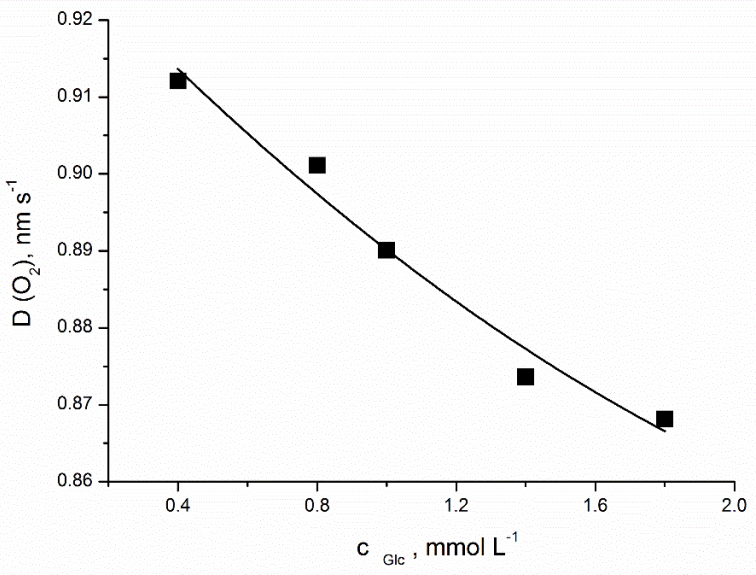

Fig. 3. 14. Diffusion rate dependence on glucose concentration, added to the buffer solution. Glc – glucose, D(O*2) – oxygen diffusion coefficient. Measurements were performed without enzymatic reaction.

In our experiments we have used the buffer solution with 0.1 M of KCl with particular concentration of glucose. Some other researchers found that diffusion coefficient of oxygen separately depends on the concentration of glucose and NaCl in water [192]. Therefore, in our case, when glucose was added to buffer solution containing several salts, it is obvious, that in such solution the diffusion coefficient of oxygen is more significantly affected by composition of the solution. To determine influence of glucose concentration to the diffusion coefficient in buffer solution, we performed experiment at the same conditions, but on the surface where the GOx was inactivated and has not consumed oxygen (Fig. 3.14). When SECM-based evaluation is performed on enzyme modified surface and enzymatic reaction is taking place, then the diffusion coefficient of oxygen is almost the same in glucose concentration range of 0.4-0.6 mM (Fig. 3.15), while measurements

without enzymatic reaction show linear dependence of diffusion coefficient on glucose concentration in glucose concentration range of 0.4-1.8 mM.

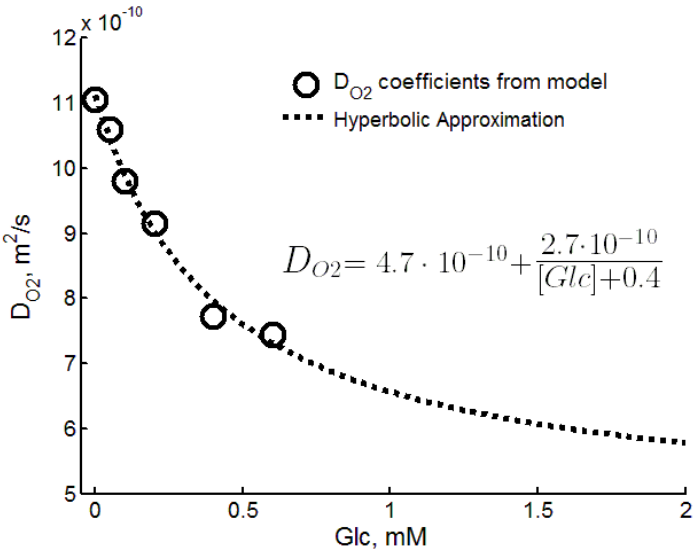

Fig. 3.15. Diffusion rate dependence on glucose concentration, added to the solution. Glc – glucose, $D(O_2^*)$ – oxygen diffusion coefficient.

Mathematical models usually are fitted to normalized current *vs* normalized distance curves. However the diffusion of measured materials is not evaluated in such a case. The diffusion coefficients could be measured using SECM technique, therefore in mathematical model different diffusion coefficients could be applied for different glucose concentrations. Additionally, the research of different redox couples, such as oxidized/reduced ferrocene (Fc^+/Fc) or benzoquinone (BQ/BQ^-), and ferrocyanide/ferricyanide, showed that the UME current response in the SECM generation-collection mode is particularly sensitive to subtle differences in the diffusion coefficients of a redox couple [190]. In particular, the diffusion coefficient ratio of the oxidized and reduced forms of a couple can readily be determined by three methods: (i) by fitting the chronoamperometric UME current at a known distance between UME and substrate; (ii) by combining measurements of the steady-state UME amperometric response at a known distance between UME and substrate with that registered when the UME is positioned far from the

substrate; (iii) by measuring the ratio of the steady-state feedback and UME current response at GC-SECM mode registered at the same distance of UME from the substrate [190]. Therefore, the fittings of not-normalized data to the model using different oxygen diffusion coefficient are also meaningful because they demonstrated real UME currents.

3.4 SEIM based measurements

EIS is based on the measurement of alternating current, which is registered when a sinusoidal excitation signal of low voltage amplitude is applied to electrochemical system. As a result, the AC-current with a shifted phase is registered by working electrode. The measured signal is based on complex impedance, which depends on the solution resistance, double layer capacitances of both working and counter electrodes, and charge-transfer resistance between these two electrodes [193]. The working electrode in here applied SEIM equipment is an UME. This electrode is scanning in all three directions and therefore it can be applied for the investigation of selected 3D space of solution. The idea of this research is coming out from results of some investigations, which were described in earlier researches: i) many researches were based on the EIS application for the evaluation of enzymatic reaction when the enzymes were immobilized on surfaces of electrodes [194]; ii) conventional SECM is very often used for the investigation of enzyme-modified insulating surfaces while applying constant potential to UME [4, 87-89]. Hence by assumption of previous achievements we have expected that it is possible to merge the EIS technique with SECM in order to get efficient SEIM system, which will be suitable for the evaluation of enzyme-modified surfaces. However, according to our best knowledge up to now no research, in the area of application of SEIM for the investigation of reaction product diffusion from enzyme-modified insulating surfaces, was reported.

The obtained data were analysed using equivalent circuit, which is represented in Fig. 3.16. The SEIM is used more rarely, than the AC-SECM, because scanning at one desired frequency takes less time. But the advantage of SEIM is that the EIS measurements are performed in wide range of frequencies at each point of the UME position. Such measurements allow to evaluate the response of the electrochemical system, to develop 3D model of the system, also to determine the most suitable equivalent circuit and their parameters, which in the most optimal way to describe the system [94]. What is the most important; such measurements allow finding the values of equivalent circuit parameters in selected volume of the electrochemical cell.

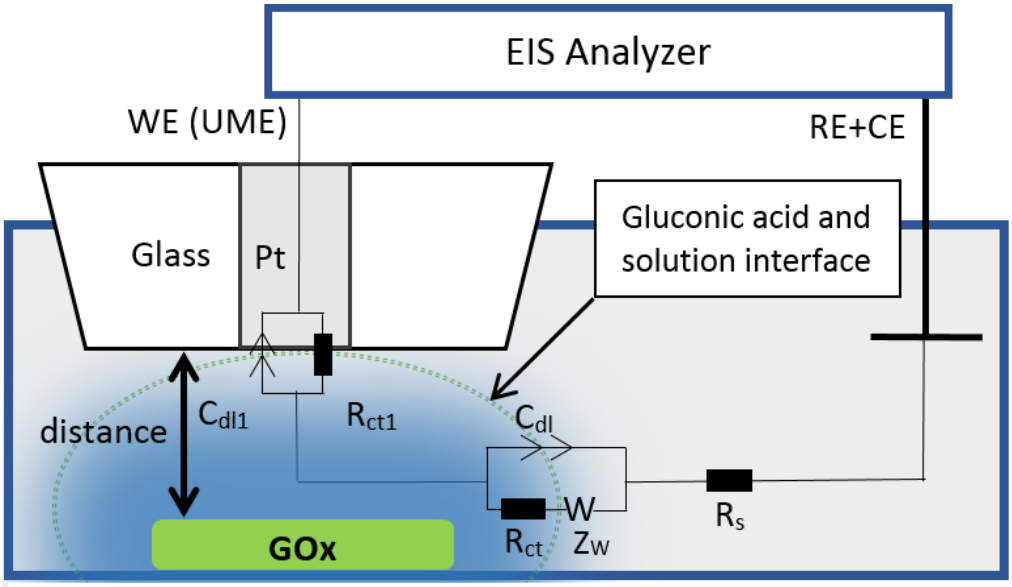

Fig. 3.16. Experimental scheme used for the measurement of EIS data. Equivalent circuit used for the fitting of EIS data was simplified to: Rs – uncompensated solution resistance, Rct – charge transfer resistance, Cdl – pseudo double layer capacitance, W – Warburg impedance. Cdl1 – double layer capacitance on UME/solution interface, Rct1 – charge transfer resistance through UME/solution interface. GOx – glucose oxidase, WE (UME) – ultramicroelectrode, which was applied as working electrode, RE+CE – platinum electrode, which was applied as reference and counter electrode.

Reaction products, which affect solution's conductivity, diffuse from the active sites of GOx-modified surface into the solution; therefore the SEIM with moving UME is one of the best choices to study the diffusion of formed reaction products in selected volume of

electrochemical cell. Due to the fact that the EIS measurements take a long time, the conductivity changes in time were also evaluated and this issue was taken into account.

The oxidation of glucose in the presence of O_2 is catalysed by GOx, and in this reaction hydrogen peroxide (H_2O_2) and D-glucono-1,5-lactone, which is rapidly hydrolysed to β-D-gluconic acid, are produced:

$$\beta - \mathrm{D} - \mathrm{glucose} \; + \; \mathrm{O_2} \xrightarrow{\mathrm{GO_x}} \mathrm{D} - \mathrm{glucono} - 1{,}5 - \mathrm{lactone} \; + \; \mathrm{H_2O_2}$$

$$\mathrm{D} - \mathrm{glucono} - 1{,}5 - \mathrm{lactone} \; + \; \mathrm{H_2O} \; \rightleftarrows \; \beta - \mathrm{D} - \mathrm{gluconic\ acid}$$

Therefore, the changes in impedance spectra are mostly related to the accumulation of gluconic acid because its concentration mainly affects the surface capacitance and ohmic-resistance of solution. Due to diffusional limits gluconic acid concentration decreases with increasing distance between UME and GOx-modified surface, this fact was approved by Faradaic SECM approach curves [4, 89].

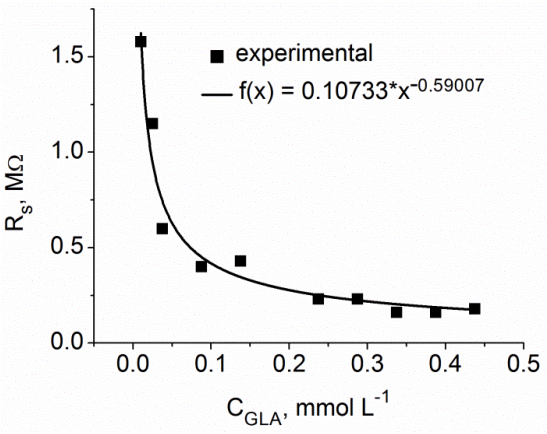

Fig. 3.17. Calibration curve of solution resistance dependence on gluconic acid (GLA) concentration.

To verify the dependence of solution resistivity on gluconic acid concentration, the impedance spectra were measured at different concentrations of gluconic acid. Equivalent circuit values were fitted corresponding to measured impedance spectra and equivalent circuit (Eq. 8), and then the dependence of solution resistance on the

concentration of gluconic acid was found (Fig. 3.17). The R_S value decreases by addition of gluconic acid to the solution.

Further, the measurements of impedance at different distances from enzyme-modified surface were performed, and the same impedance model (Eq. 8) was fitted to the results. Solution resistance was decreasing from 1.5 to 0.7 MΩ while the UME was approaching to the GOx-modified surface (3.18 A). These changes are related to the gluconic acid diffusion from GOx-modified surface into the solution. The gluconic acid concentration was recalculated according to the resistance of solution (Fig. 3.18 B). When the UME approaches towards the GOx-modified surface it first encounters the gluconic acid solution, which initially was very diluted; however while approaching closer to the GOx-modified surface the UME reached a point where the gluconic acid concentration was the highest, due to superposition of several factors: close diffusion distance from active site of the enzyme and sufficient gluconolactone/water ratio, which is necessary for both hydrolysis of gluconolactone and dissociation of formed gluconic acid. Calculated gluconic acid concentration was changing from 0.011 mM (at 1.5 mm from GOx-modified surface) to 0.040 mM (at 50 μm from the GOx-modified surface). After 5 hours of reaction course the resistance of the solution remained approximately 0.4 MΩ and it became similar in all distances, suggesting that the gluconic acid has spread in all volume of the solution. Gluconic acid concentration changed from 0.076 mM (at 1.5 mm from GOx-modified surface) to 0.093 mM (at 50 μm from the GOx-modified surface). At the distances from 250 to 1500 μm gluconic acid concentration is increasing while approaching to the GOx-modified surface. Below the distance of 100 μm the UME is entering a near-surface zone where the current of UME is blocked by limited diffusion of ions in such thin solution layer.

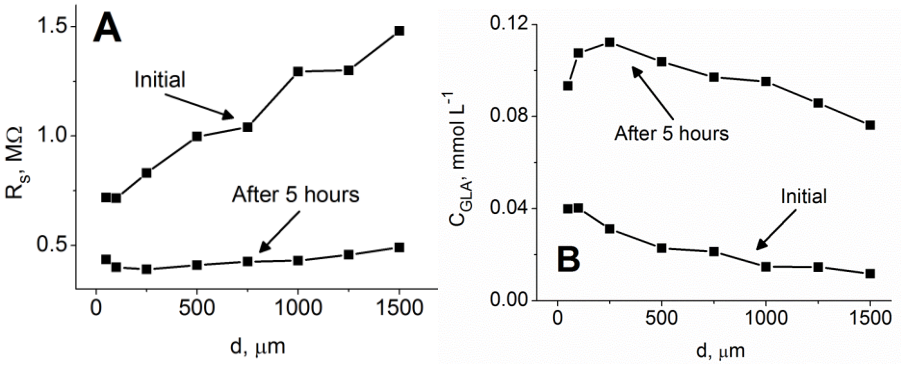

Fig. 3.18. A – Calculated solution resistance dependence on the distance of UME from the GOx-modified surface in 0.1 mM glucose solution; **B** – Dependences of calculated gluconic acid concentration on the distance of UME obtained from results presented in figure 3.18 A.

3.5 Measurement of living cells

Living cells are the most complicated and the most interesting systems, because they are in the human organism, and investigation of various effects influence to the cell processes, measured in their physiological system, should be very important.

3.5.1 Evaluation of double mediator system

The principle of the measurement of intracellular redox reactions based on a two mediator system is shown in figure 3.19. According to this scheme the NAD(P)H is oxidized to $NAD(P)^+$ as in many reactions, which are occurring in the living cells. NADH and NAD(P)H are the reduced forms of the nicotinamide adenine dinucleotide (NAD) and NAD(P) cofactors, NAD^+ and $NAD(P)^+$ are the oxidized forms. NAD is a ubiquitous biological molecule that participates in many metabolic reactions [195]. Many human diseases are associated with changes in total NAD level and/or the NAD^+ : NADH ratio [195]. In *S. cerevisiae,* the two redox mediator based system response is proposed to originate from the reduction of the lipophilic mediator by NAD(P)H produced in the pentose phosphate pathway [115]. NAD(P)H in the cell is produced by $NAD(P)^+$ and H^+ using two electrons that are received by the oxidation of glucose during glycolysis. The resulting NAD(P)H can be reoxidized

by NAD(P)H oxidizing enzymes (NOE) back to $NAD(P)^+$. The above-mentioned reactions are intracellular, and electron transport through the cell membrane is performed by the lipophilic mediator [100]. Lipophilic 9,10-phenanthrenequinone (PQ) can access the interior of the cell, where it is reduced and diffuse back through the membrane into the solution and transmits electrons to the hydrophilic $[Fe(CN)_6]^{3-}$ ion, by reducing it to $[Fe(CN)_6]^{4-}$. $[Fe(CN)_6]^{4-}$ on the electrode generates a current, which indicates NOE's activity in the yeast cell [196].

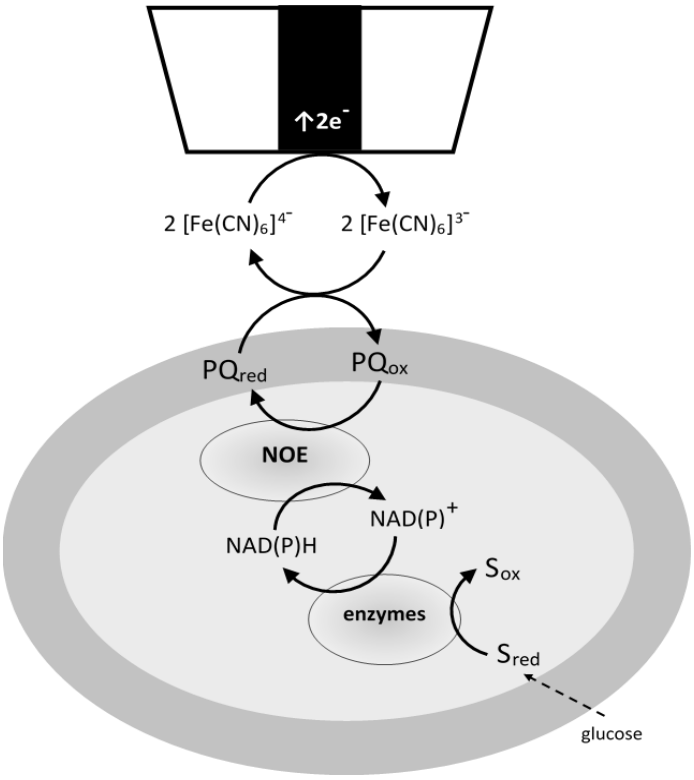

Fig. 3.19. SECM-based measurement of intracellular redox reactions using a two redox mediators based system. The PQ diffuses inside cell wall, at the inner part of cell membrane and it is reduced by NAD(P)H. Latter diffuses to the outer part of the cell membrane and in this position it passes the electrons to $[Fe(CN)_6]^{3-}$. Oxidation of the formed $[Fe(CN)_6]^{4-}$ is determined by UME amperometrically at +400 mV. The addition of glucose results in the formation of NADH and NAD(P)H mainly in glycolysis and pentose phosphate metabolic pathways. In this figure the abbreviation 'enzymes' depicts glyceraldehydes 3-phosphate dehydrogenase, glucose 6-phosphate dehydrogenase, 6-phosphogluconate, dehydrogenase and other enzymes, which are involved into glycolysis and pentose phosphate pathways and other processes of metabolism; Abbreviations 'S_{red}' and 'S_{ox}' are indicating reduced and oxidized forms of corresponding substrates of these enzymes, respectively; The abbreviation 'NOE' depicts NAD(P)H oxidizing enzymes.

When cells are immobilized on the surface, the UME is always at some distance from the surface of interest. Therefore, the measured result depends on the distance of the UME from the surface. Since the goal is not only to measure electrochemical activity, but also to get the image of activity at appropriate resolution, the distance of the UME from the surface must be chosen accurately. This goal can be achieved by recording current *vs* distance dependencies in redox competition and generation-collection modes. In the generation-collection mode of SECM, the reactions take place during the entire measurement. Therefore in order to evaluate kinetics of the evolvement of metabolic processes, the measurement started before the addition of the glucose to the sample. Our investigations of immobilized yeast cells shows that the steady-state amperometric signal can be achieved only after 18 min incubation of the yeast cells with both redox mediators (PQ and potassium ferricyanide).

3.5.2 Chronoamperometric measurements

The efficiency of four different compounds PQ, pBQ, PD, DCPIP, which are able to act as a second redox mediators in the charge transfer chain (Fig. 3.19) of not immobilized yeast cells was compared in the presence of ferricyanide dissolved in PBS (Fig. 3.20 A). The UME current, measured with PQ as a second redox mediator, was more than 3 times higher than others here evaluated redox mediators. Next chronoamperometric experiment was performed to prove that the current signal corresponds to yeast cell electrochemical activity (Fig. 3.20 B). When only potassium ferricyanide was added as redox mediator to PBS with dissolved yeast cells, then the registered UME current was very low. The UME current remained at the same level after the addition of 10 mM glucose. This confirms that if only potassium ferricyanide is used as a redox mediator its action is not very efficient because it cannot cross the membrane of the cell. But simultaneous application of two redox

mediators – ferricyanide and PQ with different properties enables to register some current by UME, even if no glucose is added to the solution. This phenomena could be explained, knowing that yeast cells still have some compounds suitable for the metabolism, therefore two redox mediators based system could transfer charge towards UME. Finally, by adding 10 mM of glucose, the UME current significantly increases. Incubation experiment with and without glucose was performed within 4 days (Fig. 3.21).

The decrease of yeast cell viability is well described by Hill's function. Better fit with Hill's function was obtained for cells, which were incubated in PBS not containing any glucose, and this could be related to the decrease of glucose and other nutrient concentrations in the cells, because under such conditions some cells have died much faster. Yeast cells, which were incubated with glucose, after 24 hours showed low viability. This could be related to the production of ethanol, which can affect the viability of the cells.

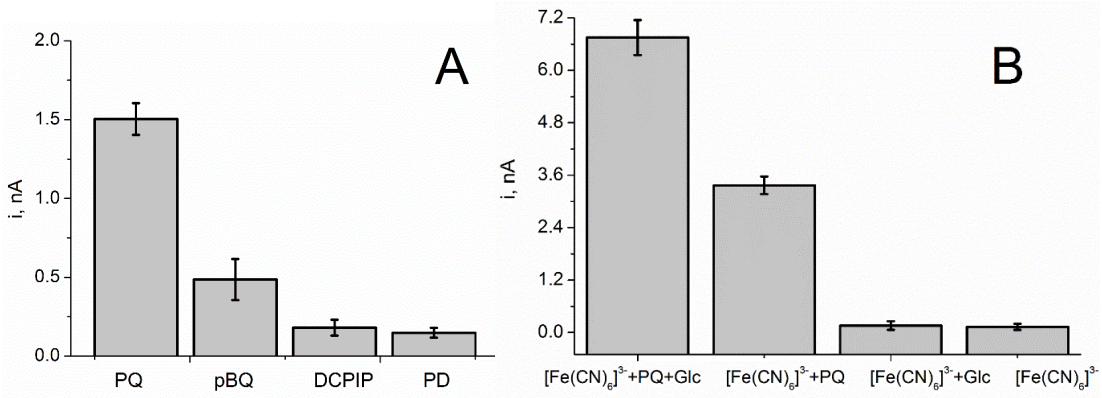

Fig. 3.20 A. Plot of steady-state currents measured by chronoamperometry at +400 mV *vs* Ag/AgCl in solutions of 6.7 mg/mL yeast, 5 mM potassium ferricyanide, 10 mM glucose (Glc), and 100 μM secondary mediator, using stirring and incubation for 10 min. **B.** Current dependence on the composition of solution registered after 10 min of incubation. PQ is 9,10-phenanthrenequinone, pBQ – p-benzoquinone, DCPIP – 2,6-dichlorophenolindophenol sodium salt hidrate, PD – 10-phenahtroline-5,6-dione, $[Fe(CN)_6]^{3-}$ – potassium ferricyanide, Glc – glucose.

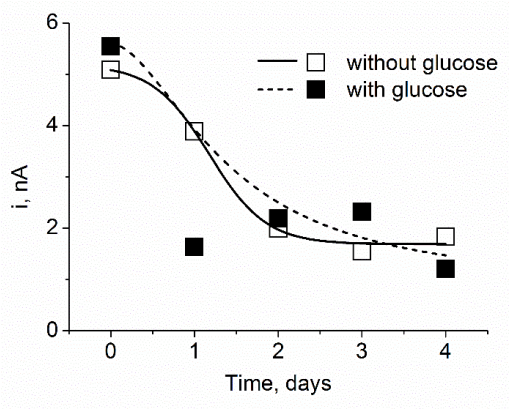

Fig. 3.21. The incubation of yeast cells with and without glucose in PBS. Chronoamperometric measurements were performed at +400 mV *vs* Ag/AgCl in the solution of 6.7 mg/mL of yeast, 5 mM of potassium ferricyanide, 100 μM of PQ, and 10 mM of glucose. Fittings were performed using Hill's equation.

The influence of pH was investigated at the same conditions. Chronoamperometric measurements were evaluated by fitting with the Hill's function, and the determination of pH dependence is shown in figure 3.22. The maximal current was obtained at pH 4.5 (Fig. 3.22 C). The results of fittings are provided in the Table 2. The fittings with Hill's function at pH lower than pH 4.5 were the most successful, but calculated i_{max} values were very small, and these pH values were not taken into account. The maximal Hill's numbers were observed at pH 5.5 (Fig. 3.22 B). At this pH the apparent Michaelis constant is at the lowest range, thus the reaction is relatively fast comparing to that at other pHs (Table 2). Since the Hill's number shows the degree of cooperativity, the maximal PQ cooperativity to yeast cells was observed at pH 5.5. At the same time the apparent Michaelis constant is at the lowest range, comparing to that calculated in other fittings observed at different pH, and it means that toxic effect of PQ is maximal at pH 5.5. Therefore, the pH 6.5 was chosen for our measurements, where the Hill's number is lower, and apparent constant is higher. Hence, such experimental conditions provide most efficient balance between the toxicity and charge transfer efficiency of second mediator and kinetics of metabolism, because here mentioned factors are mostly affecting the UME current.

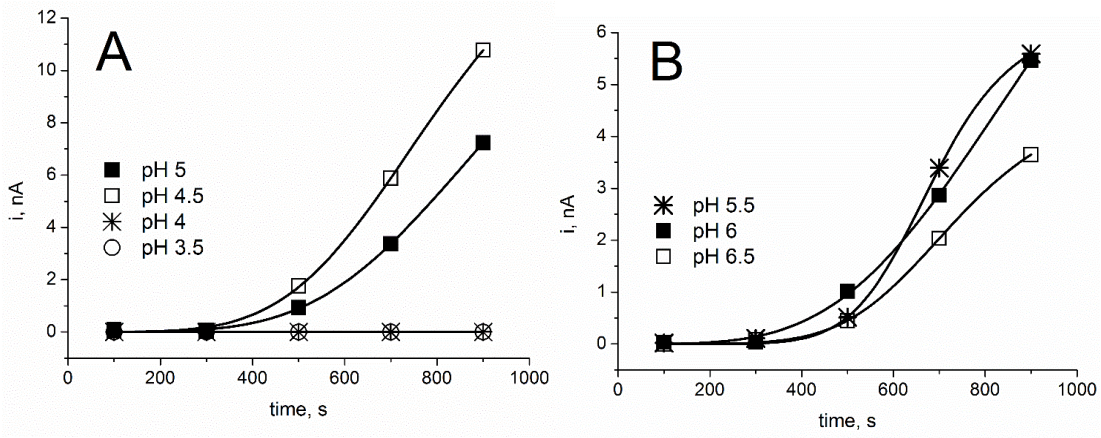

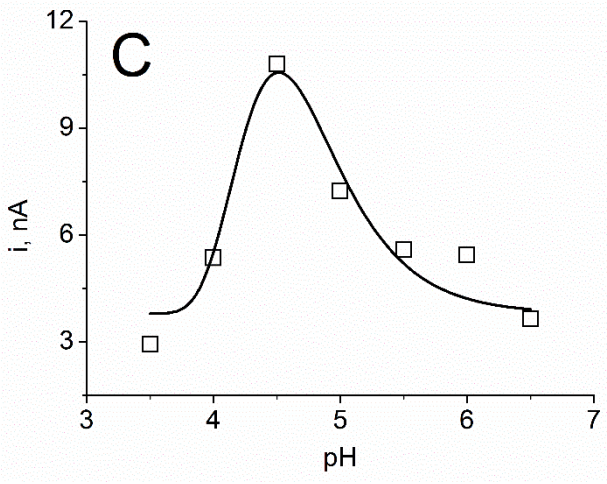

Table 2. Fitting parameters of Hill's equation at different pH

pH	i_{max}, nA	k_M, s	n
3.5	9.7	1084	4.5
4.0	6.2	683	6.9
4.5	17.5	812	4.6
5.0	16.3	947	4.4
5.5	6.3	686	7.6
6.0	12.1	947	3.8
6.5	4.8	739	5.8

Fig. 3.22. A, B. Chronoamperometric measurements at different pH at the conditions the same as in the figure 3. **C.** Current dependence on pH obtained from at time 900 s data presented in A, B parts of figure. Fitting performed using 'Extreme fit' function in Origin 8.

3.5.3 The determination of optimal concentrations of mediators

The optimal imaging conditions were determined by adjusting the concentrations of both mediators as current intensity was measured by the UME during horizontal scans of the surface. The PQ concentration was varied from 0 mM to 0.25 mM before each new horizontal scan of the surface and then the maximal current value was registered (Fig. 3.23 A). The registered UME current was the highest at lower PQ concentrations, which do not exceed 0.08 mM, while in the concentration range of 0-0.08 mM the UME current is increasing. However at higher

PQ concentrations, the decrease of current indicates a negative and probably to some extent a toxic effect on the cells [18]. The measured UME current is related to the intensity of metabolism of yeast cells, therefore the decrease of current with an increase of PQ concentration over 0.08 mM shows the reduction of cell viability. Therefore, in order to achieve a compromise between cell viability and the highest currents, which are required for efficient imaging, the concentration of PQ was chosen at half a value (0.04 mM) of the concentration of PQ at which the maximal UME current was achieved. Current *vs* PQ concentration dependence has been determined in accordance with steady state approximation based reaction kinetics (Eq. 3) with the following values: $i_{max(\text{for PQ})}$ = 0.65 nA, $K_{SX(\text{for PQ})}$ = 0.003 mM. A low value of $K_{SX(\text{for PQ})}$ depends on the efficiency of PQ to act as a redox mediator in the proposed bioelectrochemical system, and it shows that the PQ is efficiently transporting electrons from redox enzymes inside the cell and is passing them to $[Fe(CN)_6]^{3-}$, which is acting outside the cell. The half of the maximal current is achieved at 0.003 mM concentration of PQ. Therefore, this low $K_{SX(\text{for PQ})}$ value justifies the 0.04 mM concentration of PQ chosen for the SECM imaging.

To determine the optimal concentration of potassium ferricyanide, the peak current measured from every horizontal scan with different concentrations is presented in figure 3.23 B. The optimal current value from the plot of current *vs* potassium ferricyanide concentration dependence was observed at 0.6 mM of potassium ferricyanide. For potassium ferricyanide, calculated values determined from the steady state approximation based reaction kinetics model (Eq. 12) are: $i_{max(\text{for FeCN})}$ = 0.57 nA, $K_{SX(\text{for FeCN})}$ = 0.22 mM. This $K_{SX(\text{for FeCN})}$ value shows efficiency of potassium ferri-/ferro-cyanide to act as a redox mediator between PQ and the UME of SECM. The $K_{SX(\text{for FeCN})}$ is almost three times lower than that, which was chosen as an optimal one for the SECM

imaging, therefore it well justifies the concentration of potassium ferricyanide selected for SECM imaging.

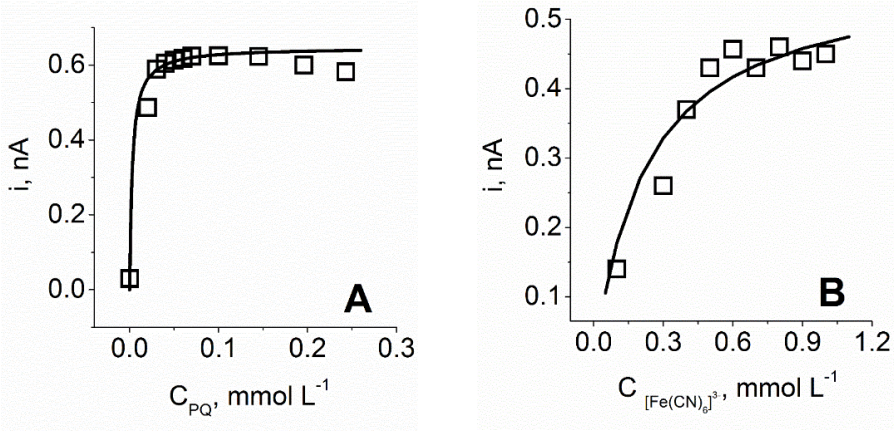

Fig. 3.23. Dependences of UME currents on the concentration of mediators in solution. **A**: Current dependence on PQ concentration (in the range from 0 until 0.25 mM) in the presence of 0.6 mM of potassium ferricyanide and 60 mM of glucose. Solid line represents approximated values calculated using the equation *2* with the parameters: $i_{max(\text{for PQ})}$ = 0.65 nA, $K_{M(\text{app. for PQ})}$ = 0.003 mM. **B**: Current dependence on the concentration of potassium ferricyanide (in the range from 0.1 until 1 mM) in the presence 60 mM of glucose and 0.04 mM of PQ. Solid line represents approximated values calculated using the equation *2* with the parameters: $i_{max(\text{for FeCN})}$ = 0.57 nA, $K_{M(\text{app. for FeCN})}$ = 0.22 mM.

3.5.4 Evaluation of cell redox activity by horizontal scanning at GC-SECM mode

Evaluation of cell redox activity was performed by horizontal linear scan of the yeast-modified spot on the surface at different time intervals after addition of 0.6 mM of potassium ferricyanide, 0.04 mM of PQ and 60 mM of glucose in buffer, pH 6.7 (Fig. 3.24). The measurements were performed every 2 minutes in different scanning directions, as it is shown in figure 3.24. The current changes with time because metabolic reactions after addition of glucose are evolving in time until ‘saturation’ of these processes is reached, which results in achievement of a steady-state current on the UME. However, scanning in opposite directions has provided also very interesting results. It should be noted that SECM scanning can be performed in desired directions, and in some particular cases one direction scanning is chosen.

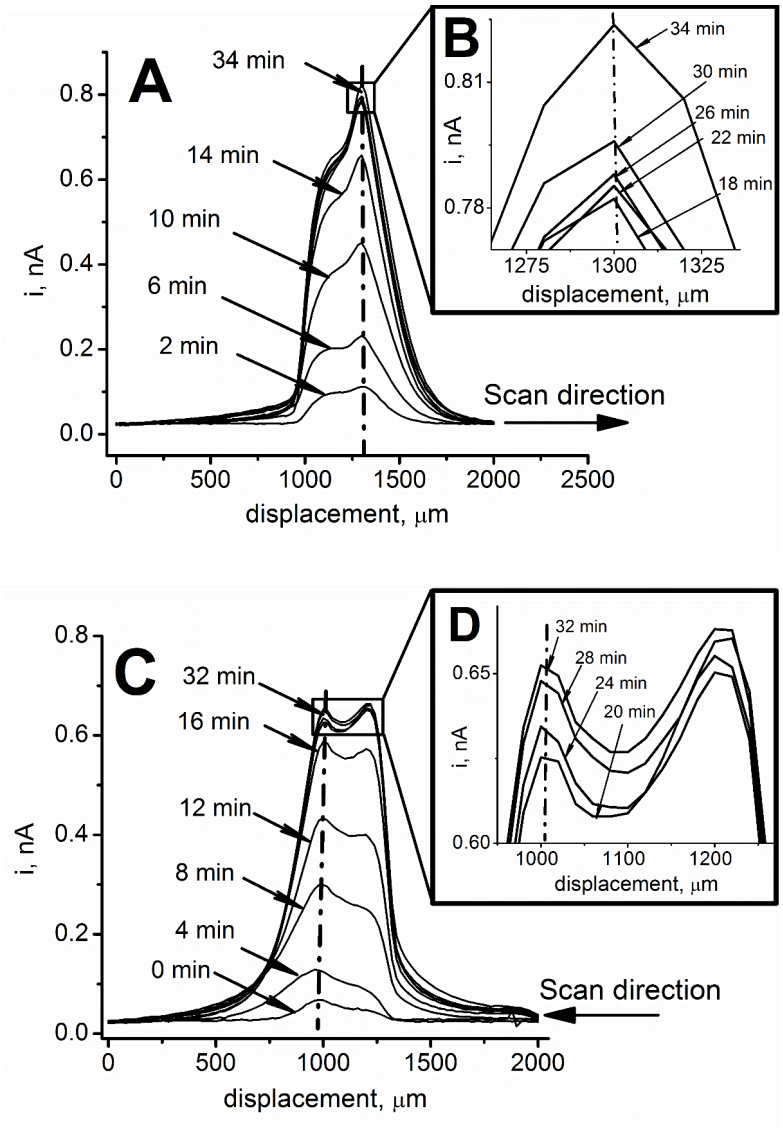

Fig. 3.24. UME current dependence on time after addition of 60 mM of glucose to the buffer, pH 6.7, containing 0.6 mM of potassium ferricyanide and 0.04 mM of PQ. The UME signal was measured at GC-SECM mode using scanning distance 20 μm, applied potential +400 mV, step of the displacement of UME between measurements is 20 μm, speed 10 μm/s. **A**: Scanned during 0-34 min, at forward direction, **B**: Scanned during 18-34 min, at forward direction. **C**: Scanned during 0-32 min, at reverse direction, **D**: Scanned during 20-32 min at reverse direction.

In such cases the UME returns to the same point and the measurement is repeated again. In our case, the first set of measurements was performed during the UME scan in one direction (Fig. 3. 24 A), the second set of measurements was performed during the UME scan in the opposite direction (Fig. 3. 24 B). The two graphs show separate data from scans in opposite directions (Fig. 3.25). It can be

seen, that scanning direction has some influence on measured current. Thus, the increase in current on the edges of the cell is related to the asymmetry in topography and/or asymmetric differences in electrochemical activity.

Additionally, measurements with optical microscopy show that cells are immobilized in toroid-shaped spot due to more quick evaporation of the solvent on the edges of the spot, where the concentration of cells becomes higher, and therefore more cells are immobilized on the edges of the spot. Hence the profile of electrochemical activity corresponds to that represented in figure 3D from 20 to 32 minutes, where the edges of the yeast-modified surface provide higher electrochemical activity. Current values at one displacement point were used for current *vs* time dependence, plot which is presented in figure 3.25. Steady-state current was obtained at 18 min after the incubation and scanning in both directions is leading almost to the same value of UME current.

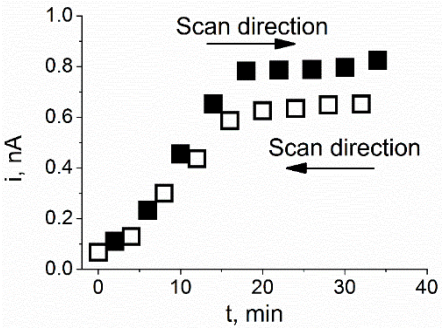

Fig. 3.25. UME current dependence on incubation time in the buffer, pH 6.7, containing 0.6 mM of potassium ferricyanide, 0.04 mM of PQ and 60 mM of glucose; Values marked with dot-dashed vertical line from figure 3A,B,C,D parts are presented in this plot.

Another set of experiments was performed by scanning the cell-modified surface at different glucose concentrations (Fig. 3.26). When the glucose concentration was 5 mM, the current change was only 0.15 nA; increasing the concentration up to 65.4 mM increases the current significantly, reaching the value of 0.55 nA. However, at maximal

glucose concentration the resolution has significantly decreased (Fig. 3.26). As mentioned above, the spot with immobilized cells is toroid-shaped with higher yeast cell concentration at the edges of the cells. The cross-section view shows that the UME signal is higher on one edge of cell-modified spot. This effect is related to different heights of edges of cell-modified toroidal-spot. Also, scanning direction is important (Fig. 3.24). Due to these limitations, at higher concentrations of glucose the profile of immobilized cells loses their shape. If on the surface of interest two or more active regions are present, then they can be correctly evaluated only if i_{max} differs by a factor 2 [74]. If this difference is lower than 2, a larger separation is required to distinguish signals from the both active regions, otherwise the overlapping of diffusion layers will dominate by the flux from both active regions [74].

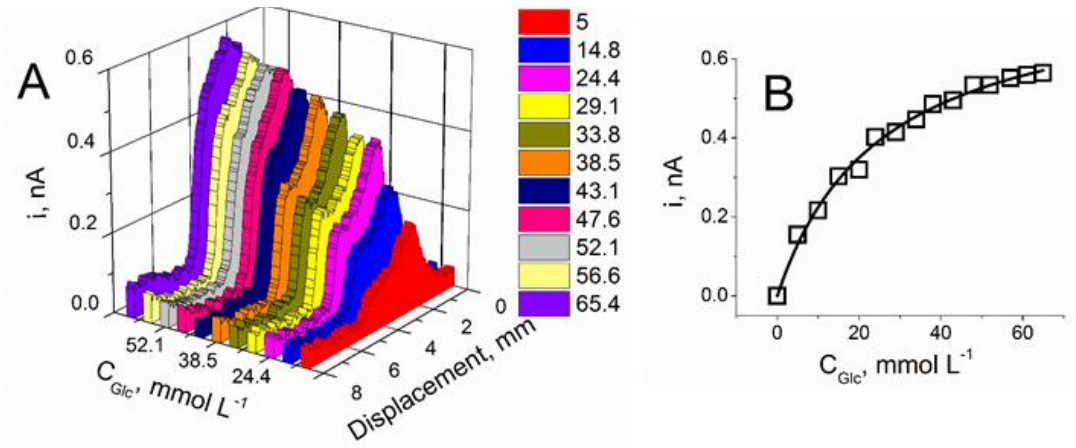

Fig. 3.26. **A**: The UME current dependence on the displacement at different glucose concentrations. Measurements were performed 18 min after the initiation of metabolic reactions by addition of glucose. **B**: The current dependence on the glucose (Glc) concentration, the solid line - values calculated from the *equation 2* with the parameters: $i_{max(\text{for Glc})}$ = 0.79 nA, $K_{M(\text{app. for Glc})}$ = 25.3 mM. Measurements were performed in buffer, pH 6.7, with 0.6 mM of potassium ferricyanide, 0 to 65.4 of glucose mM and 0.04 mM of PQ.

3.5.5 Visualization of cells

The most efficient concentrations of redox mediators, which are suitable for the visualization of the redox process of yeast cells, were determined as 0.6 mM for potassium ferricyanide and 0.04 mM for PQ in

the presence of 60 mM of glucose. These concentrations were suitable to achieve significant UME current. But lower concentrations of redox mediators could be also used, and especially the concentration of PQ, which is toxic to yeast cells. When lower concentration of PQ is used, the concentration of potassium ferricyanide also can be lowered, because in two redox mediators based system one mediator is passing electrons to another, and much higher concentration of potassium ferricyanide could not significantly improve UME current. Also, it should be noted that selected concentration of redox mediator should be proportional to the quantity and/or efficiency of immobilized cells. The immobilization by poly-L-lysine is not the most reliable way, and cells could be washed out during the measurement. Therefore in current research, we have immobilized relatively low quantity of cells. The measured current when UME approaches cell surface, is related to potassium ferrocyanide concentration, thus it was calculated using equation 1. The ferrocyanide at the cell surface is 0.48 mM, therefore almost all ferricyanide is reduced to ferrocyanide, even if low 1 μM PQ concentration was used (Fig. 3.27). For our research we chosen a distance of 20 μm as we found out that the signal is the most optimal for scanning of cell-modified surface by SECM due to the most prominent ferricyanide/ferrocyanide ions concentration changes, which are converted into variation of UME current. Figure 3.28 shows the SECM image of yeast-modified surface registered in GC mode at a constant 20 μm height and at +400 mV *vs* Ag/AgCl potential of UME.

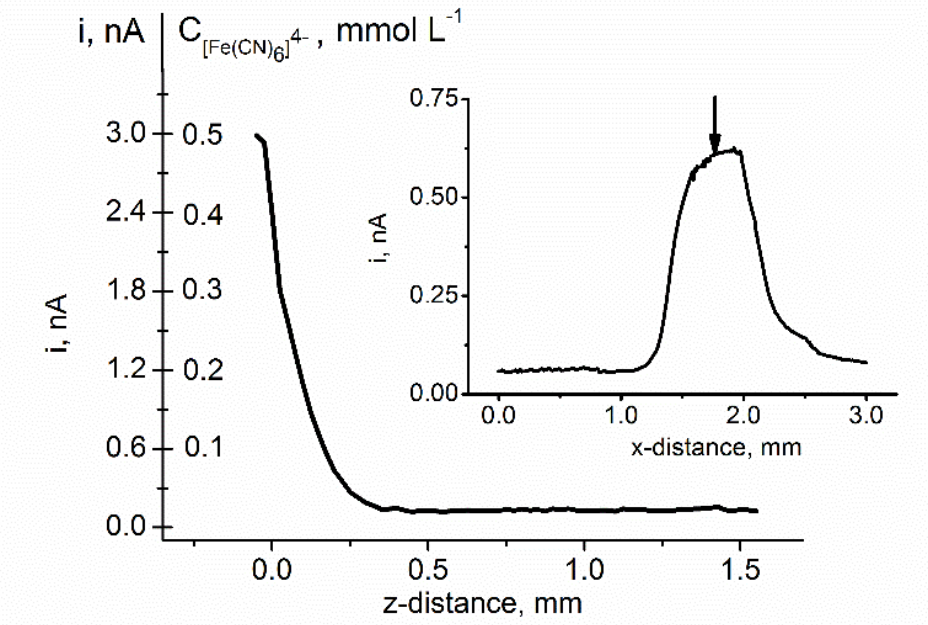

Fig. 3.27. The 'approaching curve' registered during the approaching of UME to surface modified by immobilized yeast at generation-collection mode of SECM. UME potential was + 400 mV *vs* Ag/AgCl, scanning speed 1 μm/s. Experiment was performed in the buffer solution, pH 6.5, consisting of 0.5 mM of potassium ferricyanide, 1 μM of PQ, and 10 mM of glucose. Current values were recalculated into corresponding concentrations using equation 2. **Inset:** scan at x-direction of immobilized yeast modified surface, scan was performed at 20 μm height from the modified surface, UME potential was + 400 mV, scanning speed was 10 μm/s. Experiment was performed in the solution consisting of 50 μM of potassium ferricyanide, 1 μM of PQ, and 10 mM of glucose. Arrow shows a position at which the 'approaching curve' was recorded.

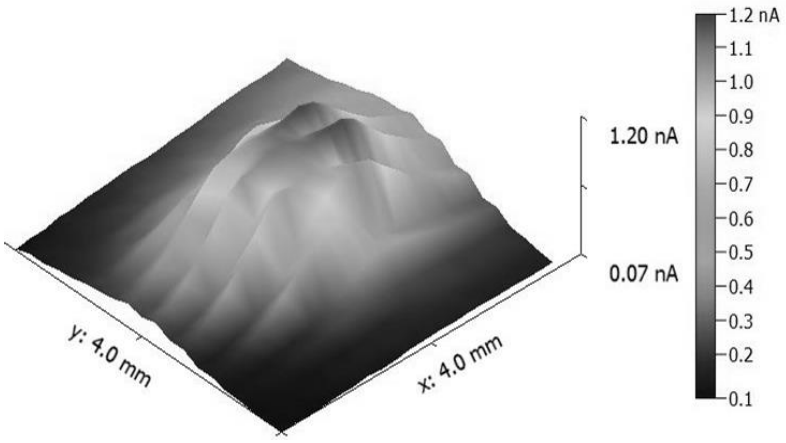

Fig. 3.28. SECM-based imaging of the spot of immobilized yeast modified surface after 18 min of the initiation of metabolic process in yeast cells; surface area is 4 × 4 mm, scanning distance - 20 μm, applied potential +400 mV, step 100 μm, speed 10 μm/s. Solution consist of 0.6 mM of potassium ferricyanide, 0.04 mM of PQ, 60 mM of glucose in buffer, pH 6.7.

It is important to determine which concentrations of glucose are optimal for the generation of maximal electrode current. The optimal glucose concentration was determined to be in the range from 50 to 65.4 mM when the glucose concentration in a solution was changed from 0 to 65.4 mM. Therefore, a 60 mM concentration of glucose was used for further imaging. A maximum current of 1.2 nA was obtained at the edge of the spot of immobilized cells. At the area outside of toroid-shaped spot of immobilized cells, the current decreases to the half of the maximum – 0.6-0.7 nA (Fig. 3.28).

3.5.6 Imaging of immobilized yeast cells by AFM

Yeast cells, deposited on microscope slide, were measured by AFM in contact mode (Fig. 3.29 A, B).

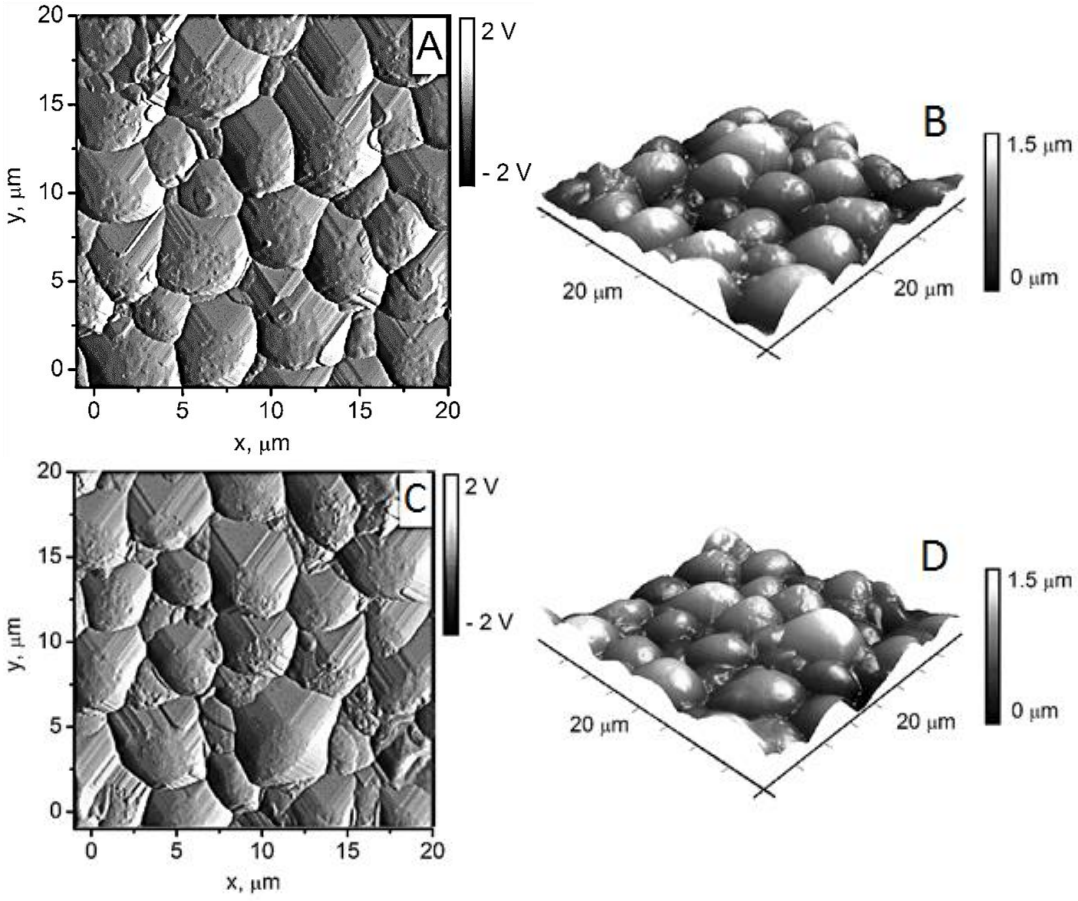

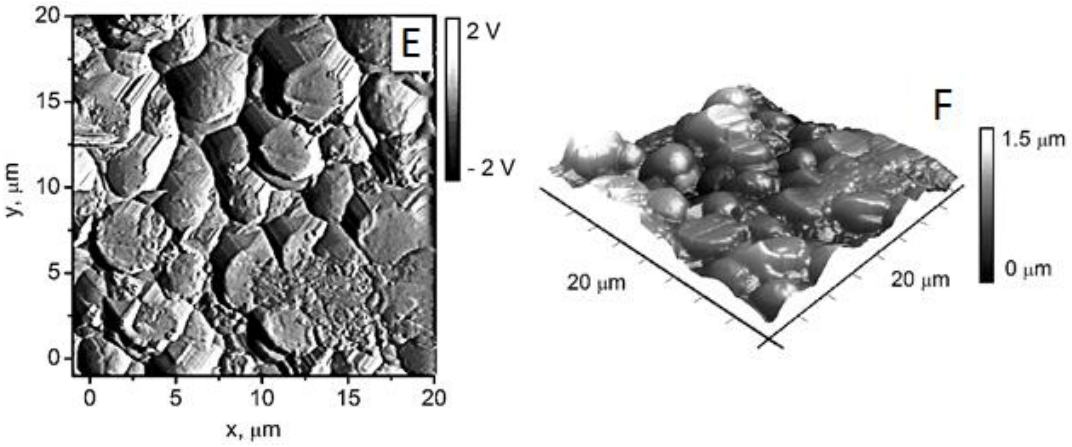

Fig. 3.29. AFM measurement of Yeast cells: **A, B**. Cells before affecting with 9,10-phenantrenequinone, **C, D**. Cells after first exposure with 9,10-phenantrenequinone, **E, F**. Cells after second exposure with 9,10-phenantrenequinone.

9,10-phenantrenequinone solution with concentration of 0.05 mM was dropped on the yeast. After drying the cells' sample again was measured by AFM (Fig. 3.29 C, D). The last procedure was repeated, and the sample again was measured by AFM (Fig. 3.29 E, F). Concentrations of 9,10-phenantrenequinone were chosen from Fig. 3.23 A. At 0.05 mM concentration the current signal was highest, therefore, it was interesting to explore cells surface at this concentration. The results show, that after exposure with 0.05 mM PQ, cells morphology was not changed extremely, but it can be seen increase in cells surface roughness (Fig. 3.29 C). After second exposure, cells surface looks more 'flatten', and it can be explained as decrease in cells viability (Fig. 3.29 E, F).

3.6 Biofuel Cell Based on Glucose Oxidase and Horseradish Peroxidase

The schematic diagram of the prepared E-BFC with GOx/PD/GRE electrode as anode and HRP/GRE electrode as cathode is presented in Fig. 3.30 and all biochemical and bioelectrochemical reactions are presented in Eqs. (34–38). The Eqs. (34–38) represent GOx catalysed glucose oxidation and the ways of non-mediated (Eqs. 34–36) and PD-

mediated electron transfer (Eqs. 37 and 38) on GOx/PD/GRE anode. The hydrogen peroxide is used as a substrate by HRP, which catalyses the reduction of hydrogen peroxide to water (Eq. 39) and during this reaction the oxidized state of HRP is recovered to its reduced state accepting electrons from the electrode directly (Eq. 40).

Anode reactions:

$$\beta\text{-D-glucose} + H_2O + GOx(ox) \rightarrow \text{D-glucono-1,5-lactone} + GOx(red) \quad (34)$$

$$GOx(red) + 1/2O_2 + H_2O \rightarrow GOx(ox) + H_2O_2 \quad (35)$$

$$H_2O_2 \rightarrow O_2 + 2H^+ + 2e^- \text{ (non-mediated ET at anode)} \quad (36)$$

$$GOx(red) + PD(ox) \rightarrow GOx(ox) + PD(red) + 2H^+ + 2e^- \quad (37)$$

$$PD(red) \rightarrow PD(ox) + 2e^- \text{ (mediated ET at anode)} \quad (38)$$

Cathode reactions:

$$HRP(red) + H_2O_2 \rightarrow HRP(ox) + 2H_2O \quad (39)$$

$$2e^- \text{ (non-mediated direct ET at cathode)} + HRP\ (ox) \rightarrow HRP\ (red) \quad (40)$$

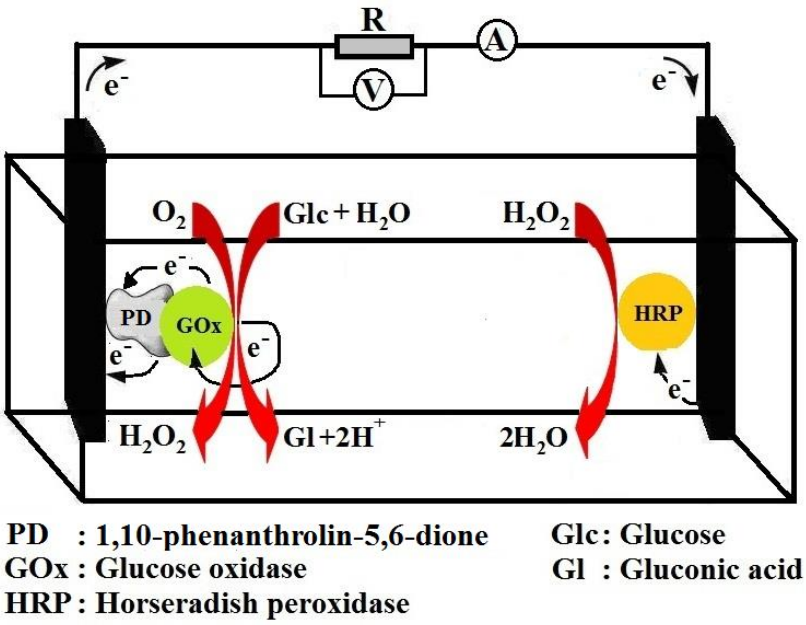

Fig. 3. 30. Principal scheme of reactions at evaluated biofuel cell electrodes.

Hence the potential difference in the E-BFC was generated by the direct ET based HRP catalysed reaction on cathode and GOx catalysed

reaction followed by PD mediated electron transfer on anode (Fig. 3.30). Before the formation of E-BFC GOx/PD/GRE and HRP/GRE electrodes were evaluated amperometrically at constant potentials. The GOx/PD/GRE electrode was evaluated at constant +150 mV *vs* Ag/AgCl/KClsat potential (Fig. 3.31 A), and apparent Michaelis constant (K_{Mapp}) for the glucose was determined as 33.73 mM , which has significantly increased in comparison with K_M of native enzyme, which is in the range 12.9–15.4 mM [197]. The increase of K_{Mapp} was influenced by additional diffusion-based limitations of substrate to the active site of immobilized GOx. Calculated I_{max} value of GOx/PD/GRE electrode was 6.99 lA. During second stage the efficiency of direct ET [122] between the HRP and GRE surface in HRP/GRE electrode was evaluated amperometrically at 200 mV *vs* Ag/AgCl/KClsat in A-PBS, pH 6.0, at different hydrogen peroxide concentrations (Fig. 3.31 B). Calculated K_{Mapp} of HRP/GRE for the hydrogen peroxide was 0.74 mM , while calculated Imax value was 2.69 μA. The K_M value of native HRP is 0.19 mM [198].

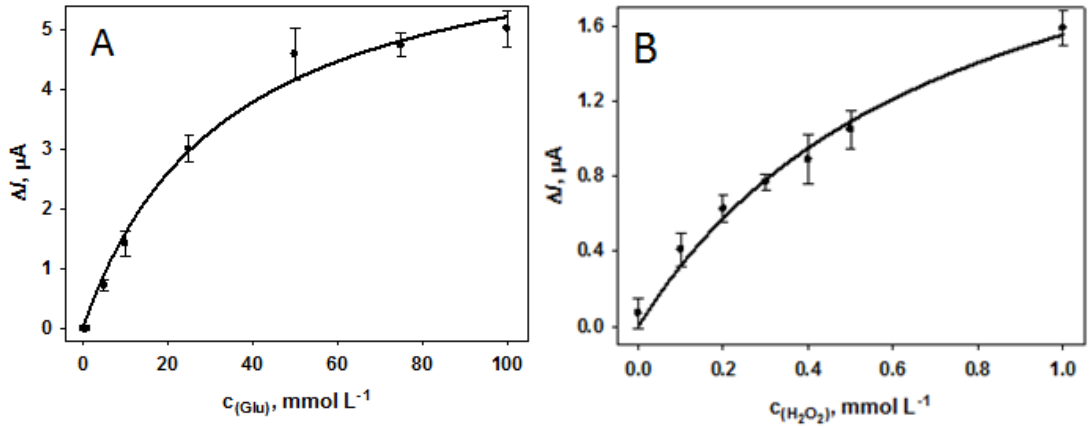

Fig. 3.31. A. Current generated by GOx/PD/GRE electrode in A-PBS, pH 6.0, at +150 mV *vs* Ag/AgCl/KClsat. **B**. Current generated by HRP/GRE electrode in A-PBS, pH 6.0, at –200 mV *vs* Ag/AgCl/KCl_{sat}.

Then the E-BFC consisting of two compartments was established and open circuit potential of E-BFC was evaluated: (i) in the presence of several different glucose concentrations in anode compartment (Fig. 3.32 A), and (ii) in the presence of several different hydrogen peroxide

concentrations in cathode compartment (Fig. 3.32 B). Two compartment based design differently from previous studies of E-BFCs [122, 129] was selected in order to investigate the influence of each substrate and/or each electrode of E-BFC to generated open circuit potential more in detail. Presented results shows, that the open circuit potential of E-BFC in the presence 200 mM of glucose in anode compartment increase up to 70 mV, while if in the presence of 200 mM glucose in anode compartment additionally 0.5 mM of H_2O_2 is added to the cathode compartment then the potential of E-BFC increase up to 640 mV. The amperometric and potentiometric studies of HRP/GRE have clearly shown that HRP is capable for the direct electron transfer if it is immobilized on the surface of GRE [122, 129].

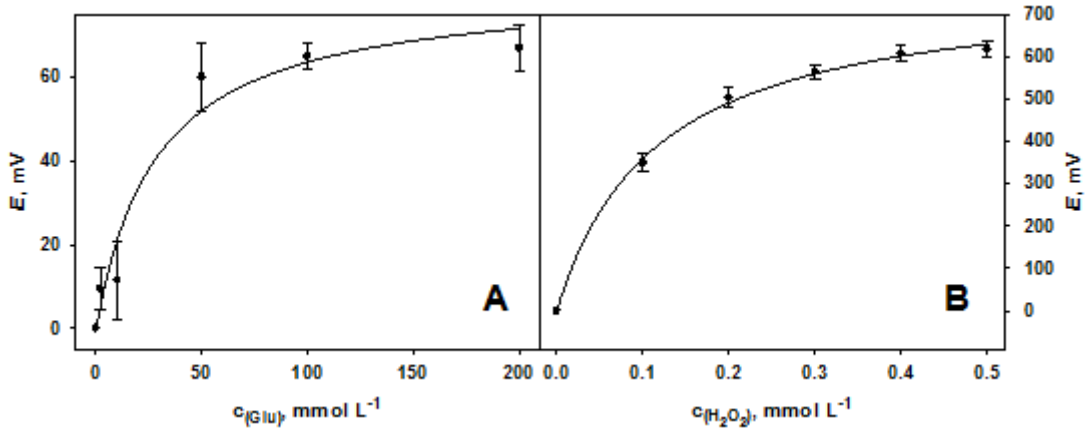

Fig. 3.32. Open circuit potential generated by BFC consisting of GOx/PD/GRE anode and HRP/GRE cathode deposited in two separated compartments switched by electrolyte-key vs: **A.** glucose concentration in anode compartment; and **B.** H_2O_2 concentration in cathode compartment in presence of 200 mM of glucose in anode compartment. A-PBS, pH 6.0, was used as solvent in both compartments.

The performance of E-BFC was tested in the presence of few different concentrations (2–200 mM) of glucose in GOx/PD/GRE anode compartment and in the absence of hydrogen peroxide in cathode compartment at different 'work-loads' ('work-load' was imitated by switching different resistances into the circuit as it is demonstrated in Fig. 3.30). It was found that the maximum power was registered at 30–60 mV and it reached 2 μW/cm (Fig. 3.33). It was determined that the maximal

voltage (Fig. 3.33 A) and power were registered in the presence of 50–200 mM of glucose. The low voltage and very moderate current was influenced by single action of only GOx/PD/GRE anode because the electron transfer out from HRP/GRE cathode in the absence of H_2O_2 was very limited. In next part of experiment the same principle was applied in order to measure potentials of E-BFC in the absence of glucose in anode compartment and the presence of different hydrogen peroxide concentrations varying in the range of 0.1–0.5 mM (Fig. 3.34). In this case the potential was also relatively low below 200 mV and power density was below 300 nA/cm.

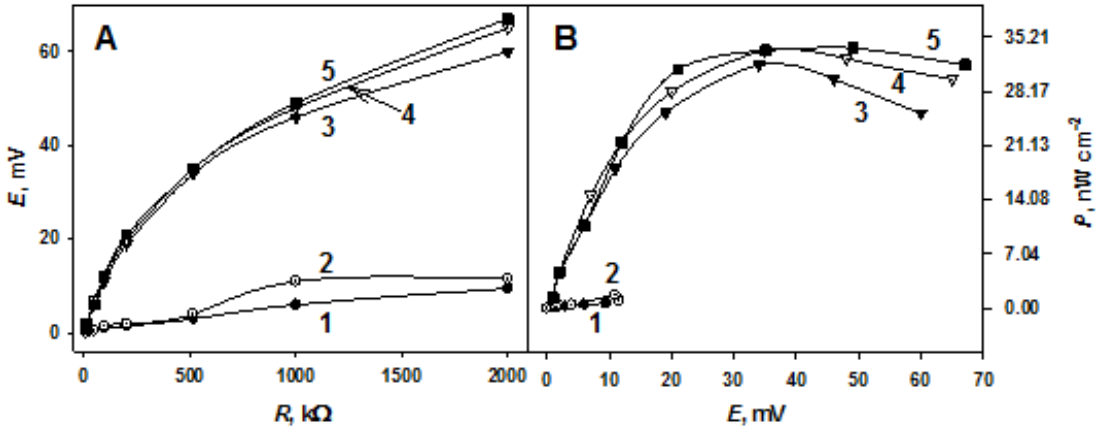

Fig. 3.33. BFC potential dependence on external resistance (A) and BFC power density dependence on generated potential (B); Biofuel cell based on GOx/PD/GRE anode and HRP/GRE cathode with 2 mM (1), 10 mM (2), 50 mM (3), 100 mM (4) and 200 mM (5) of glucose in anode compartment.

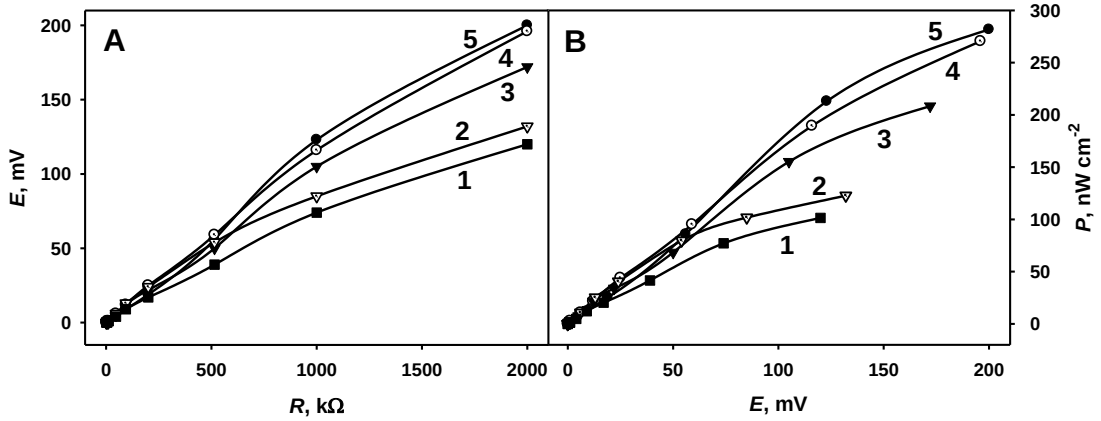

Fig. 3.34. BFC potential dependence on external resistance (**A**) and BFC power density dependence on generated potential (**B**); Biofuel cell based on GOx/PD/GRE anode and HRP/GRE cathode with 0.1 mM (1), 0.2 mM (2), 0.3 mM (3), 0.4 mM (4) and 200 mM (5) of H_2O_2 in cathode compartment.

Then the same ‘work-loads’ were applied for E-BFC, which in anode compartment contained 200 mM of glucose and in cathode compartment contained 0.1–0.5 mM of hydrogen peroxide. The voltage of the E-BFC depended on the ‘work-load’ (Fig. 3.35 A), which was switched to the circuit [4,11]. The maximal voltage of 640 mV was registered in the presence of 0.4– 0.5 mM of hydrogen peroxide in cathode compartment and 200 mM of glucose in anode compartment, while the maximal power of complete E-BFC was registered in the presence of 200 mM glucose in anode compartment and 0.5 mM of hydrogen peroxide in the cathode compartment and it was 4.2 μW/cm^2 at 530 mV (Fig. 3.35 B).

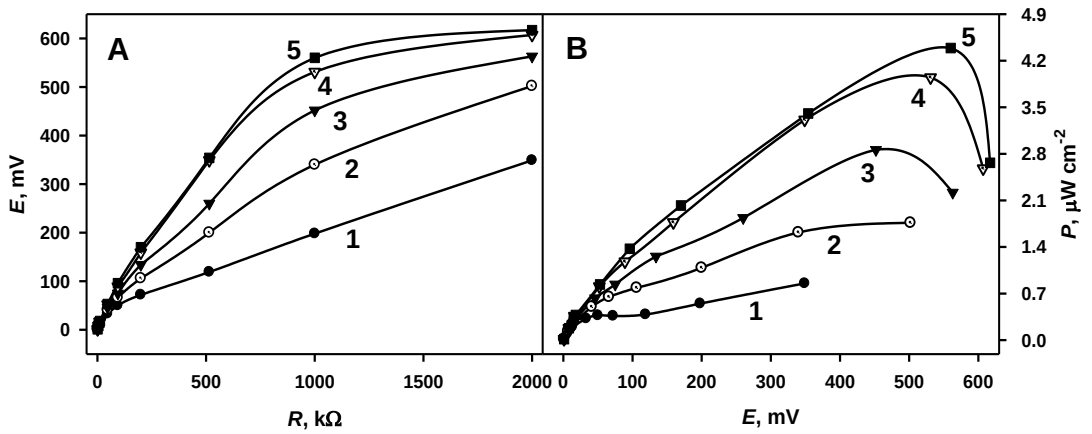

Fig. 3.35. BFC potential dependence on external resistance (A) and BFC power density dependence on generated potential (B); Biofuel cell based on GOx/PD/GRE anode and HRP/GRE cathode with 200 mM of glucose in anode compartment and with 0.1 mM (1), 0.2 mM (2), 0.3 mM (3), 0.4 mM (4) and 0.5 mM (5) of H_2O_2 in cathode compartment.

The maximal power output at 530 mV potential makes here designed E-BFC especially attractive for practical applications because this potential is already suitable for powering of low current electronics [47]. Comparison of generated potentials and E-BFC powers in the absence of one of fuels (Figs. 3.33 A, B and 3.34 A, B) with that in the presence of both fuels (Fig. 3.35 A and B), shows significant increase of both parameters in presence of both fuels, which is not equal to basic summation of that parameters registered in the absence of one of the fuels. This effect is based on the synergistic action of both electrodes,

which allowed significant increase of working potential and power of the system if fuelled by both fuels. Therefore it is clear that presence of optimal concentration of both fuels is necessary in order to gain optimal efficiency of E-BFC.

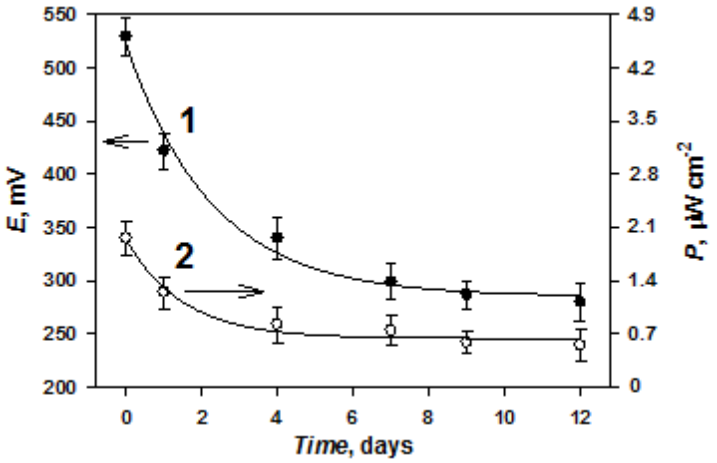

Fig. 3.36. The stability of potential (1●) and power (2○) of biofuel cell based on GOx/PD/GRE anode and HRP/GRE cathode with 200 mM of glucose in anode compartment and 0.5 mM of hydrogen peroxide in cathode compartment. Measurements performed when 2 MΩ was switched to imitate external 'work-load' of the circuit.

The stability of here designed E-BFC was tested at 20 °C. During stability test the E-BFC potential was tested by switched 2 MΩ resistance, which imitated optimal 'work-load' of circuit at initial phase of the experiment. Potential stability-tests of the complete E-BFC showed that approximately 40% of open-circuit voltage of the E-BFC was lost within 12 days (Fig. 3.36, curve 1), while the power of E-BFC at the same measurement conditions decreased by 25% (Fig. 3.36, curve 2). We predict that limited stability of the E-BFC was the mostly influenced by the instability of enzymes present in the enzymatic electrodes, what is in agreement with previous studies [4,11].

Conclusions

1. Comparing measurements at redox competition and generation-collection modes, we found that H_2O_2 diffuses very far from surface after the enzymatic reaction, while O_2 is consumed close to surface modified by GOx. Contrary the concentration of H_2O_2 is highest close to the surface, where the enzymatic reaction takes place. If horizontal scan is performed by SECM, the choose of appropriated distance is very important factor, because at closer distances measurement results can be distorted due to hindered diffusion or fast O_2 consumption. The selection of distance, which is the most suitable for the horizontal scan, should be performed taking into account concentrations of both compounds (consumed O_2 and formed H_2O_2), which appears close to the GOx-modified surface.

2. Redox competition mode of SECM is useful tool for the investigation of enzymatic reaction kinetics followed by Michaelis-Menten model. The quality of $K_{M(app.)}$ calculation can be evaluated by drawing the $K_{M(app.)}$ dependence on distance between ME-based probe and enzyme-modified surface. Conductivity of surfaces, which were used as substrates for enzyme immobilization, similarly influences the changes of $K_{M(app.)}$ *vs* distance, therefore, the RC-SECM mode is suitable for investigation of biosensors and biofuel cells, when they are operating.

3. The impedance measurements of the solution at different distances from the GOx-modified surface enabled to evaluate the concentrations of gluconic acid formed in the solution after glucose oxidation during enzymatic reaction. Here demonstrated results show that the SEIM technique could become a valuable tool for the investigation and characterization of biosensors and biofuel cells because the SEIM could be applied without any mediators, without significant perturbation of

designed bio-system, and in real-time when the biosensor or biofuel cell is operating.

4. According to our best knowledge, in present our research mathematical model of RC-SECM mode is presented for the first time. Using this model, it is possible to calculate oxygen consumption rate, to evaluate enzymatic reaction kinetics, and to determine diffusion coefficients for oxygen diffusion in the media of varying composition. The modelling of RC-SECM mode, which is taking into account both diffusion-reaction kinetics, show that the main parameter, on which depends steady-state diffusion limited current signal, is a diffusion coefficient.

5. Four redox mediators (p-benzoquinone, (pBQ), 1,10-phenanthroline-5,6-dione (PD), 2,6-dichlorophenolindophenol sodium salt hydrate (DCPIP)) and 9,10-phenantrenequinone (PQ) were tested in two redox mediators based electrochemical system in order to check the charge transfer efficiency from yeast cells at aerobic conditions. It was found that the most effective out of here evaluated lipophilic redox mediators was the PQ, the UME current in the presence of PQ was about 3 times higher compared with that registered in the presence of other three redox mediators. For the determination of cell viability at different pH the Hill's function was successfully applied.

6. Enzymatic biofuel cell based on GOx/PD/GRE anode powered by glucose and HRP/GRE cathode powered hydrogen peroxide was developed and evaluated. Such new design of biofuel cell allows to utilize glucose as a fuel for the anode, and H_2O_2 formed during the catalytic action of GOx, which is immobilized on anode, could be utilized as a fuel at the cathode of the same biofuel cell. According to our best knowledge such kind of biofuel cell design is proposed for the first time.

List of publications

Morkvenaite-Vilkonciene, Inga, Ramanaviciene, Almira, and Ramanavicius, Arunas, 9,10-Phenanthrenequinone as a Redox Mediator for the Imaging of Yeast Cells by Scanning Electrochemical Microscopy. Sensors & Actuators: B. Chemical, 2016. 228: p. 200-206.

Morkvenaite-Vilkonciene, Inga, Genys, Povilas, Ramanaviciene, Almira, and Ramanavicius, Arunas, Scanning electrochemical impedance microscopy for investigation of glucose oxidase catalyzed reaction. Colloids Surf B Biointerfaces, 2015. 126: p. 598-602.

Ramanavicius, Arunas, Kausaite-Minkstimiene, Asta, **Morkvenaite-Vilkonciene, Inga**, Genys, Povilas, Mikhailova, Raisa, Semashko, Tatiana, Voronovic, Jaroslav and Ramanaviciene, Almira, Biofuel cell based on glucose oxidase from Penicillium funiculosum 46.1 and horseradish peroxidase. Chemical Engineering Journal, 2015. 264: p. 165-173.

Morkvenaite-Vilkonciene, Inga, Ramanaviciene, Almira, and Ramanavicius, Arunas, Redox competition and generation-collection modes based scanning electrochemical microscopy for the evaluation of immobilised glucose oxidase-catalysed reactions. RSC Advances, 2014. **4**(91): p. 50064-50069.

Morkvenaite-Vilkonciene, Inga, Ramanavicius, Arunas, and Ramanaviciene, Almira, Atomic Force Microscopy as a Tool for the Investigation of Living Cells. Medicina, 2013. 49(4): p. 155-164.

Scientific conferences:

Morkvenaite-Vilkonciene, I., Sareikaite, A. Ramanavicius. 9,10-Phenanthrenequinone as a Redox Mediator for the Imaging of Yeast Cells by Scanning Electrochemical Microscopy. S5. 2nd International Conference of Chemists „Nanochemistry and Nanomaterials“, Vilnius University. October 23, 2015.

Morkvenaite-Vilkonciene, I., Genys, P., Ramanaviciene, A., Ramanavicius, A. Scanning electrochemical microscopy in combination with electrochemical impedance spectroscopy as a tool for the monitoring of glucose oxidase catalyzed reaction. Nanotechnology: research and development : conference book : Vilnius, Lithuania, 15-16 May 2014. Vilnius, Lietuvos mokslų akademija, 2014. ISBN 9789955937142. 2014. P. 72.

Morkvenaite-Vilkonciene, I., Kisieliute, A., Voronovic, J., Ramanaviciene, A., Ramanavicius, A. Investigation of electrochemical activity of Saccharomyces cerevisiae by scanning electrochemical microscopy. Advanced materials and technologies : book of abstracts of the 16-th international conference-school, Palanga, Lithuania, 27-31 August 2014. Kaunas, Technologija. ISSN 1822-7759. 2014. p. [31 p.].

Morkvenaite-Vilkonciene, I., Ramanavicius, A., Ramanaviciene, A. Scanning electrochemical microscopy for the determination of enzymatic kinetics. CEEC-TAC2 : 2nd Central and Eastern European conference on thermal analysis and calorimetry : book of abstracts, 27-30 August 2013, Vilnius, Lithuania. Vilnius, 2013. ISBN 9783940237330. 2013. p. 90.

Morkvenaite-Vilkonciene, I., Astrauskaite, I., Ramanavicius, A. Scanning electrochemical microscopy analysis in feedback mode of immobilized glucose oxidase. EcoBalt 2013 : 18th international scientific conference, Vilnius, Lithuania, October 25-27, 2013 : book of abstracts. Vilnius, Vilniaus universiteto leidykla, 2013. ISBN 9786094592416. p. 34.

Morkvenaite-Vilkonciene, I., Genys, P., Ramanavicius, A. Alternating current scanning electrochemical microscopy for investigation of conducting surfaces. ITELMS'2013 : Intelligent technologies in logistics and mechatronics systems : proceedings of the 8th international conference, May 23-24, 2013, Panevėžys, Lithuania. Kaunas, Technologija. ISSN 2345-0088. 2013.

Morkvenaite-Vilkonciene, I., Astrauskaite, I., Ramanavicius, A. Characterization of biosensor surface by scanning electrochemical microscopy. ITELMS'2013 : Intelligent technologies in logistics and mechatronics systems : proceedings of the 8th international conference, May

23-24, 2013, Panevėžys, Lithuania. Kaunas, Technologija. ISSN 2345-0088. 2013.

Morkvenaite-Vilkonciene, I. and Ramanavicius, A.. Imaging Glucose Oxidase by Scanning Electrochemical Microscopy. in 2nd International Conference on Nanotechnologies and Biomedical Engineering. 2013. Chisinau, Moldova: Technical University of Moldova.

Co-author

Ramanavicius, A., **Morkvenaite-Vilkonciene, I.**, Sareikaite, R., Kisieliute, A., Genys, P., Petroniene, J., Ramanaviciene, A. Imaging of Immobilized Enzymes and Yeast Cells by Scanning Electrochemical Microscopy. (1000-6). PITTCON 2016. March 6 -10, 2016. Atlanta, Georgia, USA.

Ramanavicius, A., German, N., Kausaite-Minkstimiene, A., **Morkvenaite-Vilkonciene, I.**, Genys, P., Voronovic, J., Petroniene, J., Ramanaviciene, A. Advances in Development of Glucose Biosensors. (980-2). PITTCON 2016. March 6 -10, 2016. Atlanta, Georgia, USA.

Kisieliute, A., **Morkvenaite-Vilkonciene**, **I.,** Andriukonis, E., Ramanavicius, A. Investigation of Yeast Modified with Polypyrrole by Scanning Electrochemical Microscopy. P4. 2nd International Conference of Chemists „Nanochemistry and Nanomaterials“ Vilnius University. October 23, 2015.

Ramanavicius, A., **Morkvenaite-Vilkonciene, I.,** Kausaite, A., Ramanaviciene, A. Electron transfer pathways in electrochemical biosensors and in some other biodevices. Photosynthetic proteins for technological applications: biosensors and biochips (PHOTOTECH) : 2nd plenary workshop and management committee meeting: information, programme and abstracts, 9-11 April, 2014, Istanbul, Turkey. Ankara, Hacettepe university. 2014. p. 4.

Curriculum Vitae

Name, Surname Inga Morkvėnaitė-Vilkončienė
E-mail inga.morkvenaite-vilkonciene@chf.vu.lt
Date of birth 1979-07-06

EDUCATION

2012-2016 Vilnius University, Faculty of Chemistry, doctoral studies, Chemistry
2009-2011 Kaunas University of Technology, Faculty of Technologies, Master degree studies, Control technology
2005-2009 Kaunas University of Technology, Faculty of Technologies, Bachelor degree studies, Electrical Engineering
2001-2004 Panevezys College, Faculty of Management and Technologies, Electrical and Automation devices

CURRENT RESEARCH AND ACADEMIC POSITIONS

2016 – … Vilnius Gediminas Technical University, Lecturer
2013 – … University of Applied Sciences, Lecturer
2013 – 2014 Center for Physical Sciences and Technology, Researcher
2008 – 2012 Panevėžys mechatronics center, Researcher

PROFESSIONAL TRAINING

2013 November Laboratory of Physical Chemistry and Microbiology for the Environment, Nancy, France.

References

[1] W. Nogala, K. Szot, M. Burchardt, M. Jonsson-Niedziolka, J. Rogalski, G. Wittstock, M. Opallo, Scanning electrochemical microscopy activity mapping of electrodes modified with laccase encapsulated in sol-gel processed matrix, Bioelectrochemistry, 79 (2010) 101-107.
[2] R. Lei, L. Stratmann, D. Schafer, T. Erichsen, S. Neugebauer, N. Li, W. Schuhmann, Imaging Biocatalytic Activity of Enzyme-Polymer Spots by Means of Combined Scanning Electrochemical Microscopy/Electrogenerated Chemiluminescence, Anal. Chem., 81 (2009) 5070-5074.
[3] G. Wittstock, W. Schuhmann, Formation and imaging of microscopic enzymatically active spots on an alkanethiolate-covered gold electrode by scanning electrochemical microscopy, Anal. Chem., 69 (1997) 5059-5066.
[4] D.T. Pierce, P.R. Unwin, A.J. Bard, Scanning electrochemical microscopy. 17. Studies of enzyme-mediator kinetics for membrane- and surface-immobilized glucose oxidase, Anal. Chem., 64 (1992) 1795-1804.
[5] G. Wittstock, M. Burchardt, S.E. Pust, Y. Shen, C. Zhao, Scanning Electrochemical Microscopy for Direct Imaging of Reaction Rates, Angewandte Chemie International Edition, 46 (2007) 1584-1617.
[6] R. Teranishi, E. Higuchi, M. Chiku, H. Inoue, Analysis of Kinetics of Oxygen Reduction Reaction in Alkaline Solution by Scanning Electrochemical Microscopy, Ecs Transactions, 41 (2011) 2179-2184.
[7] J.L. Fernández, A.J. Bard, Scanning electrochemical microscopy. 47. Imaging electrocatalytic activity for oxygen reduction in an acidic medium by the tip generation-substrate collection mode, Anal. Chem., 75 (2003) 2967-2974.
[8] H. Ye, H.S. Park, A.J. Bard, Screening of Electrocatalysts for Photoelectrochemical Water Oxidation on W-Doped BiVO4 Photocatalysts by Scanning Electrochemical Microscopy, Journal of Physical Chemistry C, 115 (2011) 12464-12470.
[9] C.H. Jung, C.M. Sanchez-Sanchez, C.L. Lin, J. Rodriguez-Lopez, A.J. Bard, Electrocatalytic Activity of Pd-Co Bimetallic Mixtures for Formic Acid Oxidation Studied by Scanning Electrochemical Microscopy, Anal. Chem., 81 (2009) 7003-7008.
[10] L. Guadagnini, A. Maljusch, X.X. Chen, S. Neugebauer, D. Tonelli, W. Schuhmann, Visualization of electrocatalytic activity of microstructured metal hexacyanoferrates by means of redox competition mode of scanning electrochemical microscopy (RC-SECM), Electrochimica Acta, 54 (2009) 3753-3758.
[11] T. Yasukawa, Y. Hirano, N. Motochi, H. Shiku, T. Matsue, Enzyme immunosensing of pepsinogens 1 and 2 by scanning electrochemical microscopy, Biosens. Bioelectron., 22 (2007) 3099-3104.
[12] C. Zhao, G. Wittstock, Scanning electrochemical microscopy for detection of biosensor and biochip surfaces with immobilized pyrroloquinoline quinone (PQQ)-dependent glucose dehydrogenase as enzyme label, Biosens Bioelectron, 20 (2005) 1277-1284.
[13] A.J. Bard, M.V. Mirkin, Scanning Electrochemical Microscopy, Marcel Dekker, NY, 2001.

[14] M. Burchardt, M. Träuble, G. Wittstock, Digital Simulation of Scanning Electrochemical Microscopy Approach Curves to Enzyme Films with Michaelis−Menten Kinetics, Anal. Chem., 81 (2009) 4857-4863.
[15] M. Pellissier, D. Zigah, F. Barriere, P. Hapiot, Optimized preparation and scanning electrochemical microscopy analysis in feedback mode of glucose oxidase layers grafted onto conducting carbon surfaces, Langmuir, 24 (2008) 9089-9095.
[16] D. Zigah, M. Pellissier, B. Fabre, F. Barriere, P. Hapiot, Covalent immobilization and SECM analysis in feedback mode of glucose oxidase on a modified oxidized silicon surface, Journal of Electroanalytical Chemistry, 628 (2009) 144-147.
[17] M. Burchardt, G. Wittstock, Kinetic studies of glucose oxidase in polyelectrolyte multilayer films by means of scanning electrochemical microscopy (SECM), Bioelectrochemistry, 72 (2008) 66-76.
[18] A.J. Bard, F.R.F. Fan, J. Kwak, O. Lev, Scanning electrochemical microscopy. Introduction and principles, Anal. Chem., 61 (1989) 132-138.
[19] T. Wilhelm, G. Wittstock, R. Szargan, Scanning electrochemical microscopy of enzymes immobilized on structured glass-gold substrates, Fresen J Anal Chem, 365 (1999) 163-167.
[20] S.A.G. Evans, K. Brakha, M. Billon, P. Mailley, G. Denuault, Scanning electrochemical microscopy (SECM): localized glucose oxidase immobilization via the direct electrochemical microspotting of polypyrrole-biotin films, Electrochem. Commun., 7 (2005) 135-140.
[21] J. Zaumseil, G. Wittstock, S. Bahrs, P. Steinrucke, Imaging the activity of nitrate reductase by means of a scanning electrochemical microscope, Fresen J Anal Chem, 367 (2000) 352-355.
[22] G. Wittstock, T. Wilhelm, Characterization and manipulation of microscopic biochemically active regions by scanning electrochemical microscopy (SECM), Anal Sci, 18 (2002) 1199-1204.
[23] T. Wilhelm, G. Wittstock, Analysis of interaction in patterned multienzyme layers by using scanning electrochemical microscopy, Angewandte Chemie (International ed. in English), 42 (2003) 2248-2250.
[24] H. Shiku, T. Shiraishi, H. Ohya, T. Matsue, H. Abe, H. Hoshi, M. Kobayashi, Oxygen consumption of single bovine embryos probed by scanning electrochemical microscopy, Anal. Chem., 73 (2001) 3751-3758.
[25] E.M.H. Amine, Visualization of local biocatalytic activity using scanning electrochemical microscopy, Bochum, Bochum, Germany, 2008, pp. 120.
[26] S. Amemiya, J. Guo, H. Xiong, D.A. Gross, Biological applications of scanning electrochemical microscopy: chemical imaging of single living cells and beyond, Anal Bioanal Chem, 386 (2006) 458-471.
[27] A. Schulte, M. Nebel, W. Schuhmann, Single Live Cell Topography and Activity Imaging with the Shear-Force-Based Constant-Distance Scanning Electrochemical Microscope, Imaging and Spectroscopic Analysis of Living Cells: Optical and spectroscopic techniques, 504 (2012) 237-254.
[28] R. Cornut, A. Bhasin, S. Lhenry, M. Etienne, C. Lefrou, Accurate and Simplified Consideration of the Probe Geometrical Defaults in Scanning Electrochemical Microscopy: Theoretical and Experimental Investigations, Anal. Chem., 83 (2011) 9669-9675.

[29] M. Nebel, S. Grutzke, N. Diab, A. Schulte, W. Schuhmann, Microelectrochemical visualization of oxygen consumption of single living cells, Faraday Discuss, 164 (2013) 19-32.
[30] M. Nebel, S. Grützke, N. Diab, A. Schulte, W. Schuhmann, Visualization of Oxygen Consumption of Single Living Cells by Scanning Electrochemical Microscopy: The Influence of the Faradaic Tip Reaction, Angewandte Chemie International Edition, 52 (2013) 6335-6338.
[31] P.M. Diakowski, Z.F. Ding, Interrogation of living cells using alternating current scanning electrochemical microscopy (AC-SECM), Physical Chemistry Chemical Physics, 9 (2007) 5966-5974.
[32] B.R. Horrocks, M.V. Mirkin, D.T. Pierce, A.J. Bard, G. Nagy, K. Toth, Scanning Electrochemical Microscopy .19. Ion-Selective Potentiometric Microscopy, Anal. Chem., 65 (1993) 1213-1224.
[33] B. Liu, W. Cheng, S.A. Rotenberg, M.V. Mirkin, Scanning electrochemical microscopy of living cells - Part 2. Imaging redox and acid/basic reactivities, Journal of Electroanalytical Chemistry, 500 (2001) 590-597.
[34] A.J. Bard, J. Kwak, Scanning Electrochemical Microscopy. Apparatus and Two-Dimensional Scans of Conductive and Insulating Substrates, Anal. Chem., 61 (1989) 1794-1799.
[35] J.P. Li, J.G. Yu, Fabrication of Prussian Blue modified ultramicroelectrode for GOD imaging using scanning electrochemical microscopy, Bioelectrochemistry, 72 (2008) 102-106.
[36] K. Borgwarth, C. Ricken, D.G. Ebling, J. Heinze, Surface analysis by scanning electrochemical microscopy: Resolution studies and applications to polymer samples, Fresen J Anal Chem, 356 (1996) 288-294.
[37] T. Yasukawa, Y. Kondo, I. Uchida, T. Matsue, Imaging of Cellular Activity of Single Cultured Cells by Scanning Electrochemical Microscopy, Chem Lett, 27 (1998) 767-768.
[38] Y. Hirano, D. Oyamatsu, T. Yasukawa, H. Shiku, T. Matsue, Scanning electrochemical microscopy for protein chip Imaging and shear force feedback regulation of substrate-probe distance, Electrochemistry, 72 (2004) 137-142.
[39] H. Shiku, T. Shiraishi, S. Aoyagi, Y. Utsumi, M. Matsudaira, H. Abe, H. Hoshi, S. Kasai, H. Ohya, T. Matsue, Respiration activity of single bovine embryos entrapped in a cone-shaped microwell monitored by scanning electrochemical microscopy, Anal Chim Acta, 522 (2004) 51-58.
[40] T. Kaya, Y.-s. Torisawa, D. Oyamatsu, M. Nishizawa, T. Matsue, Monitoring the cellular activity of a cultured single cell by scanning electrochemical microscopy (SECM). A comparison with fluorescence viability monitoring, Biosensors and Bioelectronics, 18 (2003) 1379-1383.
[41] Y.-s. Torisawa, T. Kaya, Y. Takii, D. Oyamatsu, M. Nishizawa, T. Matsue, Scanning electrochemical microscopy-based drug sensitivity test for a cell culture integrated in silicon microstructures, Anal. Chem., 75 (2003) 2154-2158.
[42] Y.-s. Torisawa, H. Shiku, T. Yasukawa, M. Nishizawa, T. Matsue, Three-dimensional micro-culture system with a silicon-based cell array device for multi-channel drug sensitivity test, Sensors and Actuators B: Chemical, 108 (2005) 654-659.
[43] L.L. Zhu, N. Gao, X.L. Zhang, W.R. Jin, Accurately measuring respiratory activity of single living cells by scanning electrochemical microscopy, Talanta, 77 (2008) 804-808.

[44] M. Ludwig, C. Kranz, W. Schuhmann, H.E. Gaub, Topography feedback mechanism for the scanning electrochemical microscope based on hydrodynamic forces between tip and sample, Rev Sci Instrum, 66 (1995) 2857-2860.
[45] A. Hengstenberg, C. Kranz, W. Schuhmann, Facilitated Tip-Positioning and Applications of Non-Electrode Tips in Scanning Electrochemical Microscopy Using a Shear Force Based Constant-Distance Mode, Chemistry – A European Journal, 6 (2000) 1547-1554.
[46] B. Ballesteros Katemann, A. Schulte, W. Schuhmann, Constant-distance mode scanning electrochemical microscopy (SECM)--Part I: Adaptation of a non-optical shear-force-based positioning mode for SECM tips, Chemistry, 9 (2003) 2025-2033.
[47] M. Nebel, K. Eckhard, T. Erichsen, A. Schulte, W. Schuhmann, 4D Shearforce-Based Constant-Distance Mode Scanning Electrochemical Microscopy, Anal. Chem., 82 (2010) 7842-7848.
[48] J.V. Macpherson, P.R. Unwin, A.C. Hillier, A.J. Bard, In-Situ Imaging of Ionic Crystal Dissolution Using an Integrated Electrochemical/AFM Probe, Journal of the American Chemical Society, 118 (1996) 6445-6452.
[49] D.J. Comstock, J.W. Elam, M.J. Pellin, M.C. Hersam, Integrated ultramicroelectrode− nanopipet probe for concurrent scanning electrochemical microscopy and scanning ion conductance microscopy, Anal. Chem., 82 (2010) 1270-1276.
[50] B. Ballesteros Katemann, A. Schulte, W. Schuhmann, Constant-Distance Mode Scanning Electrochemical Microscopy (SECM)—Part I: Adaptation of a Non-Optical Shear-Force-Based Positioning Mode for SECM Tips, Chem. Eur. J., 9 (2003) 2025-2033.
[51] P.I. James, L.F. Garfias-Mesias, P.J. Moyer, W.H. Smyrl, Scanning Electrochemical Microscopy with Simultaneous Independent Topography, Journal of The Electrochemical Society, 145 (1998) L64-L66.
[52] M.A. Alpuche-Aviles, D.O. Wipf, Impedance Feedback Control for Scanning Electrochemical Microscopy, Anal. Chem., 73 (2001) 4873-4881.
[53] K. Eckhard, H. Shin, B. Mizaikoff, W. Schuhmann, C. Kranz, Alternating current (AC) impedance imaging with combined atomic force scanning electrochemical microscopy (AFM-SECM), Electrochem. Commun., 9 (2007) 1311-1315.
[54] C. Kranz, J. Wiedemair, Scanning force microscopy based amperometric biosensors, Anal. Bioanal. Chem., 390 (2008) 239-243.
[55] J. Kwak, A.J. Bard, Scanning electrochemical microscopy. Theory of the feedback mode, Anal. Chem., 61 (1989) 1221-1227.
[56] R. Cornut, C. Lefrou, A unified new analytical approximation for negative feedback currents with a microdisk SECM tip, Journal of Electroanalytical Chemistry, 608 (2007) 59-66.
[57] R. Cornut, C. Lefrou, New analytical approximation of feedback approach curves with a microdisk SECM tip and irreversible kinetic reaction at the substrate, Journal of Electroanalytical Chemistry, 621 (2008) 178-184.
[58] A.J. Bard, M.V. Mirkin, P.R. Unwin, D.O. Wipf, Scanning Electrochemical Microscopy .12. Theory and Experiment of the Feedback Mode with Finite Heterogeneous Electron-Transfer Kinetics and Arbitrary Substrate Size, J Phys Chem-Us, 96 (1992) 1861-1868.

[59] C. Kranz, G. Wittstock, H. Wohlschlager, W. Schuhmann, Imaging of microstructured biochemically active surfaces by means of scanning electrochemical microscopy, Electrochimica Acta, 42 (1997) 3105-3111.
[60] G. Wittstock, Modification and characterization of artificially patterned enzymatically active surfaces by scanning electrochemical microscopy, Fresenius J Anal Chem, 370 (2001) 303-315.
[61] R.E. Gyurcsányi, G. Jágerszki, G. Kiss, K. Tóth, Chemical imaging of biological systems with the scanning electrochemical microscope, Bioelectrochemistry, 63 (2004) 207-215.
[62] K. Eckhard, X. Chen, F. Turcu, W. Schuhmann, Redox competition mode of scanning electrochemical microscopy (RC-SECM) for visualisation of local catalytic activity, Physical Chemistry Chemical Physics, 8 (2006) 5359-5365.
[63] A.O. Okunola, T.C. Nagaiah, X.X. Chen, K. Eckhard, W. Schuhmann, M. Bron, Visualization of local electrocatalytic activity of metalloporphyrins towards oxygen reduction by means of redox competition scanning electrochemical microscopy (RC-SECM), Electrochimica Acta, 54 (2009) 4971-4978.
[64] K. Karnicka, K. Eckhard, D.A. Guschin, L. Stoica, P.J. Kulesza, W. Schuhmann, Visualisation of the local bio-electrocatalytic activity in biofuel cell cathodes by means of redox competition scanning electrochemical microscopy (RC-SECM), Electrochem. Commun., 9 (2007) 1998-2002.
[65] W. Nogala, M. Burchardt, M. Opallo, J. Rogalski, G. Wittstock, Scanning electrochemical microscopy study of laccase within a sol-gel processed silicate film, Bioelectrochemistry, 72 (2008) 174-182.
[66] P.R. Unwin, A.J. Bard, Scanning Electrochemical Microscopy .9. Theory and Application of the Feedback Mode to the Measurement of Following Chemical-Reaction Rates in Electrode Processes, J Phys Chem-Us, 95 (1991) 7814-7824.
[67] M.V. Mirkin, A.J. Bard, Multidimensional integral equations: a new approach to solving microelectrode diffusion problems: Part 2. Applications to microband electrodes and the scanning electrochemical microscope, Journal of Electroanalytical Chemistry, 323 (1992) 29-51.
[68] Y. Selzer, D. Mandler, Scanning Electrochemical Microscopy. Theory of the Feedback Mode for Hemispherical Ultramicroelectrodes: Steady-State and Transient Behavior, Anal. Chem., 72 (2000) 2383-2390.
[69] O. Sklyar, G. Wittstock, Numerical Simulations of Complex Nonsymmetrical 3D Systems for Scanning Electrochemical Microscopy Using the Boundary Element Method, The Journal of Physical Chemistry B, 106 (2002) 7499-7508.
[70] P. Liljeroth, C. Johans, C.J. Slevin, B.M. Quinn, K. Kontturi, Disk-Generation/Ring-Collection Scanning Electrochemical Microscopy: Theory and Application, Anal. Chem., 74 (2002) 1972-1978.
[71] T. Nann, J. Heinze, Simulation in electrochemistry using the finite element method part 2: scanning electrochemical microscopy, Electrochimica Acta, 48 (2003) 3975-3980.
[72] J.L. Amphlett, G. Denuault, Scanning Electrochemical Microscopy (SECM): An Investigation of the Effects of Tip Geometry on Amperometric Tip Response, The Journal of Physical Chemistry B, 102 (1998) 9946-9951.
[73] O. Sklyar, A. Kueng, C. Kranz, B. Mizaikoff, A. Lugstein, E. Bertagnolli, G. Wittstock, Numerical simulation of scanning electrochemical microscopy experiments with

frame-shaped integrated atomic force microscopy--SECM probes using the boundary element method, Anal Chem, 77 (2005) 764-771.
[74] O. Sklyar, M. Trauble, C. Zhao, G. Wittstock, Modeling steady-state experiments with a scanning electrochemical microscope involving several independent diffusing species using the boundary element method, Journal of Physical Chemistry B, 110 (2006) 15869-15877.
[75] R.D. Martin, P.R. Unwin, Scanning electrochemical microscopy: theory and experiment for the positive feedback mode with unequal diffusion coefficients of the redox mediator couple, Journal of Electroanalytical Chemistry, 439 (1997) 123-136.
[76] T. Nann, J. Heinze, Simulation in electrochemistry using the finite element method: Part 1: The algorithm, Electrochem. Commun., 1 (1999) 289-294.
[77] F.L. Qiu, A.C. Fisher, The boundary element method: chronoamperometric simulations at microelectrodes, Electrochem. Commun., 5 (2003) 87-93.
[78] F.L. Qiu, A.C. Fisher, The dual reciprocity method: simulation of potential step voltammetry at microelectrodes, Electrochem. Commun., 2 (2000) 738-742.
[79] O. Sklyar, J. Ufheil, J. Heinze, G. Wittstock, Application of the boundary element method numerical simulations for characterization of heptode ultramicroelectrodes in SECM experiments, Electrochimica Acta, 49 (2003) 117-128.
[80] B. Haghighi, M.A. Tabrizi, Direct electron transfer from glucose oxidase immobilized on an overoxidized polypyrrole film decorated with Au nanoparticles, Coll. Surf. B, 103 (2013) 566-571.
[81] M.E. Ghica, R.C. Carvalho, A. Amine, C.M.A. Brett, Glucose oxidase enzyme inhibition sensors for heavy metals at carbon film electrodes modified with cobalt or copper hexacyanoferrate, Sens. Actuat. B-Chem., 178 (2013) 270-278.
[82] Y.P. Dong, L. Huang, X.F. Chu, L.Z. Pei, An Amperometric Glucose Biosensor Based on the Immobilization of Glucose Oxidase on the CuGeO3 Nanowire Modified Electrode, Russ. J. Electrochem., 49 (2013) 571-576.
[83] M. Ammam, J. Fransaer, Combination of laccase and catalase in construction of H2O2-O-2 based biocathode for applications in glucose biofuel cells, Biosens. Bioelectron., 39 (2013) 274-281.
[84] S. Bourigua, A. Maaref, F. Bessueille, N.J. Renault, A New Design of Electrochemical and Optical Biosensors Based on Biocatalytic Growth of Au Nanoparticles Example of Glucose Detection, Electroanal., 25 (2013) 644-651.
[85] A.S. Bandarenka, K. Eckhard, A. Maljusch, W. Schuhmann, Localized Electrochemical Impedance Spectroscopy: Visualization of Spatial Distributions of the Key Parameters Describing Solid/Liquid Interfaces, Anal. Chem., 85 (2013) 2443-2448.
[86] V. Kuznetsov, A. Maljusch, R.M. Souto, A.S. Bandarenka, W. Schuhmann, Characterisation of localised corrosion processes using scanning electrochemical impedance microscopy, Electrochem. Commun., 44 (2014) 38-41.
[87] M.V. Mirkin, W. Nogala, J. Velmurugan, Y. Wang, Scanning electrochemical microscopy in the 21st century. Update 1: five years after, Physical Chemistry Chemical Physics, 13 (2011) 21196-21212.
[88] M. Ciobanu, D.E. Taylor, J.P. Wilburn, D.E. Cliffel, Glucose and lactate biosensors for scanning electrochemical microscopy imaging of single live cells, Anal. Chem., 80 (2008) 2717-2727.

[89] B.R. Horrocks, D. Schmidtke, A. Heller, A.J. Bard, Scanning electrochemical microscopy. 24. Enzyme ultramicroelectrodes for the measurement of hydrogen peroxide at surfaces, Anal. Chem., 65 (1993) 3605-3614.
[90] K. Eckhard, T. Erichsen, M. Stratmann, W. Schuhmann, Frequency-dependent alternating-current scanning electrochemical microscopy (4D AC-SECM) for local visualisation of corrosion sites, Chem. Eur. J., 14 (2008) 3968-3976.
[91] K. Eckhard, C. Kranz, H. Shin, B. Mizaikoff, W. Schuhmann, Frequency dependence of the electrochemical activity contrast in AC-scanning electrochemical microscopy and atomic force microscopy-AC-scanning electrochemical microscopy imaging, Anal. Chem., 79 (2007) 5435-5438.
[92] P.M. Diakowski, Z.F. Ding, Novel strategy for constant-distance imaging using alternating current scanning electrochemical microscopy, Electrochem. Commun., 9 (2007) 2617-2621.
[93] B. Ballesteros Katemann, A. Schulte, E.J. Calvo, M. Koudelka-Hep, W. Schuhmann, Localised electrochemical impedance spectroscopy with high lateral resolution by means of alternating current scanning electrochemical microscopy, Electrochem. Commun., 4 (2002) 134-138.
[94] V. Kuznetsov, A. Maljusch, R.M. Souto, A.S. Bandarenka, W. Schuhmann, Characterisation of Localised Corrosion Processes Using Scanning Electrochemical Impedance Microscopy, Electrochem. Commun., (2014).
[95] C. Gabrielli, M. Keddam, N. Portail, P. Rousseau, H. Takenouti, V. Vivier, Electrochemical Impedance Spectroscopy Investigations of a Microelectrode Behavior in a Thin-Layer Cell: Experimental and Theoretical Studies, The Journal of Physical Chemistry B, 110 (2006) 20478-20485.
[96] C. Gabrielli, F. Huet, M. Keddam, P. Rousseau, V. Vivier, Scanning Electrochemical Microscopy Imaging by Means of High-Frequency Impedance Measurements in Feedback Mode, The Journal of Physical Chemistry B, 108 (2004) 11620-11626.
[97] A.S. Baranski, P.M. Diakowski, Application of AC impedance techniques to Scanning Electrochemical Microscopy, J. Solid State Electrochem., 8 (2004) 683-692.
[98] S. Ostergaard, L. Olsson, J. Nielsen, Metabolic engineering of Saccharomyces cerevisiae, Microbiology and Molecular Biology Reviews, 64 (2000) 34-50.
[99] L. Campanella, G. Favero, M. Tomassetti, Immobilised yeast cells biosensor for total toxicity testing, Science of the total environment, 171 (1995) 227-234.
[100] L. Campanella, G. Favero, D. Mastrofini, M. Tomassetti, Further developments in toxicity cell biosensors, Sensors and Actuators B: Chemical, 44 (1997) 279-285.
[101] K. Baronian, The use of yeast and moulds as sensing elements in biosensors, Biosensors and bioelectronics, 19 (2004) 953-962.
[102] M.V. Gonchar, M.M. Maidan, O.M. Moroz, J.R. Woodward, A.A. Sibirny, Microbial O 2-and H 2 O 2-electrode sensors for alcohol assays based on the use of permeabilized mutant yeast cells as the sensitive bioelements, Biosensors and Bioelectronics, 13 (1998) 945-952.
[103] E. Akyilmaz, A. Erdoğan, R. Öztürk, İ. Yaşa, Sensitive determination of l-lysine with a new amperometric microbial biosensor based on Saccharomyces cerevisiae yeast cells, Biosensors and Bioelectronics, 22 (2007) 1055-1060.
[104] E. Akyilmaz, E. Dinçkaya, An amperometric microbial biosensor development based on Candida tropicalis yeast cells for sensitive determination of ethanol, Biosensors and Bioelectronics, 20 (2005) 1263-1269.

[105] Y. Korpan, M. Gonchar, N. Starodub, A. Shulga, A. Sibirny, A. Elskaya, A cell biosensor specific for formaldehyde based on pH-sensitive transistors coupled to methylotrophic yeast cells with genetically adjusted metabolism, Anal Biochem, 215 (1993) 216-222.
[106] N. Billinton, M. Barker, C. Michel, A. Knight, W.-D. Heyer, N. Goddard, P. Fielden, R. Walmsley, Development of a green fluorescent protein reporter for a yeast genotoxicity biosensor, Biosensors and Bioelectronics, 13 (1998) 831-838.
[107] R. Hollis, K. Killham, L. Glover, Design and application of a biosensor for monitoring toxicity of compounds to eukaryotes, Appl Environ Microb, 66 (2000) 1676-1679.
[108] C.E. Rodriguez, M. Shinyashiki, J. Froines, R.C. Yu, J.M. Fukuto, A.K. Cho, An examination of quinone toxicity using the yeast< i> Saccharomyces cerevisiae</i> model system, Toxicology, 201 (2004) 185-196.
[109] C.E. Rodriguez, Z. Sobol, R.H. Schiestl, 9, 10-Phenanthrenequinone induces DNA deletions and forward mutations via oxidative mechanisms in the yeast Saccharomyces cerevisiae, Toxicology in Vitro, 22 (2008) 296-300.
[110] Y. Lei, W. Chen, A. Mulchandani, Microbial biosensors, Anal Chim Acta, 568 (2006) 200-210.
[111] D. Chen, Y. Cao, B. Liu, J. Kong, A BOD biosensor based on a microorganism immobilized on an Al2O3 sol–gel matrix, Anal. Bioanal. Chem., 372 (2002) 737-739.
[112] F.J. Rawson, A.J. Downard, K.H. Baronian, Electrochemical detection of intracellular and cell membrane redox systems in Saccharomyces cerevisiae, Scientific reports, 4 (2014).
[113] A. Heiskanen, J. Yakovleva, C. Spégel, R. Taboryski, M. Koudelka-Hep, J. Emnéus, T. Ruzgas, Amperometric monitoring of redox activity in living yeast cells: comparison of menadione and menadione sodium bisulfite as electron transfer mediators, Electrochem. Commun., 6 (2004) 219-224.
[114] J. Zhao, M. Wang, Z. Yang, Z. Wang, H. Wang, Z. Yang, The different behaviors of three oxidative mediators in probing the redox activities of the yeast Saccharomyces cerevisiae, Anal Chim Acta, 597 (2007) 67-74.
[115] K. Baronian, A. Downard, R. Lowen, N. Pasco, Detection of two distinct substrate-dependent catabolic responses in yeast cells using a mediated electrochemical method, Applied Microbiology and Biotechnology, 60 (2002) 108-113.
[116] B. Liu, W. Cheng, S.A. Rotenberg, M.V. Mirkin, Scanning electrochemical microscopy of living cells: Part 2. Imaging redox and acid/basic reactivities, Journal of Electroanalytical Chemistry, 500 (2001) 590-597.
[117] B. Liu, M.V. Mirkin, Application of scanning electrochemical microscope for probing redox activity of living cells., Abstr. Pap. Am. Chem. Soc., 221 (2001) U72-U72.
[118] C. Cai, B. Liu, M.V. Mirkin, H.A. Frank, J.F. Rusling, Scanning electrochemical microscopy of living cells. 3. Rhodobacter sphaeroides, Anal Chem, 74 (2002) 114-119.
[119] R.A. Bullen, T.C. Arnot, J.B. Lakeman, F.C. Walsh, Biofuel cells and their development, Biosensors and Bioelectronics, 21 (2006) 2015-2045.
[120] A. Kloke, B. Biller, U. Kräling, S. Kerzenmacher, R. Zengerle, F. von Stetten, A Single Layer Glucose Fuel Cell Intended as Power Supplying Coating for Medical Implants, Fuel Cells, 11 (2011) 316-326.

[121] S.C. Barton, J. Gallaway, P. Atanassov, Enzymatic biofuel cells for implantable and microscale devices, Chem Rev, 104 (2004) 4867-4886.
[122] A. Ramanavicius, A. Kausaite, A. Ramanaviciene, Biofuel cell based on direct bioelectrocatalysis, Biosensors and Bioelectronics, 20 (2005) 1962-1967.
[123] V. Soukharev, N. Mano, A. Heller, A four-electron O(2)-electroreduction biocatalyst superior to platinum and a biofuel cell operating at 0.88 V, J Am Chem Soc, 126 (2004) 8368-8369.
[124] P.K. Addo, R.L. Arechederra, S.D. Minteer, Towards a rechargeable alcohol biobattery, Journal of Power Sources, 196 (2011) 3448-3451.
[125] T.K. Tam, G. Strack, M. Pita, E. Katz, Biofuel Cell Logically Controlled by Antigen−Antibody Recognition: Towards Immune-Regulated Bioelectronic Devices, Journal of the American Chemical Society, 131 (2009) 11670-11671.
[126] T. Chen, S.C. Barton, G. Binyamin, Z. Gao, Y. Zhang, H.H. Kim, A. Heller, A miniature biofuel cell, J Am Chem Soc, 123 (2001) 8630-8631.
[127] A. Ramanavicius, A. Ramanaviciene, Hemoproteins in Design of Biofuel Cells, Fuel Cells, 9 (2009) 25-36.
[128] E. Guler, H.C. Soyleyici, D.O. Demirkol, M. Ak, S. Timur, A novel functional conducting polymer as an immobilization platform, Materials Science and Engineering: C, 40 (2014) 148-156.
[129] A. Ramanavicius, A. Kausaite, A. Ramanaviciene, Enzymatic biofuel cell based on anode and cathode powered by ethanol, Biosens Bioelectron, 24 (2008) 767-772.
[130] B.A. Gregg, A. Heller, Cross-linked redox gels containing glucose oxidase for amperometric biosensor applications, Anal. Chem., 62 (1990) 258-263.
[131] E. Nazaruk, A. Michota, J. Bukowska, S. Shleev, L. Gorton, R. Bilewicz, Properties of native and hydrophobic laccases immobilized in the liquid-crystalline cubic phase on electrodes, Journal of biological inorganic chemistry : JBIC : a publication of the Society of Biological Inorganic Chemistry, 12 (2007) 335-344.
[132] L. Stoica, N. Dimcheva, Y. Ackermann, K. Karnicka, D.A. Guschin, P.J. Kulesza, J. Rogalski, D. Haltrich, R. Ludwig, L. Gorton, W. Schuhmann, Membrane-Less Biofuel Cell Based on Cellobiose Dehydrogenase (Anode)/Laccase (Cathode) Wired via Specific Os-Redox Polymers, Fuel Cells, 9 (2009) 53-62.
[133] I. Lapenaite, A. Ramanaviciene, A. Ramanavicius, Current trends in enzymatic determination of glycerol, Crit Rev Anal Chem, 36 (2006) 13-25.
[134] Y. Ackermann, D.A. Guschin, K. Eckhard, S. Shleev, W. Schuhmann, Design of a bioelectrocatalytic electrode interface for oxygen reduction in biofuel cells based on a specifically adapted Os-complex containing redox polymer with entrapped Trametes hirsuta laccase, Electrochem. Commun., 12 (2010) 640-643.
[135] Y. Oztekin, V. Krikstolaityte, A. Ramanaviciene, Z. Yazicigil, A. Ramanavicius, 1,10-Phenanthroline derivatives as mediators for glucose oxidase, Biosens. Bioelectron., 26 (2010) 267-270.
[136] Y. Oztekin, A. Ramanaviciene, Z. Yazicigil, A.O. Solak, A. Ramanavicius, Direct electron transfer from glucose oxidase immobilized on polyphenanthroline-modified glassy carbon electrode, Biosensors and Bioelectronics, 26 (2011) 2541-2546.
[137] A. Kausaite-Minkstimiene, V. Mazeiko, A. Ramanaviciene, A. Ramanavicius, Enzymatically synthesized polyaniline layer for extension of linear detection region of amperometric glucose biosensor, Biosensors and Bioelectronics, 26 (2010) 790-797.

[138] T. Ruzgas, L. Gorton, J. Emnéus, G. Marko-Varga, Kinetic models of horseradish peroxidase action on a graphite electrode, Journal of Electroanalytical Chemistry, 391 (1995) 41-49.
[139] G. Accorsi, A. Listorti, K. Yoosaf, N. Armaroli, 1,10-Phenanthrolines: versatile building blocks for luminescent molecules, materials and metal complexes, Chemical Society Reviews, 38 (2009) 1690-1700.
[140] T. Schilling, A. Okunola, J. Masa, W. Schuhmann, M. Bron, Carbon nanotubes modified with electrodeposited metal porphyrins and phenanthrolines for electrocatalytic applications, Electrochimica Acta, 55 (2010) 7597-7602.
[141] A. Bencini, V. Lippolis, 1,10-Phenanthroline: A versatile building block for the construction of ligands for various purposes, Coordination Chemistry Reviews, 254 (2010) 2096-2180.
[142] Y. Oztekin, A. Ramanaviciene, N. Ryskevic, Z. Yazicigil, Z. Üstündağ, A.O. Solak, A. Ramanavicius, 1, 10-Phenanthroline modified glassy carbon electrode for voltammetric determination of cadmium (II) ions, Sensors and Actuators B: Chemical, 157 (2011) 146-153.
[143] J. Castillo, S. Gáspár, S. Leth, M. Niculescu, A. Mortari, I. Bontidean, V. Soukharev, S. Dorneanu, A. Ryabov, E. Csöregi, Biosensors for life quality: Design, development and applications, Sensors and Actuators B: Chemical, 102 (2004) 179-194.
[144] A. Shrier, F. Giroud, M. Rasmussen, S.D. Minteer, Operational Stability Assays for Bioelectrodes for Biofuel Cells: Effect of Immobilization Matrix on Laccase Biocathode Stability, Journal of The Electrochemical Society, 161 (2014) H244-H248.
[145] F. Giroud, C. Gondran, K. Gorgy, V. Vivier, S. Cosnier, An enzymatic biofuel cell based on electrically wired polyphenol oxidase and glucose oxidase operating under physiological conditions, Electrochimica Acta, 85 (2012) 278-282.
[146] C. Gutiérrez-Sánchez, W. Jia, Y. Beyl, M. Pita, W. Schuhmann, A.L. De Lacey, L. Stoica, Enhanced direct electron transfer between laccase and hierarchical carbon microfibers/carbon nanotubes composite electrodes. Comparison of three enzyme immobilization methods, Electrochimica acta, 82 (2012) 218-223.
[147] A. Zebda, C. Gondran, A. Le Goff, M. Holzinger, P. Cinquin, S. Cosnier, Mediatorless high-power glucose biofuel cells based on compressed carbon nanotube-enzyme electrodes, Nature communications, 2 (2011) 370.
[148] C. Pan, Y. Fang, H. Wu, M. Ahmad, Z. Luo, Q. Li, J. Xie, X. Yan, L. Wu, Z.L. Wang, J. Zhu, Generating electricity from biofluid with a nanowire-based biofuel cell for self-powered nanodevices, Adv Mater, 22 (2010) 5388-5392.
[149] F. Gao, O. Courjean, N. Mano, An improved glucose/O 2 membrane-less biofuel cell through glucose oxidase purification, Biosensors and Bioelectronics, 25 (2009) 356-361.
[150] M. Falk, V. Andoralov, Z. Blum, J. Sotres, D.B. Suyatin, T. Ruzgas, T. Arnebrant, S. Shleev, Biofuel cell as a power source for electronic contact lenses, Biosens Bioelectron, 37 (2012) 38-45.
[151] X. Wang, M. Falk, R. Ortiz, H. Matsumura, J. Bobacka, R. Ludwig, M. Bergelin, L. Gorton, S. Shleev, Mediatorless sugar/oxygen enzymatic fuel cells based on gold nanoparticle-modified electrodes, Biosensors and Bioelectronics, 31 (2012) 219-225.

[152] V. Krikstolaityte, A. Barrantes, A. Ramanavicius, T. Arnebrant, S. Shleev, T. Ruzgas, Bioelectrocatalytic reduction of oxygen at gold nanoparticles modified with laccase, Bioelectrochemistry, 95 (2014) 1-6.
[153] F. Gao, Y. Yan, L. Su, L. Wang, L. Mao, An enzymatic glucose/O 2 biofuel cell: preparation, characterization and performance in serum, Electrochem. Commun., 9 (2007) 989-996.
[154] W. Jia, C. Jin, W. Xia, M. Muhler, W. Schuhmann, L. Stoica, Glucose Oxidase/Horseradish Peroxidase Co-immobilized at a CNT-Modified Graphite Electrode: Towards Potentially Implantable Biocathodes, Chem. Eur. J., 18 (2012) 2783-2786.
[155] A. Trifonov, K. Herkendell, R. Tel-Vered, O. Yehezkeli, M. Woerner, I. Willner, Enzyme-capped relay-functionalized mesoporous carbon nanoparticles: effective bioelectrocatalytic matrices for sensing and biofuel cell applications, ACS nano, 7 (2013) 11358-11368.
[156] V. Krikstolaityte, Y. Oztekin, J. Kuliesius, A. Ramanaviciene, Z. Yazicigil, M. Ersoz, A. Okumus, A. Kausaite-Minkstimiene, Z. Kilic, A.O. Solak, Biofuel cell based on anode and cathode modified by glucose oxidase, Electroanal., 25 (2013) 2677-2683.
[157] I. Willner, G. Arad, E. Katz, A biofuel cell based on pyrroloquinoline quinone and microperoxidase-11 monolayer-functionalized electrodes, Bioelectroch Bioener, 44 (1998) 209-214.
[158] A. Pizzariello, M. Stred'ansky, S. Miertus, A glucose/hydrogen peroxide biofuel cell that uses oxidase and peroxidase as catalysts by composite bulk-modified bioelectrodes based on a solid binding matrix, Bioelectrochemistry, 56 (2002) 99-105.
[159] V.M. A.L. Yaropolov, S.D. Varfolomeev, Electroreduction of hydrogen peroxide on an electrode with immobilized peroxidase, Dokl. Akad. Nauk., (1979) 1399–1401.
[160] R. Louise Meyer, X. Zhou, L. Tang, A. Arpanaei, P. Kingshott, F. Besenbacher, Immobilisation of living bacteria for AFM imaging under physiological conditions, Ultramicroscopy, 110 (2010) 1349-1357.
[161] A. Méndez-Vilas, A.M. Gallardo-Moreno, M.L. González-Martín, Atomic force microscopy of mechanically trapped bacterial cells, Microscopy and Microanalysis, 13 (2007) 55-64.
[162] M. Nikkhah, J. S. Strobl, R. De Vita, M. Agah, The cytoskeletal organization of breast carcinoma and fibroblast cells inside three dimensional (3-D) isotropic silicon microstructures, Biomaterials, 31 (2010).
[163] S. D'Souza, J. Melo, Immobilization of bakers yeast on jute fabric through adhesion using polyethylenimine: application in an annular column reactor for the inversion of sucrose, Process Biochem, 36 (2001) 677-681.
[164] E. Ostuni, L. Yan, G.M. Whitesides, The interaction of proteins and cells with self-assembled monolayers of alkanethiolates on gold and silver, Colloids and Surfaces B: Biointerfaces, 15 (1999) 3-30.
[165] H. Wang, R. Bash, J.G. Yodh, G.L. Hager, D. Lohr, S.M. Lindsay, Glutaraldehyde modified mica: a new surface for atomic force microscopy of chromatin, Biophys J, 83 (2002) 3619-3625.
[166] A. Suchodolskis, V. Feiza, A. Stirke, A. Timonina, A. Ramanaviciene, A. Ramanavicius, Elastic properties of chemically modified baker's yeast cells studied by AFM, Surf Interface Anal, 43 (2011) 1636-1640.

[167] W. Wang, X. Liu, D. Gelinas, B. Ciruna, Y. Sun, A fully automated robotic system for microinjection of zebrafish embryos, PloS one, 2 (2007) e862.
[168] C. Fung, N. Xi, R. Yang, K. Lai, K. Seiffert-Sinha, A.A. Sinha, Development of cell fixture for in-situ imaging and manipulation of membrane protein structure, Nanotechnology, 2009. IEEE-NANO 2009. 9th IEEE Conference on, IEEE, 2009, pp. 397-400.
[169] C. Franz, P.-H. Puech, Atomic force microscopy: a versatile tool for studying cell morphology, adhesion and mechanics, Cellular and Molecular Bioengineering, 1 (2008) 289-300.
[170] C.K.M. Fung, N. Xi, R. Yang, K. Seiffert-Sinha, K.W.C. Lai, A.A. Sinha, Quantitative analysis of human keratinocyte cell elasticity using atomic force microscopy (AFM), NanoBioscience, IEEE Transactions on, 10 (2011) 9-15.
[171] H.J. Hecht, H.M. Kalisz, J. Hendle, R.D. Schmid, D. Schomburg, Crystal Structure of Glucose Oxidase from Aspergillus niger Refined at 2·3 Å Reslution, Journal of Molecular Biology, 229 (1993) 153-172.
[172] R.V. Mikhailova, T.V. Semashko, A.G. Lobanok, [Selection of Penicillium funiculosum strains with high glucose oxidase activity], Prikladnaia biokhimiia i mikrobiologiia, 38 (2002) 273-277.
[173] R.F. Beers, Jr., I.W. Sizer, A spectrophotometric method for measuring the breakdown of hydrogen peroxide by catalase, The Journal of biological chemistry, 195 (1952) 133-140.
[174] A. Kausaite-Minkstimiene, V. Mazeiko, A. Ramanaviciene, A. Ramanavicius, Enzymatically synthesized polyaniline layer for extension of linear detection region of amperometric glucose biosensor, Biosens Bioelectron, 26 (2010) 790-797.
[175] Y. Saito, A Theoretical Study on the Diffusion Current at the Stationary Electrodes of Circular and Narrow Band Types, Review of Polarography, 15 (1968) 177-187.
[176] R.H. Benjamin, W. Gunther, Biotechnological Applications, Scanning Electrochemical Microscopy, Second Edition, CRC Press 2012, pp. 317-378.
[177] S. Skale, V. Doleček, M. Slemnik, Substitution of the constant phase element by Warburg impedance for protective coatings, Corr. Sci., 49 (2007) 1045-1055.
[178] B. Csoka, B. Kovacs, G. Nagy, Investigation of concentration profiles inside operating biocatalytic sensors with scanning electrochemical microscopy (SECM), Biosens. Bioelectron., 18 (2003) 141-149.
[179] K. Eckhard, W. Schuhmann, Localised visualisation of O2 consumption and H2O2 formation by means of SECM for the characterisation of fuel cell catalyst activity, Electrochimica Acta, 53 (2007) 1164-1169.
[180] A. Kausaite, A. Ramanaviciene, A. Ramanavicius, Polyaniline synthesis catalysed by glucose oxidase, Polymer, 50 (2009) 1846-1851.
[181] A. Ramanaviciene, G. Nastajute, V. Snitka, A. Kausaite, N. German, D. Barauskas-Memenas, A. Ramanavicius, Spectrophotometric evaluation of gold nanoparticles as red-ox mediator for glucose oxidase, Sens. Actuat. B-Chem., 137 (2009) 483-489.
[182] A. Ramanavicius, A. Kausaite, A. Ramanaviciene, Self-encapsulation of oxidases as a basic approach to tune the upper detection limit of amperometric biosensors, Analyst, 133 (2008) 1083-1089.

[183] Y. Oztekin, A. Ramanaviciene, Z. Yazicigil, A.O. Solak, A. Ramanavicius, Direct electron transfer from glucose oxidase immobilized on polyphenanthroline-modified glassy carbon electrode, Biosens. Bioelectron., 26 (2011) 2541-2546.
[184] R. Cornut, P. Hapiot, C. Lefrou, Enzyme-mediator kinetics studies with SECM: Numerical results and procedures to determine kinetics constants, Journal of Electroanalytical Chemistry, 633 (2009) 221-227.
[185] B. Ungerböck, A. Pohar, T. Mayr, I. Plazl, Online oxygen measurements inside a microreactor with modeling of transport phenomena, Microfluid Nanofluid, 14 (2013) 565-574.
[186] H.J. Bright, Q.H. Gibson, The oxidation of 1-deuterated glucose by glucose oxidase, Journal of Biological Chemistry, 242 (1967) 994-1003.
[187] V. Leskovac, S. Trivić, G. Wohlfahrt, J. Kandrač, D. Peričin, Glucose oxidase from Aspergillus niger: the mechanism of action with molecular oxygen, quinones, and one-electron acceptors, The international journal of biochemistry & cell biology, 37 (2005) 731-750.
[188] Q.H. Gibson, B.E. Swoboda, V. Massey, Kinetics and Mechanism of Action of Glucose Oxidase, Journal of Biological Chemistry, 239 (1964) 3927-3934.
[189] F.O. Laforge, P. Sun, M.V. Mirkin, Physicochemical Applications of Scanning Electrochemical Microscopy, Advances in Chemical Physics, 139 (2008) 177-244.
[190] R.D. Martin, P.R. Unwin, Theory and experiment for the substrate generation tip collection mode of the scanning electrochemical microscope: Application as an approach for measuring the diffusion coefficient ratio of a redox couple, Anal. Chem., 70 (1998) 276-284.
[191] R. Baronas, Ivanauskas, F., Kulys, J. , Mathematical Modeling of Biosensors, Springer2010.
[192] M. Jamnongwong, K. Loubiere, N. Dietrich, G. Hébrard, Experimental study of oxygen diffusion coefficients in clean water containing salt, glucose or surfactant: Consequences on the liquid-side mass transfer coefficients, Chemical Engineering Journal, 165 (2010) 758-768.
[193] F. Lisdat, D. Schäfer, The use of electrochemical impedance spectroscopy for biosensing, Anal. Bioanal. Chem., 391 (2008) 1555-1567.
[194] A. Ramanavicius, P. Genys, A. Ramanaviciene, Electrochemical Impedance Spectroscopy Based Evaluation of 1,10-Phenanthroline-5,6-dione and Glucose Oxidase Modified Graphite Electrode, Electrochimica Acta, 146 (2014) 659-665.
[195] S.-J. Lin, L. Guarente, Nicotinamide adenine dinucleotide, a metabolic regulator of transcription, longevity and disease, Current opinion in cell biology, 15 (2003) 241-246.
[196] K. Nagamine, Y. Takahashi, K. Ino, H. Shiku, T. Matsue, Influence of tip size on single yeast cell imaging using scanning electrochemical microscopy, Electroanal., 23 (2011) 1168-1174.
[197] T. Semashko, R. Mikhailova, A. Ramanaviciene, A. Ramanavicius, Specificity of glucose oxidase from Penicillium funiculosum 46.1 towards some redox mediators, Appl Biochem Biotech, 171 (2013) 1739-1749.
[198] A.D. Ryabov, V.N. Goral, L. Gorton, E. Csöregi, Electrochemically and Catalytically Active Reconstituted Horseradish Peroxidase with Ferrocene-Modified Hemin and an Artificial Binding Site, Chemistry – A European Journal, 5 (1999) 961-967.